0D/1D Investigations on SI-Engines for Optimal Engine and System Efficiency

Von der Fakultät Konstruktions-, Produktions- und Fahrzeugtechnik
der Universität Stuttgart
zur Erlangung der Würde eines Doktor-Ingenieurs (Dr.-Ing.)
genehmigte Abhandlung

von

Cihat Feyyaz Negüs
aus Sisli

Hauptberichter:	Prof. Dr.-Ing. Michael Bargende
Erster Mitberichter:	Prof. Dr.-Ing. Peter Eilts
Zweiter Mitberichter:	Prof. Dr.-Ing. André Casal Kulzer

Tag der mündlichen Prüfung: 06.04.2023

Institut für Fahrzeugtechnik Stuttgart
Universität Stuttgart

2023

Preface

This work was created during my tenure as a research assistant at the Institute of Automotive Engineering (IFS) at the University of Stuttgart. I hereby want to thank Prof. Dr.-Ing. Michael Bargende for his supervision and support during this work. I also want to thank Dr.-Ing. Michael Grill for his most valuable guidance.

I would also like to thank to my project partners Alexander Kuznik, Christian Wouters, Marvin Thielen and Erich Wenz for our fruitful discussions as well as Prof. Dr.-Ing. Peter Eilts for his many contributions and also for his interest for joining the doctoral committee. I also thank to the working group and especially the chairmen Arndt Döhler and Prof. Dr.-Ing. André Casal Kulzer of the research project "ICE2025+: Ultimate System Efficiency" defined and financed by FVV. I finally want to thank Viktoria Kelich for her efforts as project manager as well as for her constant support.

My utmost gratitude goes to my colleagues and friends at IFS. Their vigorous support and positive influence inspired me to develop not only on a professional but also on a personal level. In this regard, I would like to thank especially to my office colleagues Florian Mandl, Sebastian Fritsch, Ömer Ünal as well as Dominik Rether. Further special thanks go to Jan Przewlocki, Martin Angerbauer, Markus Maul, Cornelius Wagner, Ismail Mir, Sebastian Crönert and all my other colleagues for creating a highly pleasant and enjoyable working atmosphere.

Finally, I would like to thank to my beloved parents for their endless support while pursuing my goals throughout my life.

Stuttgart, 06.04.2023 Feyyaz Negüs

Table of Contents

Preface ..... **I**

Table of Figures ..... **VI**

List of Tables ..... **XIII**

List of Abbreviations ..... **XIV**

List of Symbols ..... **XVII**

Abstract ..... **XX**

Zusammenfassung ..... **XXI**

1 Introduction **1**

2 Technology Overview and State of the Art **5**

- 2.1 Challenges to overcome for achieving higher efficiencies 5
- 2.2 Overview for technologies and measures for efficiency increase 13
  - 2.2.1 Downsizing 13
  - 2.2.2 Cylinder deactivation 15
  - 2.2.3 Exhaust gas recirculation (EGR) 15
  - 2.2.4 Miller cycle 17
  - 2.2.5 Variable compression ratio 20
  - 2.2.6 High turbulence concept 21
  - 2.2.7 High stroke-to-bore ratio 22
  - 2.2.8 Water injection 23
  - 2.2.9 Lean concept 25
  - 2.2.10 Turbocharger efficiency 26

2.2.11 Alternative fuels ... 29
2.2.12 Hybrid drivetrains ... 31

3 Modeling approach ... 34

3.1 Simulation and modeling methods ... 34
3.1.1 Combustion chamber modeling ... 34
3.1.2 Engine Modeling ... 42
3.2 Calibration of the combustion models ... 44
3.2.1 Burn rate model ... 46
3.2.2 Knock model ... 59
3.2.3 Model calibration for alternative fuels ... 64
3.3 Full Engine Modeling and Calibration ... 66

4 Investigations of Engine Concepts ... 71

4.1 Reference Engine ... 75
4.2 High Efficiency Engine ... 81
4.3 A-Segment Engine ... 92
4.4 J-Segment Engine ... 93
4.5 Methanol Engine ... 96
4.6 Short study: Blend Engine with G70M15E15 ... 102
4.7 Full Load Water Injection Engine ... 104
4.8 Lean High Efficiency Engine ... 108
4.9 Lean Full Load Water Injection Engine ... 111
4.10 Lean Methanol Engine ... 113
4.11 Discussion of the Results with the Help of Overall Powertrain Efficiencies during WLTC cycles ... 116

5 Summary and Outlook ... 123

6 References 131

Appendix 139

- A1. Model parameter C_u for experimental setups 139
- A2. Model parameter x_{ub} for experimental setups 140
- A3. Model settings, full engine models 141
- A4. Estimation of the benefits with load point shifting 144
- A5. Complementary Engine Maps 146

Table of Figures

Figure 2.1. The pressure-volume (p-v) and the temperature-entropy (T-s) diagrams of the thermodynamic cycles that represent the working cycle of internal combustion engines [5] 6

Figure 2.2. Isobaric specific heat capacity of nitrogen, calculated with NASA polynomials 9

Figure 2.3. Increase of the apparent isochoric heat capacity at high temperatures due to dissociation [8] 10

Figure 2.4. Distribution of engine operating points for various driving cycles [9] 12

Figure 2.5. Schematical representation of mfb50%, efficiency and power output of the engine with increasing intake pressure 14

Figure 2.6. Effect of LP-EGR and HP-EGR on compressor operation. The dashed line represents the high efficiency region of the compressor map 17

Figure 2.7. Different methods for realizing Miller strategy. Left: By using shortened valve durations. Right: By shifting the valve opening timing 18

Figure 2.8. p-V diagram of a reference cycle compared with the Miller cycle. 18

Figure 2.9. Laminar flame speed of various fuels in comparison to gasoline at 800 K and 50 bar according to Crönert et al. [53] ... 30

Figure 2.10. Different hybrid architectures [9] 32

Figure 3.1. The entrainment model and the flame propagation [57] 35

Figure 3.2. Laminar flame speeds as a function of air-fuel equivalence ratio according to approaches of Heywood and Gülder [59] 37

Figure 3.3. Relative change of laminar flame speed according to Hann et al. as a function of air-fuel equivalence ratio and EGR rate for different starting temperatures [59] 38

Figure 3.4. Ignition delay as a function of temperature with two-stage ignition region for gasoline [70] 41

Figure 3.5. Burn rates with TPA and simulation for a load variation at 2000 RPM with the engine layout A.. 47

Figure 3.6. Burn rates with TPA and simulation for a load variation with 50% water injection at 2000 RPM with the engine layout A..... 48

Figure 3.7. Burn rates with TPA and simulation for a load variation with 100% water injection at 2000 RPM with the engine layout A 49

Figure 3.8. Burn rates with TPA and simulation for an EGR variation at 2250 RPM, 6.5 bar IMEP with the engine layout B 50

Figure 3.9. Burn rates with TPA and simulation for an EGR variation at 2000 RPM, 11 bar IMEP with the engine layout B 51

Figure 3.10. Burn rates with TPA and simulation for an EGR variation at 2500 RPM, 16 bar IMEP with the engine layout B 52

Figure 3.11. Burn rates with TPA and simulation for an EGR variation at 2000 RPM, 11 bar IMEP with closed tumble flap (engine layout C) 54

Figure 3.12. Burn rates with TPA and simulation for an air-fuel-ratio variation at 2000 RPM, 11 bar IMEP, tumble flap closed (engine layout C) 55

Figure 3.13. Burn rates with TPA and simulation for an air-fuel-ratio variation at 2000 RPM, 8 bar IMEP with the engine layout D 57

Figure 3.14. Burn rates with TPA and simulation for a load variation at 2000 RPM, lean combustion with λ=1.5 with the engine layout D 58

Figure 3.15. The measured and simulated center of combustion for a load variation at 2000 RPM, engine layout A............................ 59

Figure 3.16. The measured and simulated center of combustion for a load variation at 2000 RPM with 100% water injection, engine layout A.. 60

Figure 3.17. The measured and simulated center of combustion for an EGR variation for two operating points: 2500 RPM 16 bar IMEP (above), 2000 RPM 11 bar IMEP (below) 61

Figure 3.18. The effect of cycle-to-cycle variations on the distribution on working cycles and knock behavior...................................... 62

Figure 3.19. The change of center of combustion with increasing air-fuel equivalence ratio. Black solid lines are measurements VKA, the other solid lines from IVB. Red dashed line is the trend line that approximately shows the average observed knock behavior. CRlow = compression ratio of 12.42, CRhigh = compression ratio of 18, RefIVC = Reference intake valve closure, LIVC = Late intake valve closure, TFo = tumble flap open, TFc = tumble flap closed, fuel is RON95E10 if not stated otherwise, the value in bar is IMEP, the value following CR is the compression ratio............ 63

Figure 3.20. Measured and simulated burn durations for gasoline and methanol, 2500 RPM, 16 bar IMEP, gasoline with the engine layout E, methanol with the engine layout F.................. 64

Figure 3.21. Measured and simulated burn durations for methanol for an air-fuel ratio variation, 2500 RPM, 16 bar IMEP with the engine layout F. The shown point for gasoline is at the same operating point with the measured and simulated with the engine layout E. 65

Figure 3.22. Measured burn durations and mfb50% for the blend fuel G70M15E15 with the engine layout F in comparison to other fuels for a load variation at 2500 RPM [29] 66

Figure 3.23. BSFC map of the Reference Engine VW EA211 TSI evo [17].. 67

Figure 3.24. Simulated BSFC map of the VW EA211 TSI evo model......... 69

Figure 4.1. Simulated brake efficiency map of VW EA211 TSI evo. The dark blue dots represent the operating points that are simulated to generate the map. 76

Figure 4.2. The effect of cylinder deactivation on efficiency at two different loads 77

Figure 4.3. The effect of early intake valve closure on efficiency and knock resistance at two different operating points..... 78

Figure 4.4. The efficiency map of the hypothetical downsized engine..... 79

Figure 4.5. Comparison of efficiencies of for three and four-cylinder downsized engines at 2500 RPM..... 80

Figure 4.6. The efficiency map of the High Efficiency Engine model 82

Figure 4.7. The relative difference in brake efficiency of the High Efficiency Engine in comparison to the Reference Engine (VW EA211 TSI evo). Green and blue indicate, that the High Efficiency Engine is better. Yellow and orange indicate that the Reference Engine is better...... 83

Figure 4.8. EGR rate map of the High Efficiency Engine 84

Figure 4.9. Compression ratio map of the High Efficiency Engine..... 85

Figure 4.10. Friction losses as the percentage of fuel energy, for the Reference Engine, the High Efficiency Engine and for the High Efficiency Engine with a constant compression ratio of 12.5 (same as the Reference Engine)..... 86

Figure 4.11. Effects of the high turbulence concept on burn durations, center of combustion and brake efficiency 87

Figure 4.12. Effect of compression ratio on knock behavior and efficiency for two different turbulence levels..... 88

Figure 4.13. Effect of EGR on burn duration, knock behavior and efficiency for two different turbulence levels..... 89

Figure 4.14. Effect of EGR on efficiency, if optimal valve timings are chosen for each EGR rate (solid lines) and if the valve timings are kept constant throughout the EGR variation (dashed lines)...... 90

Figure 4.15. Effect of stroke-to-bore ratio on efficiency at two different operating points 91

Figure 4.16. The efficiency map of the A-Segment Engine model..... 93

Figure 4.17. The efficiencies of the J-Segment Engine with different stroke-to-bore ratios at 2500 RPM..94

Figure 4.18. The efficiency map of the J-Segment Engine model 95

Figure 4.19. The efficiency map of the Methanol Engine............................96

Figure 4.20. The relative difference in brake efficiency of Methanol Engine in comparison to the High Efficiency Engine. Green and blue indicate, that the Methanol Engine is better. Yellow and orange indicate, that the High Efficiency Engine is better. 97

Figure 4.21. Comparison of achievable efficiencies with RON95E10 (Gasoline), with more knock-resistant, hypothetical versions of gasoline (Gasoline+, Gasoline++) as well as with methanol at two different operating points. The center of combustion (mfb50%) and compression ratio (ε) of each configuration is denoted above the respective column. 100

Figure 4.22. Share of energy of the mechanical output and various losses at two different loads for the four configurations with different fuels..101

Figure 4.23. Brake Efficiencies, compression ratio, center of combustions, burn durations, EGR rates and loads when cylinder deactivation is active for High Efficiency Engine, Methanol Engine and Blend Engine along the engine speed 2500 RPM...103

Figure 4.24. The efficiency map of the Full Load Water Injection Engine model...106

Figure 4.25. The relative difference in brake efficiency of the Full Load Water Injection Engine in comparison to the Reference Engine (VW EA211 TSI evo). Green and blue indicate, that the Full Load Water Injection Engine is better. Yellow and orange indicate, that the Reference Engine is better................106

Figure 4.26. The relative difference in brake efficiency of the Full Load Water Injection Engine in comparison to the High Efficiency Engine. Light green and yellow indicate that both engines have similar efficiencies, red indicates that the High Efficiency Engine is better. 107

Figure 4.27. The efficiency map of the Lean High Efficiency Engine model with black solid line representing the border between stoichiometric and lean operation 109

Figure 4.28. The comparison of stoichiometric and lean versions of the High Efficiency Engine. Green and blue indicate that the lean version is better. Yellow and orange indicate that the stoichiometric version is better. 111

Figure 4.29. The efficiency map of the Lean Full Load Water Injection Engine model with black solid line representing the border between stoichiometric and lean operation 112

Figure 4.30. The comparison of stoichiometric and lean versions of the Full Load Water Injection Engine. Green and blue indicate that the lean version is better. Yellow and orange indicate that the stoichiometric version is better. The dashed grey line represents the maximum possible reachable load with $\lambda = 1.7$. 113

Figure 4.31. The efficiency map of the Lean Methanol Engine model with white solid line representing the border between stoichiometric and lean operation 114

Figure 4.32. The comparison of stoichiometric and lean versions of the Methanol Engine. Green and blue indicate that the lean version is better. Yellow and orange indicate that the stoichiometric version is better. 115

Figure 4.33. Distribution of operating points through the engine map during a WLTC cycle for the High Efficiency Engine with P2 LV hybrid architecture, according to investigations of VKM [29] 116

Figure 4.34. Powertrain and energy flows for the Reference Engine VW EA211 TSI evo without hybridization [29] 118

Figure 4.35. Powertrain and energy flows for the High Efficiency Engine with the P1 hybrid architecture [29] 118

Figure 4.36. Powertrain and energy flows for the High Efficiency Engine with the P2 LV hybrid architecture [29] 120
Figure 4.37. Consumed fuel energy for different powertrain configurations [75] 121
Figure 5.1. Overview of the peak efficiencies for different engine models 126
Figure 5.2. Overview of the estimated efficiency benefits for different engine models, dark orange for the worst-case, light orange for the best-case scenarios 126

List of Tables

Table 2.1. Properties of investigated fuels [29] 30

Table 3.1. Engines and engine layouts named from A to F that are used for the model calibration. 45

Table 4.1. Overview of the engine models. The present technologies are marked with the symbol “x”. 73

Table 4.2. Continuation of Table 4.1: Overview of the engine models. The present features are marked with the symbol “x”. 74

Table 4.3. Mean powertrain efficiencies for different engines combined with different hybrid architectures during the WLTC cycle [29] 117

List of Abbreviations

0D	Zero dimensional
1D	One dimensional
3D	Three dimensional
3V	Three-valve (cylinder head)
4V	Four-valve (cylinder head)
BD 10-90%	Burn duration 10-90%
BDC	Bottom dead center
BMEP	Brake mean effective pressure
BSFC	Brake specific fuel consumption
CA	Crank angle
CFD	Computational fluid dynamics
CI	Compression-ignition
CR	Compression ratio
DMC+	Fuel mixture consisting of dimethyl carbonate and methyl formate
EGR	Exhaust gas aftertreatment
EIVC	Early intake valve closure
EU	European Union
FKFS	Forschungsinstitut für Kraftfahrwesen und Fahrzeugmotoren Stuttgart
FLWI	Full Load Water Injection Engine
FMEP	Friction mean effective pressure
FVV	Forschungsvereinigung Verbrennungskraftmaschinen e.V.

GT	Gamma Technologies
HEE	High Efficiency Engine
HP	High pressure
HV	High voltage
ICE	Internal combustion engine
IMEP	Indicated mean effective pressure
IVB	Institut für Verbrennungskraftmaschinen Braunschweig
LIVC	Late intake valve closure
LP	Low pressure
LV	Low voltage
mfb50%	Mass fuel burned 50%, center of combustion
NASA	National Aeronautics and Space Administration
NEDC	New European Drive Cycle
NO_X	Nitrogen oxides
NVH	Noise, vibration and harshness
P1	P1 hybrid architecture
P2	P2 hybrid architecture
PMEP	Pumping mean effective pressure
PS	Power split hybrid architecture
RDE	Real Driving Emissions
RON	Research octane number
RPM	Revolutions per minute
RWTH	Rheinisch-Westfälische Technische Hochschule
SI	Spark-ignition
TDC	Top dead center

TFc	Tumble flap closed
TFo	Tumble flap opened
TPA	Three pressure analysis
VGT	Variable geometry turbine
VKA	Institut für Verbrennungskraftmaschinen Aachen
VKM	Institut für Verbrennungskraftmaschinen und Fahrzeugantriebe
VW	Volkswagen
WLTC	Worldwide Harmonized Light-Duty Vehicles Test Cycles
WLTP	Worldwide Harmonized Light-Duty Vehicles Test Procedure

List of Symbols

Latin Letters

a_i	$J/(kgK^i)$	Coefficients of NASA polynomials, with i=1…5
A_{fl}	m^2	Flame area
b	mm	Bore
C_1, C_2, C_3	varies	Model parameter Arrhenius equation
c_p	J/(kgK)	Specific isobaric heat capacity
C_u	-	Model parameter combustion model
d	mm	Diameter
f	-	Model parameter laminar flame speed
H_u	MJ/kg	Lower heat value
k	m^2/s^2	Turbulent kinetic energy
m	kg	Mass
$\dot{m}$	kg/s	Mass flow rate
$\dot{m}_{corr}$	kg/s	Corrected mass flow rate
M_T	Nm	Tumble torque
n_{corr}	RPM	Corrected speed
p	bar	Pressure
Q	J	Heat
Q_{add}	J	Heat addition
Q_B	J	Heat release during combustion
Q_{rej}	J	Heat rejection
s	mm	Stroke

s_L	m/s	Laminar flame speed
T	K	Temperature
t	s	Time
T_{Tipp}	-	Tippelmann number
u'	m/s	Turbulent fluctuation velocity
u_E	m/s	Entrainment velocity
V	m^3	Volume
W	J	Work
W_{comp}	J	Compression work
W_{exp}	J	Expansion work
X_{EGR}	-	EGR fraction
x_{ub}	-	Model parameter knock model

Greek Letters

α	-	Model parameter laminar flame speed
β	-	Model parameter laminar flame speed
ε	-	Compression ratio
ε_{diss}	m^2/s^3	Rate of dissipation of the turbulent kinetic energy
η	%	Efficiency
κ	-	Isentropic exponent
λ	-	Air-to-fuel equivalence ratio
ρ	kg/m^3	Density
τ	s	Ignition delay time
φ	°	Crank angle

Indices

b	Burnt
BDC	Bottom dead center
C	Compressor
EIVC	Early intake valve closure
in	Intake
Miller	Miller
mix	Mixture
o	Reference boundary conditions
prod	Production
ref	Reference
T	Turbine

Abstract

There are several promising technologies, measures, ideas and concepts for increasing the efficiency of spark-ignition internal combustion engines. In this work, these technologies are investigated by using 0D/1D simulation methods. The focus is assessing the technologies by installing them into full engine models, revealing not only their advantages, but also their potential drawbacks as well as possible interactions and synergy effects between them. The objective is to design engine models that feature highest efficiencies possible for the widest operation range possible in order to demonstrate the potential of further efficiency improvement for internal combustion engines.

The measures that are considered in this work are: Downsizing, cylinder deactivation, Miller cycle with variable valve timings, increasing the compression ratio or a variable compression ratio, exhaust gas recirculation (EGR), high turbulence concept, high stroke-to-bore ratio, water injection, lean concept and alternative fuels.

Enhancements to the internal combustion engine must be realized by two means: First, a better overlapping between the high efficiency zone of the engine map and the operating window at which the engine is operated is achieved with aggressive downsizing. Secondly, the efficiencies themselves must be increased by combining appropriate technologies. During these tasks, it is imperative to use the synergy effects between technologies and avoiding technologies that are counterproductive, as they interacted with the remaining technologies or with a desirable engine setup in a disadvantageous way.

According to the results, with a stoichiometric gasoline engine setup an estimated 15-19% of efficiency improvement potential in comparison to a state-of-the-art engine during a WLTC cycle is evident. A further 5% efficiency improvement is possible, if a lean concept is adapted instead. Furthermore, methanol presented itself as an excellent alternative to gasoline due to its exceptional knock resistance and high evaporation energy. With a methanol engine an around 8% further efficiency improvement should be achieved.

Zusammenfassung

Um den Wirkungsgrad von Ottomotoren zu verbessern, kommen zahlreiche vielversprechende Technologien, Maßnahmen, Ideen und Konzepte in Frage. Im Rahmen dieser Arbeit werden diese Technologien mittels 0D/1D-Simulationsmethoden untersucht. Dabei werden die Technologien in Vollmotormodellen eingesetzt, mit dem Ziel, neben ihren Vorteilen auch die möglichen Nachteile und eventuell das Zusammenspiel zwischen den Technologien zu entdecken. Das Hauptziel dieser Arbeit ist es, Motorkonzepte zu erstellen, die möglichst hohe Wirkungsgrade für ein möglichst breites Betriebsfenster aufweisen, um das Potential der Wirkungsgradverbesserung bei Ottomotoren aufzuzeigen.

Die Maßnahmen und Technologien, die in dieser Arbeit untersucht werden, sind: Downsizing, Zylinderabschaltung, Millerzyklus mit variablen Ventilsteuerzeiten, Erhöhung des Verdichtungsverhältnisses oder ein variables Verdichtungsverhältnis, Abgasrückführung (AGR), Hochturbulenzkonzept, Erhöhung des Hub-Bohrungsverhältnisses (Langhubigkeit), Wassereinspritzung, Magerkonzept und alternative Kraftstoffe. Die Wirkungsgradverbesserungen bei den Motorkonzepten werden auf zwei Wirkpfaden erreicht: Zum einen muss eine bessere Überlappung zwischen dem Betriebsfenster und dem Bereich der höheren Wirkungsgrade des Motorkennfeldes erzielt werden. Zum anderen muss der Wirkungsgrad in Gänze durch eine sinnvolle Kombination der oben genannten Maßnahmen gesteigert werden. Dabei ist es erforderlich, sowohl die Synergieeffekte zwischen Technologien zu nutzen als auch beim Einsatz einer Technologie die negativen Quereinflüsse auf andere Technologien zu berücksichtigen.

Im Laufe der Untersuchungen wird eine Vielzahl an Motormodellen erstellt. Um die Zuverlässigkeit der Ergebnisse der Simulationen mit den Motormodellen sicher zu stellen, müssen die Untermodelle, die den Verbrennungablauf im Zylinder beschreiben, ebenfalls eine präzise Vorhersagefähigkeit aufweisen. Die Verbrennung wird mit Hilfe des sogenannten Entrainmentmodells berechnet. Dabei wird von einer

kugelförmigen Ausbreitung der Flamme ausgehend von der Zündkerze im zylinderförmigen Brennraum ausgegangen. Die zwei wichtigen Bestandteile des Entrainmentmodells sind das Verbrennungsmodell und das Klopfmodell. Das Verbrennungsmodell berechnet die Ausbreitungsgeschwindigkeit der Flamme und das Klopfmodell bestimmt das Klopfverhalten für die Regelung der Verbrennungsschwerpunktlage. Beide Modelle bestimmen die Brennrate und beeinflussen somit wichtige Größen wie den Druckverlauf im Zylinder, die Leistung des Motors oder den Wirkungsgrad. Deswegen ist es im ersten Schritt notwendig diese Untermodelle zu kalibrieren.

Die Kalibrierung der Verbrennungs- und Klopfmodelle erfolgt durch einen Vergleich mit den Messdaten, die im Laufe des FVV Forschungsprojektes „ICE2025+: Ultimate System Efficiency“ entstanden sind. Für die Kalibrierung des Verbrennungsmodells wird eine Druckverlaufsanalyse durchgeführt. Dabei werden die Brennraten mit Hilfe des am Prüfstand gemessenen Zylinderdrucks berechnet und mit den Brennraten aus dem Modell verglichen. Während dieses Prozesses wird zunächst das Klopfmodell deaktiviert und die Schwerpunktlage aus den Messdaten verwendet. Der Modellparameter, der das Turbulenzniveau im Brennraum bestimmt, wird so ausgewählt und angepasst, dass eine möglichst gute Übereinstimmung zwischen den Messdaten und den Simulationen für beliebige Last, Drehzahl, AGR-Rate, Luft-Kraftstoff-Verhältnis und Menge des eingespritzten Wassers sichergestellt wird. Im zweiten Schritt wird das Klopfmodell aktiviert und kalibriert, so dass die Verbrennungsschwerpunktlage ebenfalls mit guter Genauigkeit vorhergesagt werden kann.

Nachdem die Untermodelle angepasst wurden, wird im folgenden Schritt ein Vollmotormodell des VW EA211 TSI evo erstellt. Dies ist ein 1.5 Liter 4-Zylindermotor mit einem maximalen Drehmoment von 200 Nm und einer Nennleistung von 96 kW. Die nennenswerten Besonderheiten dieses Motors sind ein Variable-Turbinengeometrie-Abgasturbolader, Zylinderabschaltung, ein relativ hohes Hub-Bohrungs-Verhältnis von 1.15, ein relativ hohes Verdichtungsverhältnis von 12.5 und variable Ventilsteuerzeiten mit frühem Einlass-Schließt. Diese und weitere modernen Merkmale machen den VW EA211 TSI evo zu einem geeigneten Repräsentanten des Stands der Technik.

Dieses erste Motormodell hat hauptsächlich zwei Funktionen: Erstens dient es als Referenzmotormodell und ermöglicht diverse Untersuchungen der Technologien und bildet eine Basis für die Erstellung weiterer Motormodelle. Zweitens ermöglicht dieses Modell weiterhin die Kalibrierung sowie die Validierung und wenn nötig die Nachjustierung der Untermodelle.

Zur Validierung wird mit dem Motormodell ein stationäres Verbrauchskennfeld erstellt und mit dem veröffentlichten Verbrauchskennfeld verglichen. Der Vergleich zeigt eine hervorragende Übereinstimmung und weist somit auf eine gute Qualität des Modells hin. Dieses Kennfeld dient zusätzlich als eine Vergleichsbasis mit den Verbrauchs- oder Wirkungsgradkennfelder weiterer Modelle. Ziel ist es, durch Anpassungen an dem Motormodell das Kennfeld zu verbessern, entweder durch eine allgemeine Erhöhung des Wirkungsgrades oder durch eine Verschiebung des wirkungsgradoptimalen Bereiches in Richtung niedrigerer Lasten. Es gibt eine Vielzahl von Maßnahmen, die in Frage kommen, um dieses Ziel zu erreichen, die aber neben ihren Vorteilen meistens auch Nachteile mit sich bringen. Diese Vor- und Nachteile sowie das Zusammenspiel zwischen den Technologien - auch untermauert von den Simulationsergebnissen - werden im Folgenden erläutert:

Downsizing ist eine sehr effektive Methode für Kraftstoffeinsparung durch eine Erhöhung der Wirkungsgrade in unteren Teillastbereich. Mit Downsizing wird der Motor bei gleichem Drehmoment mit höheren Mitteldruck betrieben und dadurch die Ladungswechselverluste sowie der Anteil der Reibungs- und Wandwärmeverluste reduziert. Der Nachteil von Downsizing liegt bei höheren Lasten, da der Motor aufgrund des Klopfens mit späteren Schwerpunktlagen und somit mit niedrigerem Wirkungsgrad betrieben werden muss. Ein aggressives Downsizing ist in der Regel sehr begehrenswert, weil der Motor hauptsächlich im unteren Teillastbereich betrieben wird.

Zylinderabschaltung ist ebenfalls eine effektive Methode, höhere Wirkungsgrade bei niedrigeren Lasten zu erreichen, insbesondere durch die Reduktion der Ladungswechselverluste. Die Vorteile der Zylinderabschaltung nehmen allerdings mit steigenden Lasten schnell ab. Die Reduzierung der Ladungswechselverluste können auch mit anderen Maßnahmen wie variable Ventilsteuerzeiten oder AGR erfolgen. Außerdem kann der Motor auch bei der niedrigeren Teillast zum Klopfen kommen, da die aktiven Zylinder mit höheren individuellen Lasten betrieben werden.

AGR hat vielseitige Wirkungsgradvorteile. Durch die Verdünnung durch das gekühlte Abgas wird die adiabate Flammentemperatur reduzierten. Dies verbessert die Kalorik, indem Verluste durch Dissoziation verringert werden. Außerdem werden durch die reduzierten Temperaturen die Wandwärmeverluste niedriger. Bei höheren Lasten sind weitere Vorteile durch Reduzierung der Klopfneigung und bei niedrigeren Lasten durch Reduzierung der Ladungswechselverluste ersichtlich. Obwohl der Einsatz der AGR in der Regel zu erheblichen Wirkungsgradvorteile führt, kommt es durch die Verlangsamung der Verbrennung zu einer schlechteren thermodynamischen Prozessführung und unvollständigen Verbrennung, was den Wirkungsgradvorteil teilweise aufhebt.

Ein variables Verdichtungsverhältnis ermöglicht die optimale Wahl des Verdichtungsverhältnis je nach Betriebspunkt. Bei unteren Teillasten kann der Motor mit einem höheren Verdichtungsverhältnis gefahren werden, ohne dass es zum Klopfen kommt. Bei höheren Lasten kann das Verdichtungsverhältnis reduziert werden, um die Klopfneigung und damit die Verbrennungsschwerpunktlage zu verbessern. In beiden Fällen wird der Wirkungsgrad verbessert. Außerdem ergänzt das variable Verdichtungsverhältnis ein aggressives Downsizing sehr gut, weil ein sehr niedriges Verdichtungsverhältnis bei Volllast gewählt werden kann, ohne den Wirkungsgrad bei niedrigen Lasten zu beeinträchtigen.

Das Hochturbulenzkonzept wird durch eine Anpassung der Geometrien der Einlasskanäle oder durch eine Tumbleklappe erzielt, mit dem Ziel, eine besonders intensive Ladungsbewegung zu realisieren. Dies führt zu einem erhöhten Turbulenzniveau während der Verbrennung und dadurch zu einer kürzeren Brenndauer. Eine schnellere Verbrennung an sich führt zu einer Verbesserung der Klopffestigkeit und somit zu einer Verbesserung des Wirkungsgrades bei höheren Lasten. Die wichtigsten Vorteile des Hochturbulenzkonzeptes zeigen sich allerdings durch Synergieeffekte mit anderen Maßnahmen: Die erhöhte Klopffestigkeit kann dafür benutzt werden, um das Verdichtungsverhältnis zu erhöhen. Ferner können durch die erhöhte Brennrate die Nachteile der AGR aufgehoben werden. Mit dem

Hochturbulenzkonzept bleibt die Brenndauer auch bei hohen AGR-Raten moderat und das Verbesserungspotential durch die AGR wird besser ausgeschöpft. Der Nachteil des Hochturbulenzkonzeptes ist die Verschlechterung des Ladungswechsels, was sich in erhöhten Ladungswechselverlusten zeigt. Allerdings haben sich diese Nachteile während der Untersuchungen als wenig signifikant erwiesen. Mit seinen zahlreichen Synergieeffekten und kaum Nachteilen ist das Hochturbulenzkonzept für ein hocheffizientes Motorkonzept sehr empfehlenswert.

Mit dem frühen Schließen der Einlassventile (auch Miller genannt) kann eine Verbesserung bei der thermodynamischen Prozessführung erreicht werden. Es wird durch die Kombination der variablen Ventilsteuerzeiten und verkürzten Ventilöffnungsdauer realisiert. Der Nachteil einer Miller-Strategie mit verkürzten Öffnungsdauer ist die Absenkung des Turbulenzniveaus. Durch eine Ventilmaskierung kann dieser Nachteil größtenteils behoben werden. Bei der Anwendung der Miller-Strategie ist darauf zu achten, dass die Einlassventile nicht beliebig früh geschlossen werden dürfen, weil die benötigte Zylinderfüllung für die Lastanforderung sichergestellt werden muss. Die Miller-Strategie befindet sich gewissermaßen in Konkurrenz mit der AGR. Beide Technologien erzielen ähnliche Vorteile und bei Erhöhung der AGR-Rate muss aufgrund der Problematik der Zylinderfüllung eine mildere Miller-Strategie verwendet werden. Daher sind die Kombinationen entweder aggressive Miller-Strategie ohne AGR oder milde/keine Miller-Strategie mit hoher AGR-Rate oder eine moderate Miller-Strategie mit moderater AGR-Rate mögliche Lösungen. Die optimale Kombination der Ventilsteuerzeiten und AGR-Rate hängt vom Betriebspunkt und Turbulenzniveau ab. Je höher das Turbulenzniveau ist, desto stärker wird der Wirkungsgradvorteil durch AGR und desto höhere AGR-Raten kombiniert mit milderen Miller-Strategie werden erstrebenswert.

Eine weitere vielversprechende Maßnahme für die Verbesserung des Wirkungsgrades ist die Langhubigkeit, d.h. die Erhöhung des Hub-Bohrungs-Verhältnisses. Dadurch wird ein noch höheres Turbulenzniveau erreicht und ähnliche Vorteile wie bei dem Hochturbulenzkonzept kommen vor. Ferner werden durch die Verbesserung der Motorgeometrie die Wandwärmeverluste reduziert. Der Nachteil einer hohen Hub-Bohrungsverhältnis ist allerdings der erschwerte Ladungswechsel durch die Verkleinerung des Zylinderkopfes und der Ventile bei gleichbleibendem Zylindervolumen. Obwohl die Langhubigkeit Wirkungsgradvorteile an sich bringt, erschwert sie gleichzeitig den Einsatz anderen wichtigen Maßnahmen wie Miller-Strategie oder Downsizing und wirkt somit eher kontraproduktiv auf den Wirkungsgrad. Eine weitere deutliche Erhöhung des Hub-Bohrungs-Verhältnisses ausgehend von dem Stand-der-Technik-Motoren ist deswegen nicht empfehlenswert.

Wassereinspritzung ist eine weitere, sehr effektive Maßnahme um die Klopfneigung zu reduzieren und den Wirkungsgrad zu erhöhen. Allerdings gilt der Wasservorrat in einem Fahrzeug als begrenzt und daher ist mit dem Wasser in der Regel sparsam umzugehen. Deswegen ist Wassereinspritzung ein Werkzeug, das nur bei der Volllast einzusetzen ist, um bei einem Motor mit aggressivem Downsizing gleichzeitig ein hohes Verdichtungsverhältnis zu ermöglichen. Die Wassereinspritzung ist hiermit eine kostengünstigere Alternative zu dem variablen Verdichtungsverhältnis.

Unter den bisher genannten Maßnahmen ist die Abmagerung mit Abstand die effektivste Einzelmaßnahme, um den Wirkungsgrad zu verbessern. Der Wirkmechanismus ist ähnlich wie bei der AGR. Im Vergleich zum AGR ist die Abmagerung bei der Bekämpfung der Ladungswechselverluste und beim Reduzieren der Wandwärmeverluste effektiver, aber bei der Klopfminderung weniger effektiv. Bei der Anwendung des Magerkonzeptes muss auf die Stickoxidemissionen geachtet werden. Für die Absenkung der Rohemissionen ist ein hohes Maß an Abmagerung nötig. Damit dies nicht zu Flammeninstabilitäten und -auslöschung führt, ist die Kombination eines Magerkonzeptes mit dem Hochturbulenzkonzept ein Muss. Eine weitere Herausforderung ist die Aufladung wegen des deutlich erhöhten Ladedruckbedarfs und gleichzeitig deutlich verringerter Abgastemperaturen. Wegen der erhöhten Flammeninstabilität und der erschwerten Aufladung, müssen auf AGR oder Miller-Strategie beim Magerkonzept verzichtet werden. Da diese beiden effektiven Maßnahmen für Klopfminderung fehlen, ist ein Magermotor in der Regel klopffreudiger als ein wirkungsgradoptimierter stöchiometrischen Motor. Deswegen ist der Wirkungsgradvorteil, der durch Magerkonzept erzielt werden kann, nicht so hoch, wie durch das Wirkungsgraderhöhungspotential der Abmagerung als Einzelmaßnahme ursprünglich angedeutet wird.

Die Verwendung von alternativen Kraftstoffen mit überlegenen Eigenschaften verglichen mit Benzin führt ebenfalls zu einer Wirkungsgradsteigerung. Ein gutes Beispiel hierfür ist Methanol. Methanol hat eine deutlich höhere Klopffestigkeit wie Benzin und ermöglicht somit einen klopffreien Betrieb auch mit signifikant erhöhtem Verdichtungsverhältnis. Außerdem hat Methanol eine sehr hohe Verdampfungsenthalpie. Die Prozesstemperaturen sind daher niedriger, wodurch sowohl eine bessere Kalorik, als auch eine Reduzierung der Wandwärmeverluste erzielt werden können. Als Resultat kann ein Methanolmotor erheblich höhere Wirkungsgrade als ein Benzinmotor erreichen, sowohl bei niedrigen als auch bei höheren Lasten. Ähnliche Wirkungsgradvorteile können durch eine Beimischung von Methanol in Benzin erzielt werden.

Das Referenzmotormodell ist von den obengenannten Maßnahmen mit Zylinderabschaltung und Miller-Strategie ausgerüstet. Somit erreicht er einen Maximalwirkungsgrad von 38,4 %. Die höchsten Wirkungsgrade sind bei ca. 70 % Last zu finden. Dies stellt die Ausgangssituation dar, die zu verbessern ist.

Die erste Modifikation zum Referenzmotormodell ist ein aggressives Downsizing, das zu einer Verschiebung des Hochwirkungsgradfensters in Richtung niedrigeren Lasten führt. Dies muss jedoch von einem variablen Verdichtungsverhältnis begleitet werden. Außerdem bleibt beim Downsizing die Anzahl der Zylinder unverändert, damit eine effiziente Zylinderabschaltungsstrategie noch immer möglich ist. Zusätzliche Wirkungsgradvorteile werden durch AGR und Hochturbulenzkonzept erzielt. Die optimalen AGR-Raten, Ventilsteuerzeiten und Verdichtungsverhältnisse werden für das gesamte Kennfeld iterativ bestimmt. Dieser neu entworfene, effizientere Motor „High Efficiency Engine“ demonstriert das Wirkungsgradsteigerungspotential bei einem stöchiometrischen Benzin-Ottomotor. Er hat einen Maximalwirkungsgrad von 41,4 %, der bei ca. 40 % Last zu finden ist. Die Wirkungsgradverbesserung im Vergleich zu dem Referenzmotor bei einem WLTC-Zyklus wird zwischen 15 % und 19 % geschätzt.

Bei einem weiteren Modell wird das variable Verdichtungsverhältnis bei dem Motor High Efficiency Engine mit Wassereinspritzung ersetzt. Mit

Wassereinspritzung kann die gleiche Leistungsdichte mit einem hohen Verdichtungsverhältnis realisiert werden. Mit dieser Konstellation kann ein Spitzenwirkungsgrad mit gleichem Niveau zu dem High Efficiency Engine erreicht werden (41,2 %), allerdings wird der Bereich höchster Wirkungsgrade schmaler. Dadurch ist der Wirkungsgrad beim WLTC-Zyklus um ca. 2 % geringer als bei dem High Efficiency Engine.

Wenn höhere Wirkungsgrade erwünscht sind, muss das Magerkonzept eingesetzt werden. Dafür wird der „Lean High Efficiency Engine“ bei niedrigen bis mittleren Lasten mit Abmagerung betrieben. Dabei wird auf AGR und teilweise auf die Miller-Strategie verzichtet. Dieser Motor erreicht einen Maximalwirkungsgrad von 43,0 % und ermöglicht eine weitere Wirkungsgradverbesserung um ca. 5 % im Vergleich zum stöchiometrischen High Efficiency Engine.

Der Nutzen der alternativen Kraftstoffe wird anhand eines Methanolmotors demonstriert, der „Methanol Engine“ genannt wird. Er ist ähnlich wie der Motor High Efficiency Engine aufgebaut und mit den gleichen Technologien ausgerüstet. Der Hauptunterschied zum Motor High Efficiency Engine ist die erheblich erhöhte Verdichtungsverhältnisse. Wegen dies, der optimalen Schwerpunktlage sowie der hohen Verdampfungsenthalpie erweist sich der Methanol Engine als deutlich effizienter als der High Efficiency Engine. Er erreicht einen Maximalwirkungsgrad von 45,3 %. Die Wirkungsgradverbesserung im Vergleich zu dem Referenzmotor ist bei einem WLTC-Zyklus zwischen 24 % und 29 % geschätzt.

Die höchsten Wirkungsgrade werden durch Kombination des Methanols mit der Abmagerung erreicht. Bei dem so entstandenen „Lean Methanol Engine“ Konzept wird ein maximaler Wirkungsgrad von 46,8 % erreicht. Die Wirkungsgradverbesserung im Vergleich zu dem Referenzmotor liegt damit zwischen 29 % und 34 % bei einem WLTC-Zyklus. Diese Ergebnisse demonstrieren, dass der Verbrennungsmotor immer noch ein signifikantes Verbesserungspotential bezüglich der Wirkungsgrade hat.

1 Introduction

Since the beginning of the industrial revolution, the humanity has been handling the environment recklessly. As a consequence, the climate change and global warming start becoming serious issues, which -if further ignored- can pose an existential threat to the entire ecosystem as well as to the humanity itself. Therefore, in the current age, it is the utmost responsibility of engineers and scientists to find environmentally friendly and sustainable solutions to today's problems in many areas as possible. One such critical area is the mobility, which for example in EU is responsible for the one-third of the total primary energy consumption [1], and one major task here is to increase the efficiency of the drivetrains, which will reduce CO_2 emissions while decreasing the consumption the non-renewable resources. Despite the rising popularity of pure electrical drivetrains as a promising way of addressing these problems, they are still far from making internal combustion engines obsolete or even being widespread enough to make a significant impact. In fact, the global market for the internal combustion engines is expected to further grow steadily in the coming years [2]. Thus, it is imperative to put further effort in developing highly efficient, eco-friendly internal combustion engines.

For this reason, this work is dedicated to investigate the methods to increase the efficiency of spark-ignition internal combustion engines. The challenge here is that the internal combustion engine already exists for more than 150 years and can be considered as a close-to-perfected technology with little room for further improvement. Yet still, there are several promising ideas, concepts, measures and technologies that are suggested to make the efficiency of the internal combustion engines better.

Naturally, there is already intensive research ongoing on those technologies and yet many of this research concentrates on investigating individual technologies separately. Although this type of research is useful for spotting potentially beneficial technologies, it is often neglected how the technologies might interact with each other. This interaction can be a positive as well as a negative one: Synergy effects between technologies might occur so that the total efficiency improvement of a technology combination might be greater than the sum of the efficiency improvements of individual technologies. The opposite is also possible, i.e. technologies might cancel each other’s benefits out to some extent or even the presence of a technology might do more harm than good in a certain engine setup. Thus, this kind of research often fails to demonstrate their true benefits of the investigated measure. Apart from this, there is also research for combining as many suitable technologies as possible in an attempt to reach a certain impressive efficiency at a certain operating point, a notable example being how an efficiency beyond 45% with a gasoline engine can be achieved [3]. In this case, however, it remains unanswered, whether the chosen engine setup is also suitable for the remaining operating range of the engine. Since so much effort is put to optimize the efficiency at a single operating point, it can be implied that at least some of the features of this engine is sub-optimal for remaining operating window and it is unclear, whether how much the overall efficiency of an engine can be increased. Therefore, this kind of study is also not helpful for demonstrating the efficiency improvement potential of internal combustion engines.

This present work neither focuses on individual technologies nor aims for maximal peak efficiencies. The focus lies rather on demonstrating the interactions or synergy effects between technologies, revealing not only their advantages but also their drawbacks and challenging aspects. By doing so, the most suitable combination of technologies can be figured out that leads to highest efficiencies for a widest engine map region possible. The objective of this work is to propose engine configurations for future concepts for hybrid architectures with greatest overall drivetrain efficiencies.

Given the number of many possibilities for improving the efficiency of internal combustion engines, 0D/1D engine simulation methods are the only viable option for this investigation. 0D/1D simulation methods provide a great flexibility and many degrees of freedom while adjusting engine parameters as well as while adding and removing engine technologies, enabling much more thorough investigation in comparison to experimental setups or 3D-CFD investigations. Furthermore, due to the high quality and predictive capabilities of the underlying sub-models, these results are by no means just rough estimates, but they are indeed expected to represent the reality with a relatively high precision comparable to other highly detailed and yet much more time-consuming research methods. Over the course of this work, several full engine models equipped with various technologies are designed along with the model of a state-of-the-art reference engine. The engine models are used for generating stationary efficiency maps. The engine models and their respective efficiency maps are used for demonstrating the effects of various technologies as well as revealing the potential for further efficiency improvement for spark-ignition internal combustion engines in the future.

This objective of achieving highest efficiencies is pursued in several steps, starting from the state-of-the-art stoichiometric gasoline engine. There are several ways of achieving this objective, examples being increasing the knock resistance, decreasing the pumping losses due to throttling, reducing losses due to wall heat transfer and improving caloric by avoiding too high temperatures. Furthermore, shifting the high efficiency regions of the engine maps towards the regions where the engine is mostly operated is also of utmost importance. For achieving these sub-goals, several measures can be considered: Downsizing, cylinder deactivation, exhaust gas recirculation (EGR), Miller strategy with variable valve timings, variable compression ratio, high turbulence concept, high stroke-to-bore ratio and water injection. At the end of this step, it is demonstrated how much the efficiency of state-of-the-art engines can further be improved and what technologies can be recommended for this purpose.

Even with these measures, however, the efficiency potential of the spark-ignition internal combustion engine is still far from being fully exploited, since significant improvements are possible with lean combustion. In fact, among all the technologies mentioned above, the lean concept is likely to be by far the most promising single measure efficiency-wise. Therefore, in the second step of this work, engine models operated under lean conditions should also be designed and a comparison with the stoichiometric engine models should be conducted.

Apart from these measures, alternative fuels can further improve the efficiency significantly, while potentially being an environmentally sound solution for the mobility problem, assuming renewable sources are used for the synthesis of these fuels. For example, methanol presents itself as a superior alternative to gasoline, most notably due to its excellent knock resistance. Thus, methanol is considered in this work as a fuel and engine models optimized for methanol fuel are designed in order demonstrate the potential of alternative fuels. Furthermore, a blend fuel that is composed of gasoline, methanol and ethanol should also be tested.

This work is structured as follows: Chapter 2 opens up with a discussion about the energy losses at internal combustion engines. Then, the technologies that counteract these losses and their potential benefits are presented along with a discussion about potential drawbacks, challenges as well as potential interactions with other technologies. In Chapter 3, the modeling methods along with the most relevant sub-models are described. Then, the model calibration is shown. Then in the main part, Chapter 4, simulative investigations follow. Here, technologies implemented, assessed, several engine maps are generated and compared with each other. In the first section, the stoichiometric gasoline engines are considered. Then follows an assessment of methanol and the blend fuels. Finally, lean concept is introduced to the engine models, aiming for the maximal efficiency. The chapter closes with a discussion about overall drivetrain efficiencies for these engines in combination with various hybrid architectures. In the final chapter, Chapter 5, a brief summary of the results of this work is found.

2 Technology Overview and State of the Art

2.1 Challenges to overcome for achieving higher efficiencies

The way of achieving higher efficiencies is by reducing the losses of the engine. The losses during the operation of an engine can be listed as follows: Losses through non-ideal thermodynamic cycle, wall heat losses, losses through incomplete combustion, pumping losses and friction losses [4]. For a better understanding of the engine process, thermodynamics of the engine cycle should be considered thoroughly.

The operating cycle of an internal combustion engine can be roughly modeled by an idealized closed thermodynamic cycle combined with an ideal gas model (i.e. the specific heat capacity of the working fluid is constant) [4]. The thermodynamic cycle consists of the following separate processes, as shown in Figure 2.1:

- Adiabatic and reversible (therefore isentropic) compression (1→2)
- Heat addition (isochoric, isobaric or dual process) (2→3)
    - A: Isochoric heat addition
    - B: Isobaric heat addition
    - C: Dual process, i.e. isochoric heat addition followed by an isobaric heat addition, also known as the Seilinger cycle
- Adiabatic and reversible (therefore isentropic) expansion (3→4)
- Isochoric heat rejection (4→1)

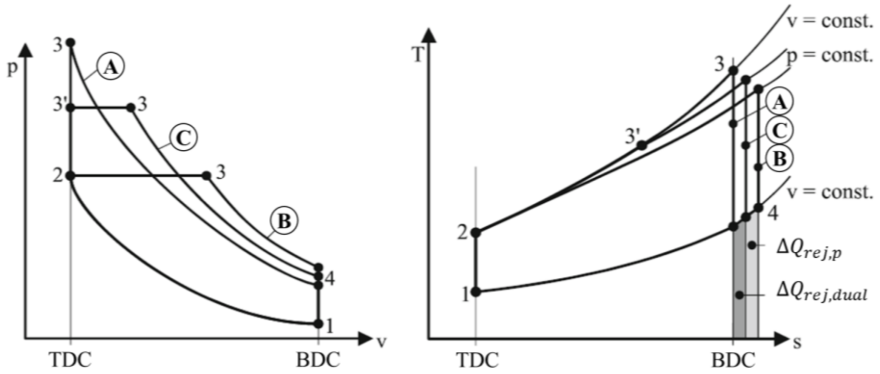

Figure 2.1. The pressure-volume (p-v) and the temperature-entropy (T-s) diagrams of the thermodynamic cycles that represent the working cycle of internal combustion engines [5]

The energy balance of the thermodynamic cycle is given by a sum of compression work W_{comp}, heat addition Q_{add}, expansion work W_{exp} and the heat rejection W_{rej} as in the following equation:

$$W_{comp} + Q_{add} + W_{exp} + Q_{rej} = 0 \tag{2.1}$$

And the efficiency of the thermodynamic cycle η is given by:

$$\eta = \frac{W_{comp} + W_{exp}}{Q_{add}} = \frac{-Q_{add} - Q_{rej}}{Q_{add}} = 1 - \frac{|Q_{rej}|}{Q_{add}} \tag{2.2}$$

In other words, if the quantity of the added heat is constant, the lower the quantity of the rejected heat is, the higher the efficiency becomes. Because of this, the isobaric and dual processes are efficiency-wise inferior to the isochoric process. This can be illustrated with the help of the grey areas in Figure 2.1: In the case of a dual process or isobaric process instead of an isochoric process, the heat rejection is increased by $\Delta Q_{rej,dual}$ or by ($\Delta Q_{rej,dual}$+ $\Delta Q_{rej,p}$) respectively.

Traditionally, the spark-ignition (SI) internal combustion engine cycle is approximated by the isochoric process. In this case, the efficiency η of the idealized engine cycle is governed by the following equation:

$$\eta = 1 - \frac{1}{\varepsilon^{\kappa-1}} \tag{2.3}$$

whereas ε is the compression ratio and κ is the isentropic exponent of the working fluid. For example, the efficiency is calculated as 61.7%, if the compression ratio is assumed as 11 and isentropic exponent as 1.4. However, a SI internal combustion engine of a passenger vehicle typically has a peak efficiency lower than 40% and this efficiency decreases dramatically towards lower loads. Because, on contrary to the simplified thermodynamic cycle, the combustion does not occur spontaneously at the top dead center. The combustion is also incomplete which further affects the efficiency. Also, no phase of the thermodynamic process can be considered as adiabatic and significant losses occur in shape of wall heat transfer, since cylinder walls and the piston need to be cooled. Friction losses are caused by moving parts of the engine which cannot be neglected. Lastly, pumping losses occur due to air resistance as well as the difference between the exhaust backpressure and intake pressure - an aspect which is not considered at the simplified thermodynamic cycle at all.

Friction losses are caused by friction at main and connecting-rod bearings, between piston and cylinder wall, at valve train. Energy for the operation of auxiliary equipment like oil pump, cooling water pump, fuel pump also counts as friction losses [6]. Possibilities for decreasing friction losses include changing the number and dimensions of the cylinders, changing the sizes and weights of valves, reducing cornering force or average piston speed by changing the stroke-to-bore ratio of the engine. Friction losses have an especially dominant effect on the efficiency at lower loads.

Pumping losses should be considered separately at lower and higher loads for turbocharged engines. At lower loads, the pumping losses can be reduced, if throttling losses can be decreased and an intake pressure can be kept close to the atmospheric pressure. Here, measures such as EGR, lean combustion, Miller cycle or cylinder deactivation are thinkable. At higher loads, the exhaust backpressure is increased because of the turbine that needs to provide the compressor with the necessary energy. Therefore, increasing the turbocharger efficiency can be considered to keep pumping losses under control, since the necessary boosting pressure can be reached with a lower pressure ratio at the turbine, thus reducing the exhaust backpressure.

Wall heat losses are influenced by the temperatures, the heat transfer coefficient and the area through which the heat transfer occurs. Therefore, coating for heat insulation and decreasing the number of cylinders while keeping the displacement volume constant as well as decreasing the combustion temperatures by measures like EGR, lean combustion or water injection can come into consideration for reducing wall heat losses.

The most interesting part of the energy balance is the real thermodynamic process during the engine cycle. A spontaneous combustion cannot be achieved since the combustion speed cannot be infinite, but the efficiency still profits from shorter burn durations, since the combustion gets more similar to an isochoric than the isobaric process. A further drawback of longer burn durations that they might result in a low combustion efficiency. The combustion efficiency is the measure how much of the heat content of the fuel is converted during the cycle. A value lower than unity indicates an incomplete combustion. The slower the combustion proceeds, the lower percentage of the fuel energy tends to be converted until the end of the expansion phase.

An optimal center of combustion (the position of where the 50% of the fuel mass burned (mfb50%)) also plays an integral part on the resulting efficiency, however it cannot be maintained all the times, mainly because of the phenomenon known as knocking. Knocking is among the central problems of a SI internal combustion engine. It is described as an undesired, potentially damaging auto-ignition of the unburnt air-fuel mixture in the cylinder that occurs during the combustion phase. Knocking should be avoided or at least the number of knocking cycles should be limited in order to protect the engine. Knocking is a statistical phenomenon and its tendency increases with increasing temperatures and pressures in the cylinder.

In order to prevent knocking, the timing of the spark-ignition of the engine is retarded. As a result, the combustion occurs later in the expansion phase, and the high pressures and temperatures are avoided. The downside is that the efficiency of the thermodynamic process is compromised due to a late, suboptimal mfb50%, because once again the combustion takes a more isobaric character. Furthermore, although the Equation (2.3) suggests that efficiency can be increased with increasing compression ratios, a too high compression ratio will result in higher temperatures and pressures, thus increasing knock tendency. Therefore, a too high compression ratio can be counterproductive regarding the efficiencies as well. As can be seen in following chapters, a central aspect of this work is to control the knock and design a knock resistant engine by combining many technologies and measures that enhance the knock resistance.

The constant specific heat capacity for the idealized thermodynamic cycle process is also a rough assumption: Firstly, the specific heat capacity has a temperature dependency and increases with increasing temperatures. This increase can be approximated well with the so-called NASA-polynomials in the form of:

$$c_p(T) = a_1 + a_2 \cdot T + a_3 \cdot T^2 + a_4 \cdot T^3 + a_5 \cdot T^4 \tag{2.4}$$

where c_p is the isobaric specific heat capacity, T is the temperature and a_1-a_5 are coefficients specific for the considered material. The coefficients a_1-a_5 can be found in [7]. Since nitrogen has the greatest portion in the working fluid, its isobaric specific heat capacity is calculated by using the NASA polynomials and plotted in Figure 2.2 as an example:

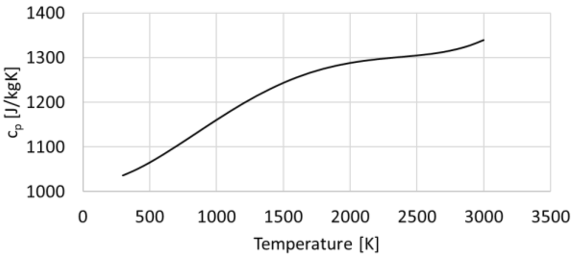

Figure 2.2. Isobaric specific heat capacity of nitrogen, calculated with NASA polynomials

As can be seen, the isobaric specific heat capacity of nitrogen increases from 1040 J/(kgK) at room temperature to 1310 J/(kgK) at 2500 K. Furthermore, at higher temperatures, the apparent specific heat capacity of burnt gas increases further as a result of dissociation. This effect is especially dominant at temperatures higher than 2000 K. For example, according to the calculations of Grill [8], the apparent isochoric heat capacity of burnt gas is almost doubled, if the temperature is increased from 2000 K to 2500 K, as illustrated in Figure 2.3.

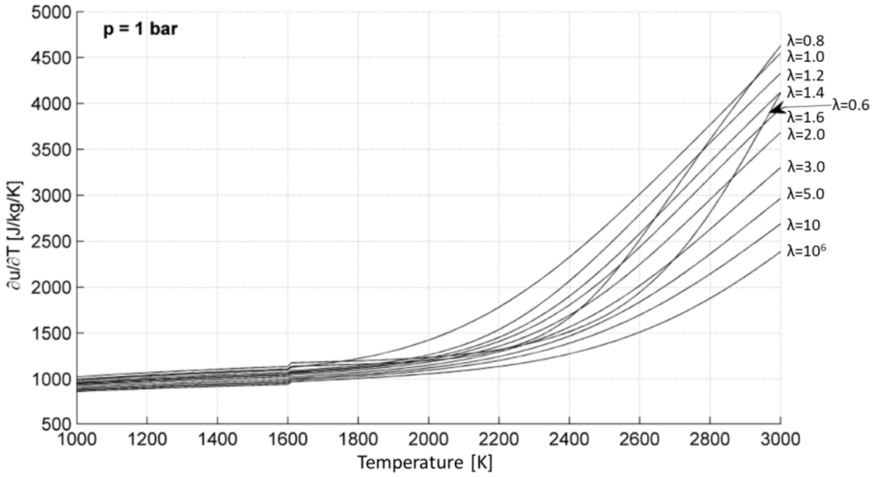

Figure 2.3. Increase of the apparent isochoric heat capacity at high temperatures due to dissociation [8]

The increase of the specific heat capacity is detrimental for the efficiency. This is because the same amount of heat addition results in a lower temperature (and therefore lower pressure) increase, and therefore less work is performed during the expansion phase.

A further factor that results in efficiency losses it the cycle-to-cycle variations. No working cycle is identical and there is some fluctuation between cycles regarding quantities such as burn rate, burn duration or mfb50%. However, if a high variation for working cycles is present, this would mean that some cycles would have especially high burn durations, late mfb50% or a low combustion efficiency. These single cycles might have significantly worse efficiencies than the average cycle and will reduce the average efficiency of the engine.

A further aspect regarding the engine efficiency is how the engine is operated. The efficiency of the engine differs from operating point to operating point because the aforementioned losses affect the efficiency to different extents at different loads and different engine speeds. For a good overall efficiency or fuel economy it is important that there is a good overlapping between the engine map regions with high efficiency and engine map regions where the engine is actually operated. How the internal combustion engine is designed influences directly the characteristics of the engine map and in which region the engine map has its “sweet spot”. Apart from that, a start-stop system and hybrid vehicle drivetrain also help achieving a better fuel economy by avoiding or reducing idling. Similarly, operation of the internal combustion engine at operating points with low efficiencies can also be avoided with load point shifting to some extent.

A possibility for measuring the overall quality of fuel economy is driving cycles. One such driving cycle is the New European Driving Cycle (NEDC). During the NEDC, the fuel consumption and emissions are measured on a roller test bench during a predefined driving cycle procedure, which consists of four identical urban driving cycles followed by an extra-urban driving cycle. However, NEDC has serious shortcomings: The velocities and accelerations are unrealistically low, speeds higher than 120 km/h are not tested. The comfort functions such as air conditioning, seat heating, radio are not taken into account. A high power demand due to a higher speeds, a dynamic driving style or driving uphill are not considered. As a result, a large portion of the engine map is not covered at all by NEDC. Today, NEDC, although still used occasionally, can be considered obsolete.[9] In 2015 the Worldwide harmonized Light vehicles Test Procedure (WLTP) with the intent of replacing NEDC. The associated driving cycle WLTC still measures the emissions and fuel consumption at a roller test bench, but the driving cycle much closely represents a realistic driving behavior and considers higher velocities and accelerations. Therefore, WLTC is more reliable for evaluating the fuel consumption and efficiency of an engine.[9] Furthermore, a regulation of the European Parliament and of the Council sets a limit of 95 g CO_2/km during

WLTC for the new car fleet average since 2020, with stricter limitations to be expected 2025 onwards [10].

A further driving cycle the Real Driving Emissions (RDE) cycle, which is mainly introduced for measurement nitrogen oxides (NO_X) and particulate emissions under realistic conditions. On contrary to NEDC and WLTC, RDE cycle is executed under real-world conditions. During the driving cycle, certain conditions like the portion of urban, extra-urban and highway routes, altitude changes, speed and acceleration should be met so that the driving cycle is both realistic and representative. [9]

An exemplary distribution of engine operating points for NEDC, WLTC and two different RDE cycles is shown in Figure 2.4. WLTP covers a greater operating range than NEDC, but is also mostly limited to medium loads and low engine speeds. The distribution of operating points for an RDE cycle heavily depends on the chosen route. While a more moderate RDE cycle can have a similar range to a WLTC cycle, a more aggressive or challenging cycle can cover up to the full load.

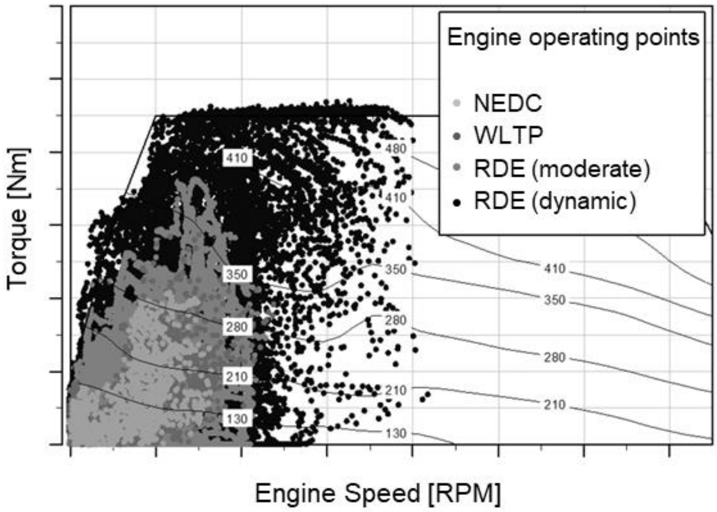

Figure 2.4. Distribution of engine operating points for various driving cycles [9]

2.2 Overview for technologies and measures for efficiency increase

In the previous chapter, the sources of energy losses at internal combustion engines are discussed. In this chapter, the measures that can potentially counteract these losses and increase the efficiency of SI internal combustion engines are covered in greater detail.

2.2.1 Downsizing

Downsizing comes into consideration as an effective method for reducing the overall fuel consumption of a vehicle. With downsizing, a similar power capacity is aimed with a smaller displacement volume, mainly by boosting the intake air with a turbocharger. This means that at a given operating point, the engine is operated with a higher specific load in terms of brake mean effective pressure (BMEP). At lower loads, this leads to a shift of the operating point towards engine map regions with higher efficiency: With increased loads, both the relative friction and wall heat losses decrease, since the absolute value of these losses increase underproportionally with increasing loads. Furthermore, as the intake pressure gets closer to the atmospheric pressure, the throttling losses are decreased. [11]

A simulative study is conducted by Fraser et al. [12] for demonstrating the efficiency improvement potential due to downsizing. Here, a SI-engine with a 2.0 liter displacement volume is compared with a heavily charged 1.2 liter displacement volume generated with the help of the MAHLE Downsize Demonstrator [13]. Both engine models have with very similar peak torque curves. It is found that a fuel consumption reduction of almost 15% is possible with the 1.2 liter engine for a D class vehicle during a NEDC. The study also advocates a two-stage boosting concept for an aggressive downsizing. Possible configurations include utilizing two turbochargers, a mechanically coupled supercharger as well as an electric compressor.

The most noteworthy drawback of downsizing is the increased pressures and temperatures in cylinder which increases the knock tendency and compromising the efficiency at higher loads. This is pointed out by Schmid et al. at their simulative study about various degrees of downsizings with different turbocharging concepts [14]. For instance, as a result of the downsizing from a 2.2 liter naturally aspirated engine to a 1.6 liter turbocharged engine, the brake specific fuel consumption (BSFC) is increased for loads higher than 100 Nm (which is approximately 50% load of the naturally aspirated engine) reaching 8% BSFC increase in the region of the low-end torque. Nevertheless, their study can also demonstrate a remarkable BSFC reduction at lower loads with an aggressive downsizing.

Furthermore, due to the increasing knock tendency at full load, only a certain degree of downsizing is possible. This can be explained schematically with the help of Figure 2.5.

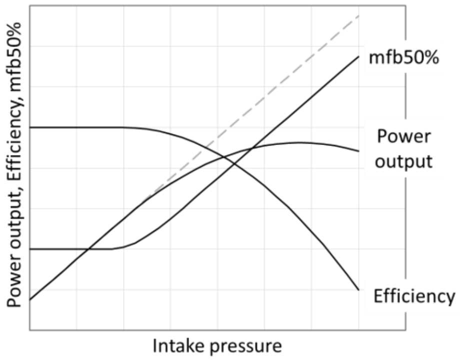

Figure 2.5. Schematical representation of mfb50%, efficiency and power output of the engine with increasing intake pressure

With increasing intake pressure at a constant engine speed, the power output of the engine should increase more or less proportionally, assuming that the air-fuel ratio and the efficiency stay similar. Once knock starts to occur with increased intake pressure, the mfb50% has to be retarded. As a result, the efficiency decreases. Due to this efficiency decrease, the power increase can no longer be proportional and the curve for the power output starts flatten out. As the efficiency decrease becomes too strong, the power will eventually start dropping despite increasing boost pressures. Thus, a downsizing beyond a certain degree while maintaining a certain rated power is not possible, at least not without further measures or adjustments to the engine that reduce the knock tendency.

2.2.2 Cylinder deactivation

Cylinder deactivation is a further suitable concept for increasing the efficiency at lower engine loads. In this case, one or more cylinders are deactivated, i.e. for the deactivated cylinders the valves are kept closed and no fuel is injected. As a result, the remaining active cylinders are operated at higher individual loads in order to reach the desired engine torque. Cylinder deactivation is an efficient method for decreasing throttling losses. Also, the remaining cylinders that are operated at higher loads would have higher efficiencies during the combustion cycle. As a result, the engine efficiency can be considerably improved, especially at very low loads. For example, investigations by Ternel et al. [15] show that the pumping losses at 2000 RPM and 1 bar BMEP are decreased from more than 0.8 bar pumping mean effective pressure (PMEP) to 0.4 bar PMEP by cutting of half of the cylinders of a 4-cylinder engine. This translates into a more than 20% reduction of fuel consumption at this operating point. Furthermore, the same investigation suggest that the fuel consumption could be reduced by 12.5% during a NEDC with the same cylinder deactivation strategy. Due to the high benefits, cylinder deactivation is applied to numerous engines with six [16], four [17] and even three cylinders [18].

With increasing loads, the cylinder deactivation loses its advantages. For example, the fuel consumption reduction of the cylinder deactivation from the aforementioned study is reduced to around 5% at 2000 RPM 5 bar BMEP [15]. Furthermore, the necessary dethrottling effect can be achieved with other measures such as EGR and variable valve timings. Also, knock might start occurring in the active cylinders, as they are operated at high individual loads which will have a detrimental effect on the efficiency.

2.2.3 Exhaust gas recirculation (EGR)

An external, cooled exhaust gas recirculation (EGR) reduces the adiabatic flame temperature of the gas mixture in the combustion chamber due to dilution. A lower combustion temperature has various benefits: The knock tendency is reduced and the wall heat losses are decreased as well. Avoiding high temperatures in general also improves the thermodynamic process, because of steep increase of the specific heat capacity due to increasing dissociation beyond certain temperatures. In addition, EGR can be used at low loads to reduce throttling and thus pumping losses.

Tabata et al. [19] conducts an experimental study at a low load, where they made an EGR variation at a low load point without knocking. They found out that a fuel consumption reduction by around 6% is possible with around 28% EGR, where main benefits come through reduced pumping and heat losses. In the case of a further EGR increase, an intensive cycle-to-cycle variation is observed and the efficiency starts decreasing.

EGR at or close to the rated power comes also into consideration as a replacement for fuel enrichment [20]. The purpose of the fuel enrichment is to protect the turbocharger turbine from too high exhaust temperatures: The injection of excess fuel leads to lower process and exhaust temperatures due to the evaporation of the fuel. Same temperature reduction can be achieved with cooled EGR and fuel enrichment can be avoided, resulting in remarkable efficiency improvement at or close to the rated power. Ganser et al. [21] show that a fuel consumption decrease of around 15% around full load is possible, as a result of avoided enrichment as well as an improved knock behavior.

Two architectures may come into consideration for realizing cooled EGR at turbocharged SI engines: High pressure (HP) EGR or low pressure (LP) EGR. The combination of both is also possible. At HP-EGR, the exhaust gas is taken before the turbine and introduced after the compressor. At LP-EGR the exhaust gas is taken downstream of the turbine and introduced before the compressor. Both HP-EGR and LP-EGR have their drawbacks: In order to HP-EGR to function properly, the pressure before the turbine must be higher than after the compressor. This is often not the case at the low-end torque region. In other words, HP-EGR is not eligible for the whole engine map whereas LP-EGR is available at all times. Furthermore, the HP-EGR has higher exhaust temperatures and thus a higher cooling power is necessary. If the exhaust gas cannot be cooled sufficiently, the resulting intake temperature would be higher, which would have a detrimental effect on knock behavior.

Furthermore, the HP-EGR puts a greater strain on the compressor, which is illustrated schematically with the help of a compressor map in Figure 2.6. With LP-EGR, both the mass flow and the pressure ratio at the compressor are increased. On the other hand, with HP-EGR only the pressure ratio is increased. As a result, the compressor is operated closer to the surge limit with HP-EGR and would prove lower efficiencies.

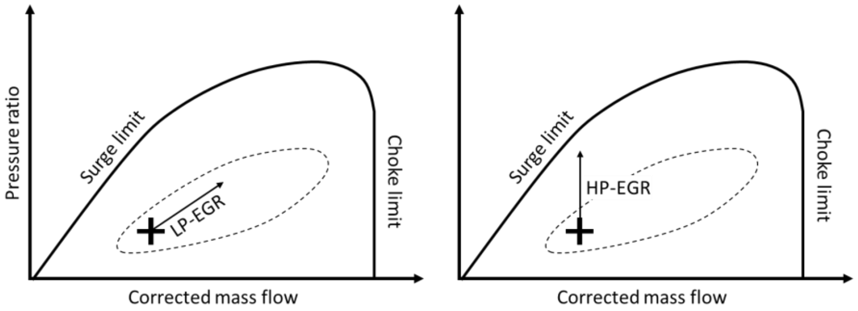

Figure 2.6. Effect of LP-EGR and HP-EGR on compressor operation. The dashed line represents the high efficiency region of the compressor map

Despite the aforementioned drawbacks, the HP-EGR architecture is significantly more widespread than LP-EGR architecture. The poor transient behavior of the LP-EGR due to longer response times makes its application significantly more challenging.

2.2.4 Miller cycle

The Miller cycle is characterized by the early intake valve closure (EIVC), i.e. intake valves are closed before the piston reaches the bottom dead center (BDC) during the intake stroke. It can be realized by a shorter valve opening duration, by variable valve timings or a combination of both. Both methods are shown in Figure 2.7.

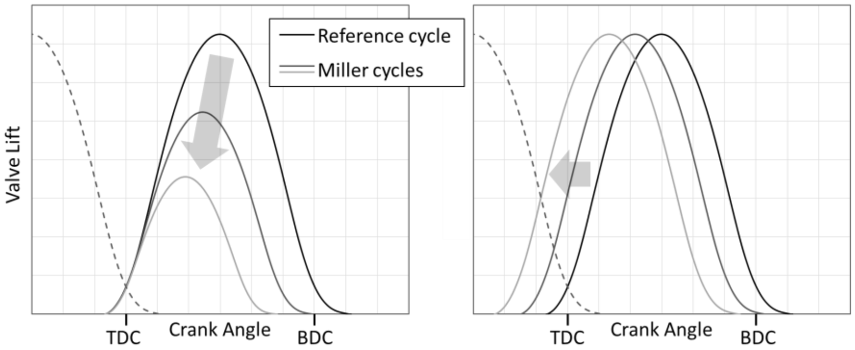

Figure 2.7. Different methods for realizing Miller strategy. Left: By using shortened valve durations. Right: By shifting the valve opening timing

The effect of EIVC can be demonstrated with the help of the thermodynamic process that is illustrated in Figure 2.8: Here, the intake and the compression phases of the engine cycle with an EIVC is compared with a reference cycle, which has an intake valve closure at BDC.

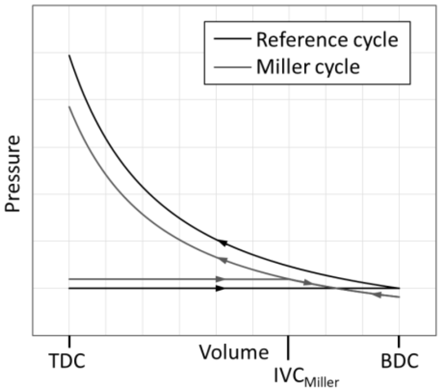

Figure 2.8. p-V diagram of a reference cycle compared with the Miller cycle.

For both cycles, the intake temperature and the mass trapped in cylinder is taken as identical. In this case, the intake pressure of the Miller cycle has to be higher, because the same mass must be trapped in a smaller volume, i.e. the volume at the time point of EIVC:

$$V_{EIVC} < V_{BDC} \implies p_{in,Miller} > p_{in,ref} \tag{2.5}$$

After the EIVC, the temperature in the cylinder decreases as a result of the expansion. Since the density at the BDC must be identical for both the reference and the Miller cycles, the pressure of the Miller cycle at BDC must also be lower:

$$\begin{gathered}\rho_{BDC,Miller} = \rho_{BDC,ref} \; and \; T_{BDC,Miller} < T_{BDC,ref} \\ \Rightarrow p_{BDC,Miller} < p_{BDC,ref}\end{gathered} \tag{2.6}$$

Since the Miller cycle has both a lower temperature and a lower pressure at the begin of the compression phase, the temperature and the pressure at the end of the compression phase has to be lower as well. As a result, the Miller cycle has a better knock resistance than the reference cycle. As an example, Kapus et al. suggest that at the operating point 2500 RPM 18 bar BMEP, about 4% fuel consumption reduction is possible, if a mild Miller strategy is applied and if the compression ratio would be increased by 1 unit additionally [22].

Furthermore, the Miller cycle can be beneficial, while the engine is operated at lower loads. Due to higher intake pressure with the Miller cycle, the throttling losses can be reduced and the efficiency of the engine can be increased. Bozza et al. demonstrates that instead of throttling down to 0.55 bar intake pressure at a low load operating point, an operation with almost 1 bar intake pressure combined with an appropriate Miller strategy is possible and this leads to an almost 5% less fuel consumption [23].

One drawback of Miller cycle with shortened valve lift durations and the resulting decreased valve lift is the reduction of tumble intensity. This can be counteracted with valve masking, which causes a particularly strong tumble at very low valve lifts. An example of valve masking can be found in the EA211 TSI evo engine of VW [17]. A potential problem for Miller cycle realized through shifting the valve opening event is the increased valve overlapping (see Figure 2.7) which may lead to a high portion of burned residuals, which has a detrimental effect on burn duration and flame stability. Moreover, an aggressive Miller strategy is challenging to combine with a high power density, because of the increased boost pressure requirement.

2.2.5 Variable compression ratio

Today’s conventional SI engines has to have more modest compression ratios in comparison to their compression ignition (CI) counterparts. The compression ratio of the spark-ignition engine is limited due to knock behavior of the engine at higher loads.

Theoretically, with a variable compression ratio, the compression ratio can be chosen freely and optimally for every operating point. At lower loads, a high compression ratio can be chosen, because knock tendency is already low. At higher loads, a low compression ratio would be more suitable to reduce knocking and as a result improving mfb50% and thus the efficiency. Variable compression ratio can also be combined well with extreme downsizing and very high power density. At full load, a very low compression ratio can be chosen in order to keep knocking under control while still maintaining high compression ratios at lower loads.

In real engines, the compression ratio can either be varied continuously within a given range or can be varied in two or more stages. A continuous variation can be expected to lead to best efficiencies, but a two-stage system can be preferred, if aspects such as simplicity, robustness, cost or size overweight the efficiency benefit.

A variable compression ratio concept for a SI-engine is developed by Nissan and introduced at [24]. Here, a continuous variation of the compression ratio between 8 and 14 is enabled with significant alterations and additions to the connection between the connecting rod and the crankshaft. A noteworthy feature of this system is that the connection rod stays almost at a vertical position during the working cycle. Therefore, the piston shear forces are lower and friction losses between cylinder walls and the piston is reduced. This reduction compensates the increased friction losses at the bearings, and the resulting friction losses with the variable compression ratio system are similar or even lower in comparison to the friction losses at a conventional crank-drive. A vehicle equipped with the engine described above is commercially available since 2019 [25].

Examples for a two-stage variable compression system are investigated by Wittek et al. [26] and by Fraidl et al. [27]. In both systems, the compression ratio can be switched back and forth between a high and a low compression ratio with a hydraulically driven variable length connecting rod system. Both publications suggest that the strongest argument for a two-stage instead of a continuous variable compression ratio system is that no fundamental change of the engine architecture is required and the system can be fitted into existing engine families with relative ease.

2.2.6 High turbulence concept

The high turbulence concept is realized by a special design of the intake manifold or by a tumble flap with the intention of creating a strong tumble during the intake. The tumble decay in the combustion chamber during the compression phase leads to an intensive turbulence. Due to this high level of turbulence the combustion becomes quicker and the air-fuel mixture in the cylinder is consumed faster. As a result, the available time for a self-ignition is decreased, which leads to an improved knock resistance of the engine. This enables an operation with a better mfb50%. Also, with decreased burn durations, the isobaric portion of the heat input decreases and the isochoric portion increases, which further contributes to the efficiency improvement. Further benefits of a quicker combustion are increased flame stability, decreases cycle-to-cycle variations and a higher combustion efficiency.

Several experimental investigations are conducting that proposes ways for generating intensive tumble and shows the benefits of the high turbulence in the combustion chamber. Berntsson et al. [28] use restriction plates to generate different tumble levels and show that with increased level of tumble the burn durations can be shortened and the knock tendency can be decreased. Thielen et al. [29] show the crucial effect of different cylinder head designs on the burn duration. They also demonstrate that the turbulence level can further be increased by a tumble flap. In the same publication, Wouters et al. reaches even shorter burn durations with a different test engine, i.e. burn durations 10-90% (BD 10-90%) lower than 12°CA can be observed [29].

The synergy effect that can be achieved with the high turbulence concept are also noteworthy: The higher knock resistance can be combined with an increase of the compression ratio of the engine to yield optimal efficiency benefits. For a similar reason, the high turbulence concept can complement variable compression ratio technology well. Also, the shortened burn duration can be especially useful in case of EGR. The higher turbulence level can compensate for the decreased laminar flame speed, thus keeping the burn durations, flame stability and cycle-to-cycle variations at an acceptable level even at high EGR rates. The same applies also to a lean concept with high air-fuel ratios.

A disadvantage of the high turbulence concept is the increased pumping losses, since the intake manifold is no longer designed for a smooth flow optimized for maximizing the air intake. Furthermore, short burn duration would lead to a higher maximum pressure and the increase of the mechanical stress should be taken into account. Similarly, a high pressure gradient is also an outcome, which leads to a higher noise, vibration and harshness (NVH) level that also needs to be considered.

2.2.7 High stroke-to-bore ratio

By increasing the stroke-to-bore ratio, a stronger tumble and thus a higher turbulence level can be realized, which amplifies the previously discussed advantages with a high turbulence concept. This is verified by the investigations of Thielen et al. [29] where the increased stroke of the single cylinder test engine lead to shorter burn durations. In addition, a higher stroke-to-bore ratio leads to lower wall heat losses: A large part of the wall heat losses is generated during combustion, which takes place, while the piston is near top dead center (TDC). If a low stroke-to-bore ratio is chosen, the shape of the combustion chamber resembles a flat disc around at TDC. The higher the stroke-to-bore ratio becomes, the more the combustion chamber gets a spherical shape at and near TDC. As a result, the proportion between the wall area and displacement volume of the combustion chamber decreases and becomes more favorable, reducing wall heat losses. A theoretical investigation by Filipi et al. [30] show that wall heat losses can be decreased by 7%-13%, if the stroke-to-bore ratio is increased from 0.7 to 1.3, whereas higher gains are associated with lower engine speeds. Further experimental data also supports that efficiency benefits with can be achieved with a high stroke-to-bore ratio [3, 29].

The drawback of a long stroke concept is that cylinder head has to be dimensioned smaller for a given displacement volume which results in smaller valve diameters. This leads to a more challenging gas exchange. As a result, the pumping losses are increased, especially at higher loads and higher speeds, where the mass flow rate through the valves is high. For the same reason, the combination of a high stroke-to-bore ratio with aggressive downsizing as well as with early or late intake valve closure (EIVC, LIVC, also called Miller strategy) might be unsuitable, since the boost pressure requirement would already be higher with these measures. Similarly, combination of a high stroke-to-bore ratio with EGR, lean concept might also be challenging, since a higher mass flow would be necessary for realizing the same fuel energy and as a result a similar load level. However, from another point of view, the EGR and lean concept can also profit from the increased turbulence levels with a high stroke-to-bore ratio.

2.2.8 Water injection

The water injection is a further way to increase the efficiency of the engine. The evaporation of water during the intake and compression phases results in a cooling down effect, which results in an improved knock resistance. Since the heat of evaporation of water is about six times higher than of the gasoline, water injection can also replace fuel enrichment at full load and offers itself as an efficient and yet much more environmentally sound solution.

Mainly two water injection strategies come into consideration: Intake port water injection and direct water injection. The intake port water injection is simpler and more straightforward to apply than the direct water injection. However, as the experimental data suggests, the direct water injection brings higher benefits regarding the knock resistance [31]. For example, in the operating point 2500 RPM 15 bar IMEP, mfb50% can be advanced from 13°CA to 8°CA by direct water injection with a water-to-fuel mass ratio of 20%. With indirect water injection and with the same amount of water, an improvement from 13°CA to 11°CA is evident. Vacca et al. suggest that with direct water injection a better control of the in-cylinder temperature is possible, which explains its superiority [31]. Similarly, experimental investigations at a single cylinder engine with direct water injection by Hunger et al. show that at 2500 RPM 20 bar IMEP, the center of combustion can be advanced by 16°CA with 50% water-to-fuel mass ratio, which results in a reduction of fuel consumption by 10.5% [32]. Vacca et al. also demonstrate in a separate 3D-CFD numerical investigation that direct water injection increases the turbulence level through an optimal spray targeting, further enhancing its benefits [33]. However, it should be noted that the application of direct water injection is more challenging: An extra injector has to be brought to the already crowded cylinder head and an injection system with higher injection pressure is necessary.

A central question of water injection is, how the water is supplied. Apart from simply filling water up, Böhm et al. advocate for recovering water from condensation at the air conditioning system, but also suggest recovering water by condensing the vapor from the exhaust gas or collecting the water from the vehicle surface as viable options [34]. Regardless, the trade-off between the efficiency improvement and the quantity of the injected water has to be considered carefully. In a theoretical study by Franzke et al. [35] intake port water injection is used for increasing the efficiency of a reference engine. For this purpose, the compression ratio of the engine is increased from 9.5 to 13. In the process, water injection is utilized for torques higher than around one-third of the maximal engine torque, whereas the water-to-fuel ratio is increased gradually with increasing loads – up to a maximum water-to-fuel ratio of 70%. The necessary water quantities are calculated for a WLTC and a moderate RDE cycles as 0.85 l/100 km and 0.84 l/100 km respectively. However, for a more dynamic RDE cycle, the required water quantity is estimated to be almost doubled. In another part of the same study, instead of increasing the compression ratio, the water injection is used for increasing the power output of the engine by increasing its knock resistance. Here, the power output of the engine can be increased by around 15% by using 50% water-to-fuel ratio [35].

Results of the aforementioned publications strongly suggest that water injection not only offers direct benefits by increasing the knock resistance at but also indirect benefits by allowing a more aggressive downsizing and/or a significant increase of compression ratio.

2.2.9 Lean concept

The lean concept works similar to external, cooled EGR, whereas the former uses charge air for dilution and the latter the recirculated exhaust gas. The main drawback of the lean concept is that the engine is no longer operated under stoichiometric conditions and an alternative exhaust gas after treatment system to the three-way catalyst is necessary. In this case, keeping the raw NOx emissions low becomes a priority as well. This can be only be achieved, if the combustion temperatures can be kept low, i.e. if the engine is operated with a high air-fuel ratio. However, a too high air-fuel ratio will result in high cycle-to-cycle variations and even misfires, which would lead lower efficiencies and a compromised operation of the engine. Therefore, it is important to combine lean operation with a high turbulence concept.

Research of Thielen et al. as well as Wouters et al. [29] with their respective single cylinder engines show that the lean concept offers a greater potential for efficiency improvement than EGR. This can be explained by the fact that more dilution with air is possible than with the cooled exhaust gas without the combustion becoming too instable. As a result, both the wall heat losses and the losses through throttling can be reduced more efficiently. The disadvantage of lean concept over EGR is the knock behavior. With EGR the knock behavior can be significantly improved consistently, whereas mixed results are observed with the lean concept. Overall, a slight improvement of the knock behavior is observed, if the air-fuel ratio gets close its maximum value with still reasonable cycle-to-cycle variations. It should be noted that EGR's advantage over lean concept regarding the knock behavior is not unexpected because dilution with an inert gas should have a higher impact on auto-ignition behavior than diluting with air.

2.2.10 Turbocharger efficiency

A turbocharger consists of a turbine after the exhaust manifold and a compressor before the intake manifold that are connected by an axle. The intake air is compressed by the compressor, which is powered by the turbine that uses the exhaust gas energy. The compressor of the turbocharger is almost always followed by an intercooler that cools down the intake air, reducing its density, thus enhancing the benefits of the turbocharger. The cooling also negates the effect of increased intake temperature on knocking.

The purpose of the turbocharger is enabling a higher power density in comparison to a naturally aspirated engine. As a result, the benefits due to downsizing as discussed in Chapter 2.2.1 are achieved. Alternatively, a downspeeding can be pursued: The increased maximum torque of the engine by boosting enables the operation with higher loads but with lower speeds for a given power output. The increasing load leads to similar benefits as the downsizing, while the decreased engine speed leads a further decrease of the friction losses.

Regarding the load control, there are mainly two types of turbochargers: The wastegate turbochargers and variable geometry turbochargers (VGT). In the case of a wastegate turbocharger, a certain amount of the exhaust gas can be bypassed for controlling the power output of the turbine. In the case of a VGT, controlling the power output is enabled by movable vanes are implemented at the turbine entry. The vanes can be rotated and their angles determine the pressure ratio over the turbine.

The efficiency of the turbine and the compressor or the turbocharger overall play an important part on the overall engine efficiency. A turbocharger with low efficiency will require a higher pressure ratio at the turbine for providing the desired amount of boost pressure. As a result, the exhaust backpressure and the pumping losses will increase. The work on improving turbocharger efficiencies is intense and several possibilities are proposed both for wastegate and for VGT turbochargers, which indicates for a great further potential of efficiency improvement for turbochargers.

A significant portion of the losses at a turbomachine is caused due to the clearance between rotary parts and the housing. Reducing the clearance or sealing it prevents the working fluid from moving through the clearance, thus reducing the losses. A possible method is used for aircraft turbine engines and goes as follows: During the first start-up of the turbomachinery, the blades of the turbomachinery are strained due to the centrifugal force and come into contact with the housing, cutting a groove on its surface. This groove serves then as a sealing at the clearance. For this purpose, an abradable coating for the housing is used [36]. Arnold et al. proposes using the same principle for turbocharger compressors [37].

A further possibility for reducing the clearance losses is using the ball bearings instead of sliding bearings. Zeppei et al. show that by replacing sliding bearings with ball bearings, the compressor efficiencies can be increased by around 3% absolute and turbine efficiencies by around 4% absolute. [38]

Another recent improvement is the development of the VGT specifically designed for spark-ignition engines. The new, shorter design of the vanes enables higher efficiencies if the normalized flow rate is above 50%, which fits especially well to SI engines operated with Miller strategy. [39]

The recent developments of the milling techniques specifically for turbocharger compressors impellers are likely to reduce production costs and allow an easy realization of more complex geometries and high precision as demonstrated by Chen et al. [40]. With those new possibilities, a greater freedom for innovative and aerodynamically optimized shapes for impellers become possible. In addition, the impeller shape can be used to influence the efficiency distribution along the compressor map. The 3D inverse design impeller, for example, can improve the efficiency of the compressor by 3% at higher mass flow rates and pressure ratios, but causes simultaneously a slight efficiency drop at lower mass flow rates and pressure ratios [41]. Further ideas tested for increasing the efficiency of compressors include variable geometry systems with variable inlet guide vanes as well as with variable geometry vaneless diffusers. Whitman et al. investigated a variable inlet valve design with the intent of creating a prewhirl, but could not demonstrate a worthwhile advantage over conventional designs [42]. In another study again from Whitman et al. the vaneless diffusor with variable angle and cross sections is investigated and efficiency advantages at lower mass flows can be found [43].

An alternative to the wastegate turbochargers is proposed by Steglich et al. [44]. The idea is to replace the wastegate with a nozzle. The nozzle serves the same purpose as the wastegate by bypassing the excess exhaust gas. In contrary to the wastegate, the bypassed exhaust gas is blown into the turbine outlet with a high speed which results in an acceleration of the gas. The acceleration creates a pressure drop at the turbine outlet, according to the Bernoulli's principle. Since the turbine experiences a lower backpressure, the turbine inlet pressure drops as well, under the assumption that the power output and thus the pressure ratio of the turbine stays similar. A lower turbine inlet pressure is equivalent to a lower exhaust backpressure during the gas exchange of the internal combustion engine, leading to reduced pumping losses.

Thermal resistance of the materials that are used for the turbine are also of high importance. The standard material for turbine wheels is a nickel-based heat resistant alloy known as Inconel [45]. Conventional wastegate turbines are limited to a turbine inlet temperature of around 980°C [46], while conventional VGT turbines are limited to a lower temperature of 950°C [47] due to increased number of moving components and a more fragile design. Considering that the exhaust gas temperatures of SI gasoline engines are around 200°C higher than diesel engines [45], at higher loads the fuel enrichment might be necessary to cool down exhaust gases to protect the turbine, which is harmful regarding both the fuel economy and the environment. Or, an integrated water-cooled exhaust manifold [48] is required. Thus, usage of materials with high thermal resistance can prove to be advantageous due to a better fuel economy as well as due to a higher flexibility during the engine design. Matsumoto et al. report that through using MarM, another nickel-based heat resistant alloy with greater strength at higher temperatures, as turbine wheel material, a wastegate turbine could be developed that resist exhaust gas temperature of 1050°C [45]. A VGT turbocharger with the same exhaust temperature capability is also commercially available [49].

2.2.11 Alternative fuels

Alternative fuels other than gasoline can also be used for SI internal combustion engines. If synthetized from renewable sources and/or by using renewable energy, alternative fuels can be considered as an environmentally sound, CO_2-neutral solution to the mobility. These fuels may either already have desirable properties for enhancing the efficiency of internal combustion engines or can be tailored specifically for this purpose. Also, they can be used purely, as mixture of two or more alternative fuels, or can be mixed into gasoline.

When assessing the quality of an alternative fuel, many aspects are taken into account: Factors such as knock sensitivity, laminar flame speed, evaporation enthalpy, stoichiometric air-fuel ratio, heat value can directly influence the efficiency that can be achieved with an alternative fuel. A lower carbon ratio in the fuel can help reducing local CO_2 emissions, making it easier to reach emission targets set by laws and regulations. The presence of oxygen atoms in the fuel molecules can inhibit soot generation. The boiling point, spray, droplet breakup, evaporation and mixture formation behaviors can influence the NO_X and hydrocarbon emissions. [50–52].

In this work, aside from gasoline blended with 10% ethanol with a research octane number (RON) of 95, the pure methanol fuel as well as a blend fuel consisting of 70% gasoline, 15% methanol and 15% ethanol (G70M15E15) are investigated. Some of the properties of these fuels are shown in Table 2.1.

According to this data, most notable advantage of methanol over gasoline is its much higher knock resistance which is directly characterized by RON and further enhanced by the high evaporation energy. A further advantage of methanol is its high laminar flame speed. Crönert et al. determined the laminar flame speeds for gasoline and methanol simulatively for boundary conditions relevant for internal combustion engines [53]. As an example, a comparison of laminar flame speeds for gasoline and methanol (among other fuels) for a temperature of 800 K and a pressure of 50 bar as a function of the equivalent ratio is shown in Figure 2.9.

Table 2.1. Properties of investigated fuels [29]

	Gasoline RON95E10	Methanol CH_3OH	Blend G70M15E15
Carbon mass fraction [-]	0.829	0.375	0.708
Hydrogen mass fraction [-]	0.134	0.125	0.132
Oxygen mass fraction [-]	0.037	0.500	0.160
Lower heating value [MJ/kg]	41.73	19.94	35.71
RON [-]	95	109	100.8
Stoichiometric air-fuel ratio [kg/kg]	13.91	6.43	12.01
Specific enthalpy of vaporization [kJ/kg]	350	1177	720

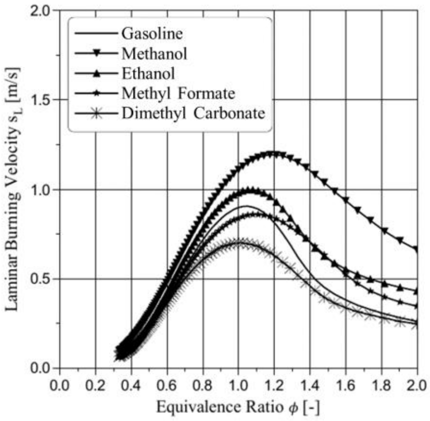

Figure 2.9. Laminar flame speed of various fuels in comparison to gasoline at 800 K and 50 bar according to Crönert et al. [53]

Despite its advantages, methanol raises health concerns due to its high toxicity. Therefore, usage of pure methanol as fuel is in general not permitted and its admixture to conventional fuel is also restricted. For example, current EU regulations allow only a 3% blend-in of methanol in gasoline [54]. Furthermore, a pure methanol engine must be significantly different than a conventional gasoline engine. For example, the lower heat value of methanol means that a higher amount of methanol must be injected for the same fuel energy and as a result a different injection system might be necessary. Due to these factors, it is unlikely that the pure methanol fuel to make a significant impact in short and middle term.

A drop-in fuel where modest amounts of other substances are mixed into gasoline, as in the case of the blend fuel, addresses both those problems. It can be expected in a nearer future for regulations to change increasing the allowed fraction of methanol in gasoline fuel. Also, since the blend fuel is still similar to gasoline, the currently available engines can be operated with it without any modifications. In other words, the blend fuel can be considered as a gasoline fuel with enhanced attributes and although its benefits are expected to be more modest, it can make a more short-term impact.

2.2.12 Hybrid drivetrains

Broadly speaking, the meaning of a hybrid drivetrain is the combination of a conventional internal combustion engine with an electric motor. This opens up a variety of possibilities for better efficiencies. Although this work concentrates solely on efficiency of the internal combustion engine, a brief introduction for hybrid drivetrains is still required in sake of completeness as well as for the discussion of the results that are to be presented in the incoming chapters.

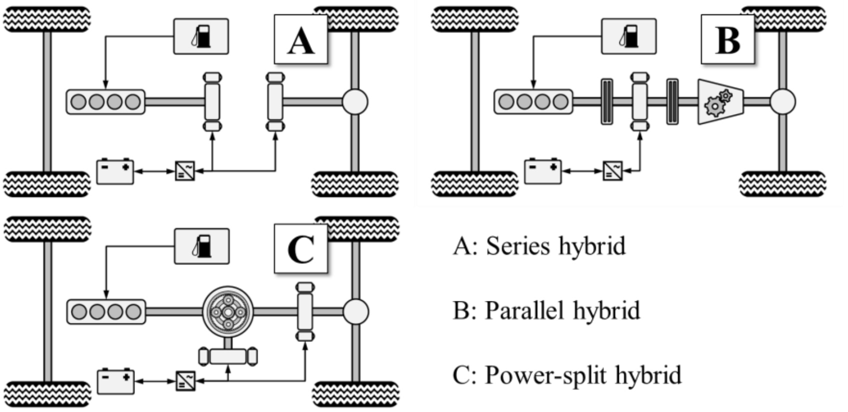

Figure 2.10. Different hybrid architectures [9]

In Figure 2.10, different hybrid architectures are shown. In the case of the series hybrid, the is no mechanical connection between the internal combustion engine and the wheels. The internal combustion engine drives the generator and generated electrical energy is used for operating the vehicle and/or for charging the battery. This configuration enables a free choice of the operating point of the internal combustion engine, thus the internal combustion engine can always be operated with the highest efficiency possible.

In case of parallel hybrid, the internal combustion engine and the electric machine are mechanically connected with the drivetrain. Here, different positions for the electric machine come into consideration which are typically named with the letter P combined with a numeral. For example, in case of the so-called P1 hybrid, the electrical machine is placed at the crank train. In this case, the connection between the internal combustion engine and the electric machine cannot be decoupled. On the other hand, the P2 hybrid places the electric machine further downstream of the drivetrain. This opens up the possibility of decoupling the internal combustion engine from the rest of the drivetrain and enabling a pure electric driving.

A further alternative hybrid architecture is the power-split (PS), which aims for a compromise between parallel and series configurations. In this configuration, a generator is connected to the drivetrain with a planetary gearset and operated constantly, converting a portion of the mechanical energy from the internal combustion engine into the electrical energy. A second electric machine is positioned directly on the drivetrain, and can be used for assisting the internal combustion engine if a high torque is demanded or can be used as a generator for recuperating the brake energy.

The advantages of the hybrid drivetrains over conventional ones are various. With the hybrid, the operating points with low efficiencies can be avoided: A simple example is start-stop system, where the internal combustion engine can be shut down instead of idling, when the vehicle is not moving. Similarly, low engine loads can be avoided by pure electrical driving. A further possibility is the load point shifting. Here, the internal combustion engine is typically operated at a higher, efficiency-wise more desirable loads despite a lower torque demand from the wheels. The excess energy is converted into electrical energy and stored in the battery. Conversely, the electric motor can be used to support the internal combustion engine, in which case a greater flexibility while dimensioning and designing the internal combustion engine is provided, which can contribute to the overall efficiency of the drivetrain. Lastly, a considerable amount of the braking energy can be recuperated with a hybrid drivetrain. [9] Naturally, the type and amount of the benefits are dependent on the chosen hybrid architecture as well as the degree of the hybridization of the vehicle, i.e. the power electronics, the power of the generator and electric motors and battery capacity.

3 Modeling approach

3.1 Simulation and modeling methods

For the investigations in this work, 0D/1D modeling and simulation methods are used. For this purpose, the software GT-Power [55] combined with the cylinder object FKFS UserCylinder® [56] is utilized. With the help of these tools, engine models are to be created, simulations are to be run, technologies to be assessed and the potential of the efficiency improvement is to be determined.

The 0D/1D simulation methods which are utilized during the course of this work allow a great flexibility while varying engine parameters which enables discovering interactions between technologies, finding the optimal engine setup and determining the highest efficiencies in relative ease. This process would be excessively resource and time consuming with experimental setups or for 3D-CFD simulations, especially considering parameters such as engine dimensions, compression ratio, the turbulence level or turbocharger fitting. Therefore, 0D/1D simulation methods are the only viable option for the investigations conducted during this work. However, the predictive capabilities of the engine models and the accuracy and reliability simulation results rely heavily on their sub-models. In the following, these sub-models should be described in more detail. These sub-models can be put into two categories: Sub-models that concern the processes in the combustion chamber and other sub-models that concern the engine model as a whole.

3.1.1 Combustion chamber modeling

The combustion in the cylinder is described with the help of the entrainment model [8]. Here, the gas in the cylinder is divided into burnt and unburnt zones. The two zones are separated by the flame front, which propagates spherically as the combustion progresses. The entrainment model is schematically shown in Figure 3.1.

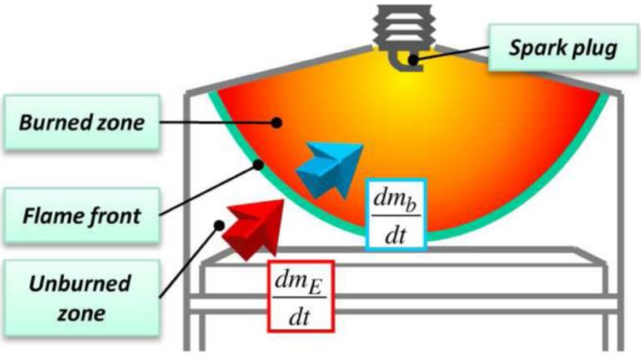

Figure 3.1. The entrainment model and the flame propagation [57]

The mass conversion rate is determined by entrainment speed of the flame front u_E, the area of the flame front A_{fl} and the density of the unburned zone ρ_{ub} as shown in the following equation:

$$\frac{dm_b}{dt} = \rho_{ub} \cdot A_{fl} \cdot u_E \tag{3.1}$$

There is a direct proportion between the mass conversion rate and heat release rate, i.e. the burn rate:

$$\frac{dQ_B}{dt} = \frac{dm_b}{dt} \cdot H_{u,mix} \tag{3.2}$$

where $H_{u,mix}$ is the lower heat value of the gas-fuel-mixture in the cylinder. More commonly, the heat release rate is expressed as heat release per degree crank angle. In this case, instead of (dQ_B/dt) with the unit of J/s, the expression $(dQ_B/d\varphi)$ with the unit of J/°CA is used.

In the next step, the entrainment speed of the flame should be considered. The entrainment speed of the flame front results from the laminar flame speed s_L and turbulent fluctuation velocity u', as well as the model parameter C_u.

$$u_E = s_L + C_u \cdot u' \tag{3.3}$$

The laminar flame speed and the turbulent fluctuation rate are calculated separately. For the calculation of the laminar flame speed, there have been common empirical approaches that are suggested by Heywood [4] and Gülder [58]. Both of those approaches share a similar formula, which describes the laminar flame speed as a function of temperature T, pressure p and the EGR rate X_{EGR}:

$$s_L(T, p, \lambda, X_{EGR}) = s_{L,0}(\lambda) \cdot \left(\frac{T}{T_0}\right)^{\alpha} \cdot \left(\frac{p}{p_0}\right)^{\beta} \cdot (1 - f \cdot X_{EGR}) \tag{3.4}$$

Here, $s_{L,0}(\lambda)$ is a reference value for a given air-fuel equivalence ratio λ, while T_0 and p_0 being reference temperatures and pressures respectively. α, β and f are model parameters.

Since the both approaches suggest a linear dependency of the laminar flame speed and the EGR mole fraction, both approaches predict negative laminar flame speed values for high EGR rates unrealistically. Furthermore, both approaches predict the laminar flame speeds very differently, especially at higher air-fuel ratios, as shown exemplary in Figure 3.2 [59]. A further overall challenge for modeling the laminar flame speed is the absence of reliable measurement data, because most of the laminar speed measurements are conducted with boundary conditions that are irrelevant to the engine operations. This is due to restrictions of technical limits as well as thermodiffusive and hydrodynamic instabilities. [59]

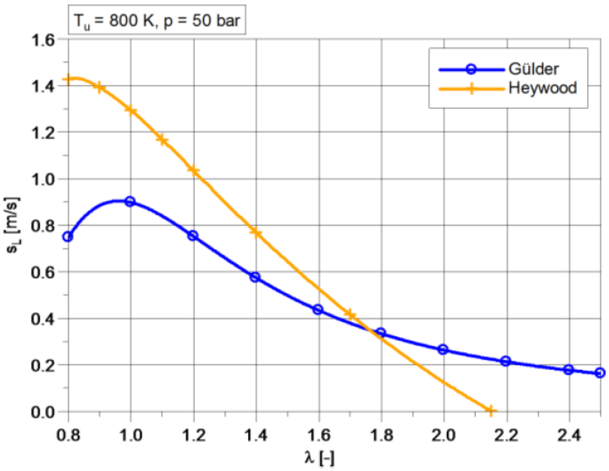

Figure 3.2. Laminar flame speeds as a function of air-fuel equivalence ratio according to approaches of Heywood and Gülder [59]

Therefore, reaction kinetics calculations should be relied on for determining the laminar flame speeds. Such an approach is developed by Hann et al. and their methods are described thoroughly in [60]. An exemplary result for laminar flame speeds with mixture dilution shown in Figure 3.3 differs greatly than the approaches of both Gülder and Heywood and shows plausible trends. In fact, the validation results presented in [59] suggest an excellent agreement between the measured and simulated burn rates. The laminar flame speed models are developed for a variety of fuels by Hann et al., most notably being gasoline, methane, methanol, methyl formate as well as ethanol admixture to gasoline or admixtures of hydrogen, ethane, propane or butane to methane at any proportions [60, 61]. For the calculation of laminar speeds in this work, the approach of Hann et al. and their respective sub-models is adopted.

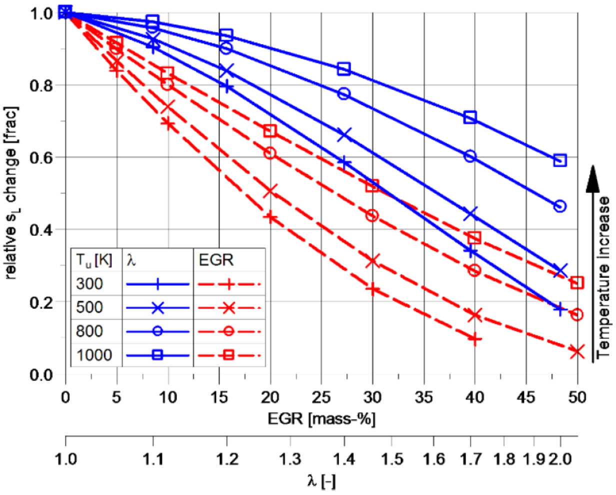

Figure 3.3. Relative change of laminar flame speed according to Hann et al. as a function of air-fuel equivalence ratio and EGR rate for different starting temperatures [59]

The second component of the flame propagation rate -the turbulent fluctuation velocity- is determined by the turbulent kinetic energy *k*. For isotropic turbulence, this relation is given by:

$$u' = \sqrt{\frac{3}{2} \cdot k} \tag{3.5}$$

The calculation of the turbulent kinetic energy is based on the *k*-ε turbulence model [62]. Here, ε stands for turbulent dissipation rate. As shown in the following formula, the change of the turbulent kinetic energy *(dk/dt)* results from the turbulence production rate (first term) and the turbulence dissipation rate (second term), which counteract each other:

$$\frac{dk}{dt} = \left(\frac{dk}{dt}\right)_{prod} - \varepsilon_{diss} \tag{3.6}$$

For 0D-simulation purposes, the turbulence production rate is considered by Bossung et al. [63] as an addition of separate turbulence production terms: Turbulence production terms due to inflow, due to piston movement, due to tumble decay and due to compressibility. This approach is further expanded by Fasse et al. [64] by an additional term for wall influence. The turbulence dissipation is calculated based on the classical approach of Wilcox et al. [65] but this too is expanded by an additional term that takes wall effects into account [63].

For the turbulence level in the combustion chamber, the tumble intensity plays an integral role. The generation of the tumble during the intake phase is modeled with the help of Tippelmann numbers. The Tippelmann number T_{Tipp} is determined at a stationary flow test bench by measuring the mass flow rate and torque generated the tumble as a function of the valve lift [66]:

$$T_{Tipp} = \frac{M_T \cdot b \cdot \rho}{2 \cdot \dot{m}^2} \tag{3.7}$$

whereas, M_T being the torque that is caused by the tumble, b the bore diameter, ρ the density of the gas, $\dot{m}$ the mass flow rate.

The Tippelmann numbers are then used in the model to calculate the torque of the tumble, i.e. the tumble intensity, by simply rephrasing the Equation (3.7). Fritsch et al. suggest that the direct injection can have a significant effect on both the turbulence and the tumble intensity and that the calculation methods for these should be expanded accordingly with additional terms [67]. Moreover, Hann et al. indicate that the type of fuel has a significant effect on the turbulent flame speed due to combustion of different fuels influence the flame wrinkling differently [61].

The model parameter C_u in Equation (3.3) determines the relationship between the turbulence intensity and entrainment velocity and is to be varied in order to calibrate the model. For the high turbulence concept, this value can simply be increased in order to realize the desired level of burn durations. At the same time, it is recommended to decrease the discharge coefficient of the intake valves to simulate the more difficult gas exchange due to a tumble flap or a different geometry of the intake ports.

For the prediction of the knock behavior and for determining the center of combustion, the knock model developed by Fandakov et al. is used [68]. The model evaluates whether an auto-ignition occurs and whether the auto-ignition is harmful or not, if the engine is operated with the desired mfb50% (in general 8°CA which leads to the highest efficiency). If a harmful auto-ignition i.e. knock is predicted, the knock controller adjusts mfb50% so that no harmful auto-ignition occurs. Therefore, the model should not only be able to predict the ignition delay for determining the auto-ignition behavior, but it also requires a criterion which distinguishes between a harmful and non-harmful auto-ignition.

Conventionally, the auto-ignition behavior in 0D-simulations of SI engines is modeled by the Livengood-Wu integral also known as the knock integral [69]:

$$1 = \int_{t=0}^{t=t_{ignition}} \frac{1}{\tau} dt \tag{3.8}$$

with *t* being time and *τ* being the ignition delay time that can be approximated with an Arrhenius type equation:

$$\tau = C_1 \cdot p^{C_2} \cdot e^{C_3/T} \tag{3.9}$$

with Arrhenius parameters C_1, C_2 and C_3.

The idea behind the Livengood-Wu integral is that the right-hand side of the Equation (3.8) increases gradually with each time step until the value of the integral reaches 1, at which point the auto-ignition occurs. What differentiates the knock model of Fandakov et al. from its predecessors is that it takes the two-stage ignition behavior of gasoline into account. This behavior is related to the negative temperature coefficient of gasoline at certain temperature range, which leads to an increase of ignition delay despite increasing temperatures, as illustrated in Figure 3.4. The solution of Fandakov et al. is to calculate the knock integral each for the low-temperature and high-temperature ignitions separately.

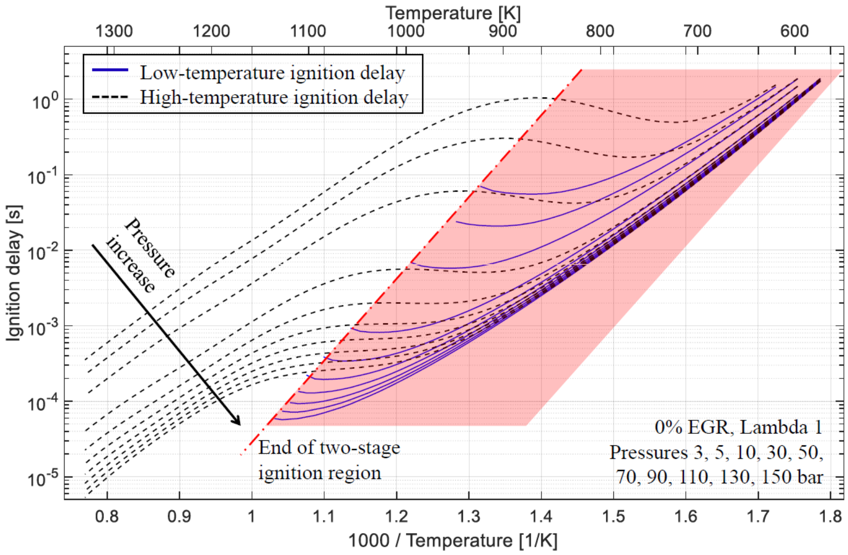

Figure 3.4. Ignition delay as a function of temperature with two-stage ignition region for gasoline [70]

In the knock model of Fandakov et al., the criterion for whether the auto-ignition harmful or not, is also innovative. Commonly used models such as the one developed by Franzke [71] or by Worret [72] use the mass fraction of the unburnt gas as a criterion. The idea is that if the mass of the unburnt gas at the time point of auto-ignition is low, the auto-ignition can be considered as non-harmful. Fandakov et al. proposes the usage of unburnt mass fraction in the thermal boundary layer as a more reliable criterion instead. This value is the primary calibration parameter of the model. If the mass fraction at the boundary layer is higher than the pre-defined threshold x_{ub} at the time of the auto-ignition, the auto-ignition is considered as not harmful, i.e. no knock occurs. [68]

An integral component of combustion chamber modeling is the wall heat modeling. For the prediction of wall heat losses, the approach of Woschni is used, which models the heat transfer coefficient between the wall and the gas in cylinder [73]. The wall heat transfer is then calculated with the help of the temperatures of the burnt and unburnt zones in each cylinder together with the wall areas of the both zones, temperatures of both the oil and the coolant, the heat transfer coefficients between cylinder, cylinder head and the piston and the coolant and the oil. Naturally, the wall heat modeling cannot be considered independently from the previously described combustion models: The combustion models influence the temperature and the flame propagation in the combustion chamber, thus providing the boundary conditions for the wall heat model. The wall heat model on the other hand influences the temperature in the combustion chamber which affects both the combustion and the knock models.

3.1.2 Engine Modeling

The remaining sub-models can be considered relatively independently from the previously discussed combustion chamber models. Here, two sub-models are of highest importance regarding the efficiency of the engine: The friction model which determine the friction losses and the turbocharger models which determine the pumping losses.

For friction modeling, the method of Fischer et al. [74], which is common for 0D/1D simulations, is used. However, this model is modified in order to simulate effects that are not considered in the original approach: First, a compression ratio dependency is implemented. Here, FMEP increases with increasing compression ratio, because of the increasing pressures in cylinders. Also, the change of FMEP with different number of cylinders is considered. Both those modifications are done in accordance to the findings of Huß et al. [6]. Furthermore, it is assumed that the FMEP remains constant with changing stroke-to-bore ratios, since opposing effects are present: With an increased stroke-to-bore ratio, the mean piston speed becomes higher, which suggests an increase of friction losses. On the other hand, the lateral forces on the piston are decreased and also losses for the valve train are reduced as a result of the reduced inertia of mass of the smaller valves. Moreover, it is assumed that the friction in not affected by the presence of a variable compression ratio system, as suggested in [24].

In the engine model, the compressor and the turbine of the turbocharger are represented as maps. These maps are generated with a set of tabulated data that include reduced mass flow, reduced speed, pressure ratio and the efficiency. The corrected mass flow and speed are defined respectively as:

$$\dot{m}_{corr} = \dot{m} \cdot \frac{\sqrt{T}}{p} \qquad n_{corr} = n \cdot \frac{1}{\sqrt{T}} \tag{3.10}$$

with T and p being the intake temperature and pressure of the turbomachine respectively, $\dot{m}$ being the mass flow through the turbomachine and n being the speed of the turbomachine. In case of the VGT, several maps are used for different rack positions and the map for any rack position is calculated via interpolation.

The maps for already existing turbochargers are generally generated according to the measurement data. For the generation of maps of virtual turbochargers, which is necessary during this work, an internal tool is used. The tool uses data from several commercially available turbochargers to generate further realistic maps. The tool first generates compressor and turbine maps according to a desired flow coefficient. As long as a plausible flow coefficient is chosen, compressor and turbine maps can be acquired that closely resembles real maps. In the next step, those maps are scaled to model turbomachines of any desired size. The diameter d is here the scaling factor. The corrected mass flow through the turbomachinery is proportional to its area, therefore:

$$\dot{m}_{corr} \sim d^2 \tag{3.11}$$

The maximum speed at the tip of the blade is limited to values that are somewhat below the speed of sound, therefore the larger the turbomachinery becomes the lower its speed should get:

$$n_{corr} \sim \frac{1}{d} \tag{3.12}$$

Furthermore, a larger turbomachine tends to have a higher efficiency, because the portion of losses, for example the previously discussed clearance losses, decrease with increasing size of the turbomachine. The proposed correlations between the diameter and the efficiency of the compressor and the turbine are:

$$\eta_c \sim d^{0.16} \qquad \eta_T \sim d^{0.10} \tag{3.13}$$

Over the course of this study, several high-efficiency, high-technology engines are modeled, which are assumed to have high-technology turbochargers, which should also have higher efficiencies than the state-of-the-art turbochargers. In this case, the efficiencies are corrected further and for the corrections following assumptions are made based on the aforementioned research in Chapter 2.2.10: For compressors, efficiency can be increased by 3% absolute by decreasing the clearance losses by either using abradable seal compressor housing or by using ball bearings and 2% absolute with advanced milling techniques. For turbines, 4% absolute improvement can be achieved with ball bearings and 3% absolute with an optimized diffusor geometry. Furthermore, it is assumed that further 3% absolute improvement for both turbine and compressor efficiencies are expected in coming years, either by using diverse further optimization and enhancement or by newly invented technologies. As a result of these considerations, in case of a high-technology compressors and the turbines, their efficiencies are multiplied by 1.11 and 1.14 respectively.

Aside from the individual turbine and compressor efficiencies, two further factors that influence the overall efficiency of the turbocharger are considered in the model. First, the friction losses that occur on the connecting shaft between compressor and turbine and which is proportional with the turbocharger speed. Second factor is the heat transfer between from turbine to the compressor. As a result of this heat transfer, the gas temperature at the turbine is decreased so that slightly less energy is available in comparison to an adiabat turbine and compressor. As a result of those two factors, the overall efficiency of the turbocharger model is slightly reduced.

3.2 Calibration of the combustion models

The combustion models are calibrated with the help of the measurement data generated by Thielen et al. from IVB of the University of Braunschweig and

Wouters et al. from VKA of the RWTH Aachen University during the FVV research project ICE2025+: Ultimate System Efficiency [29] and with the models of their respective single cylinder engines. The investigations at IVB include load, EGR rate, air-fuel ratio variations as well as studies with water injection. Over the course of their work, they modify their engine setups several times: Replacing the four-valve (4V) cylinder head with a three-valve (3V) cylinder, increasing the stroke of their engines, changing the compression ratio, opening and closing the tumble flap in order to influence the tumble intensity and thus turbulence level. The investigations at VKA concentrate more on evaluation of alternative fuels, while also varying load, EGR rate, air-fuel ratio as well as the compression ratio. They also modified their compression ratio during their investigations in order to better demonstrate the knock resistance of the alternative fuels. The detailed description of their engines and engine setups and the complete results of their experimental work can be found in the end report of the research project [29]. On Table 3.1, a brief overview of the engine layouts is given that are relevant for the model calibration.

Table 3.1. Engines and engine layouts named from A to F that are used for the model calibration.

Layout	A	B	C	D	E	F
Institute	IVB	IVB	IVB	IVB	VKA	VKA
Cylinder Head	4V	3V	3V	3V	4V	4V
Stroke [mm]	90	90	90	90	113.2	113.2
Bore [mm]	60	60	60	60	75	75
Displacement [cm^3]	255	255	255	255	500	500
s/b	1.5	1.5	1.5	1.5	1.51	1.51
CR	12.2	12.2	12.2	18	10.8	15
Tumble flap	open	open	closed	closed	-	-

To determine the burn rate from the measured pressures, the three-pressure-analysis (TPA) [56] is used. The objective of the combustion model calibration is to find out, whether any corrections or adaptations are necessary for achieving a good agreement between measured and simulation burn rates. This acquired information will then be used to adjust the combustion model of the full engine models.

Combustion model calibration is done in two steps. In the first step, the aim is to reach the best agreement possible between the measured and simulated burn rates. During this step, the mfb50% is adopted from the measurement and set constant. In the second step, the knock model is activated (i.e. mfb50% is no longer constant) and calibrated for the best agreement between the measured and simulated mfb50%. The calibration parameter for the burn rate model is the C_u, for the knock model it is x_{ub} as introduced in Chapter 3.1. The exact values for C_u and x_{ub} for the calibration process can be found in the Appendix.

3.2.1 Burn rate model

Load variation

For first step of the calibration for the burn rate model, the load variation conducted by IVB of the University of Braunschweig at 2000 RPM with the engine layout A. In Figure 3.5, the comparison between the burn rate predicted by the model and the burn rate acquired by TPA is shown.

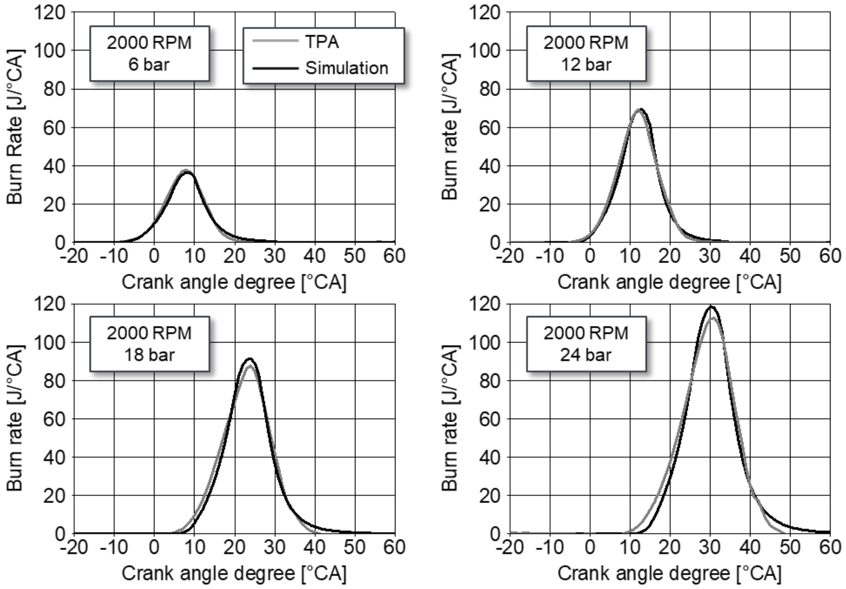

Figure 3.5. Burn rates with TPA and simulation for a load variation at 2000 RPM with the engine layout A

The model parameter is calibrated at only one operating point, and kept constant. No correction is necessary for different operating points. A very good agreement between the TPA and simulation is observed.

Water injection

The same load variation with the same engine layout A is conducted with water injection at the intake port, with different injected water masses at each time. In the first variation, the mass of the injected water is 50% of the mass of the injected fuel. In the second variation, the mass of the injected water is equal (100%) to the mass of the injected fuel. The comparison for the TPA and modeled burn rates for 50% and 100% water injections are shown in Figure 3.6 and Figure 3.7 respectively.

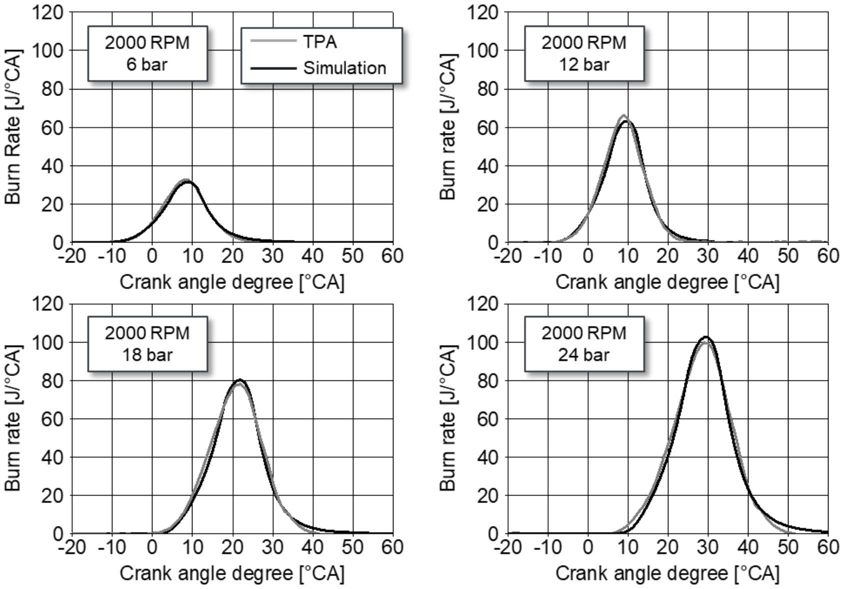

Figure 3.6. Burn rates with TPA and simulation for a load variation with 50% water injection at 2000 RPM with the engine layout A

As in the previous case, a calibration for different loads is not necessary and the model can predict the burn rate throughout the load variation with water injection very accurately. However, it is found that the burn rate model slightly underestimated the decrease of the combustion speed as a result water injection and were calibrated accordingly, so that the parameter C_u is increased by around 10% for 50% water injection and around 20% for 100% water injection.

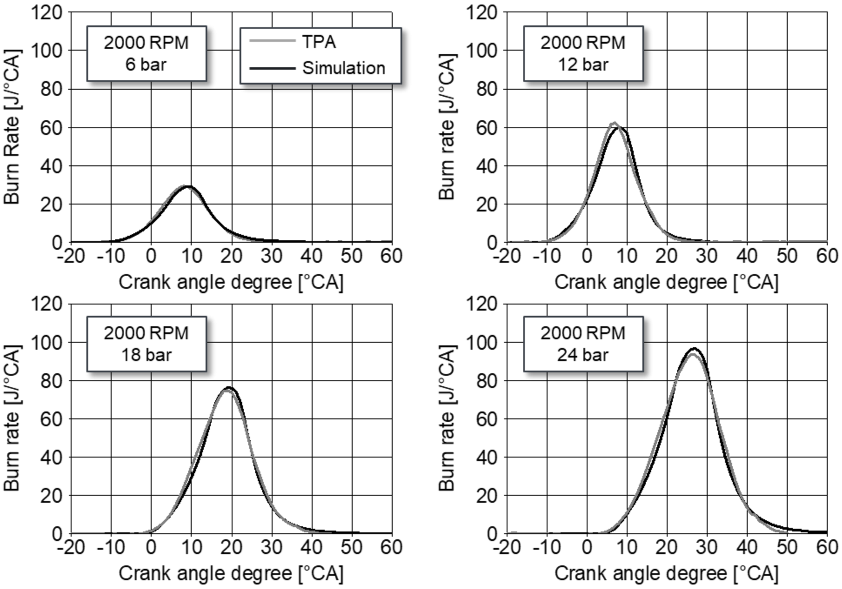

Figure 3.7. Burn rates with TPA and simulation for a load variation with 100% water injection at 2000 RPM with the engine layout A

EGR variation

The model calibration for EGR is conducted at several operating points with the engine layout B. The first operating point is 2250 RPM and 6.5 bar IMEP and EGR rate is varied from 0% to 25% with 5% steps. The burn rates with TPA and simulation are compared and the comparison is shown in Figure 3.8.

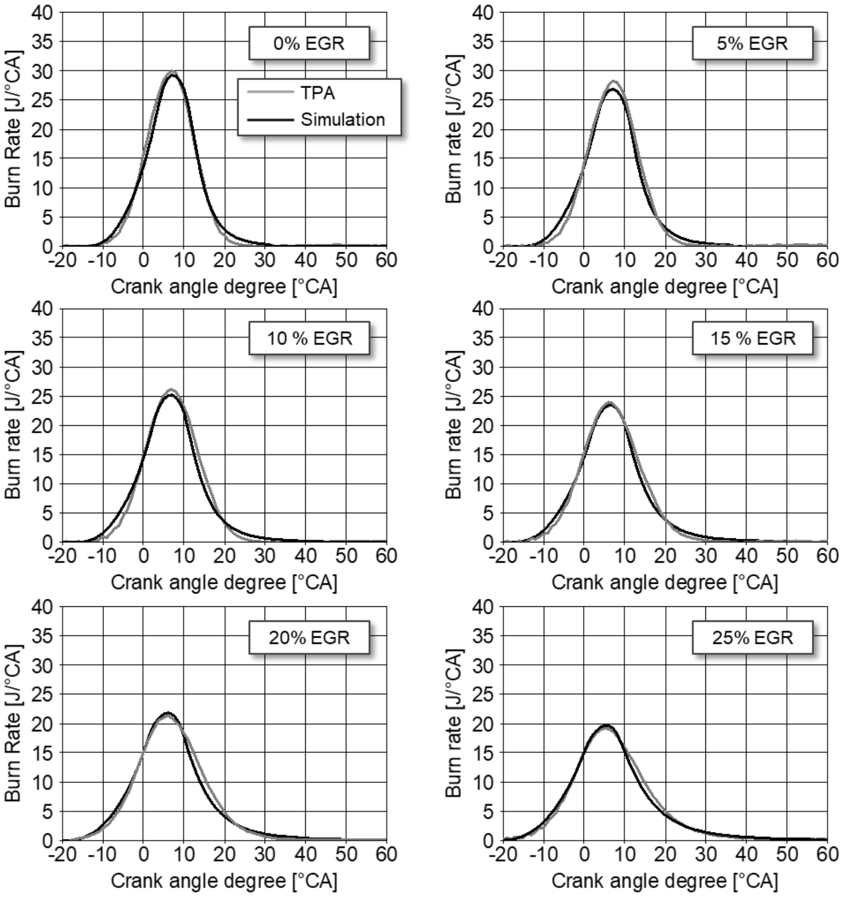

Figure 3.8. Burn rates with TPA and simulation for an EGR variation at 2250 RPM, 6.5 bar IMEP with the engine layout B

A similar comparison is conducted at 2000 RPM and 11 bar IMEP and 2500 RPM and 16 bar IMEP. The results are shown in Figure 3.9 and Figure 3.10 respectively.

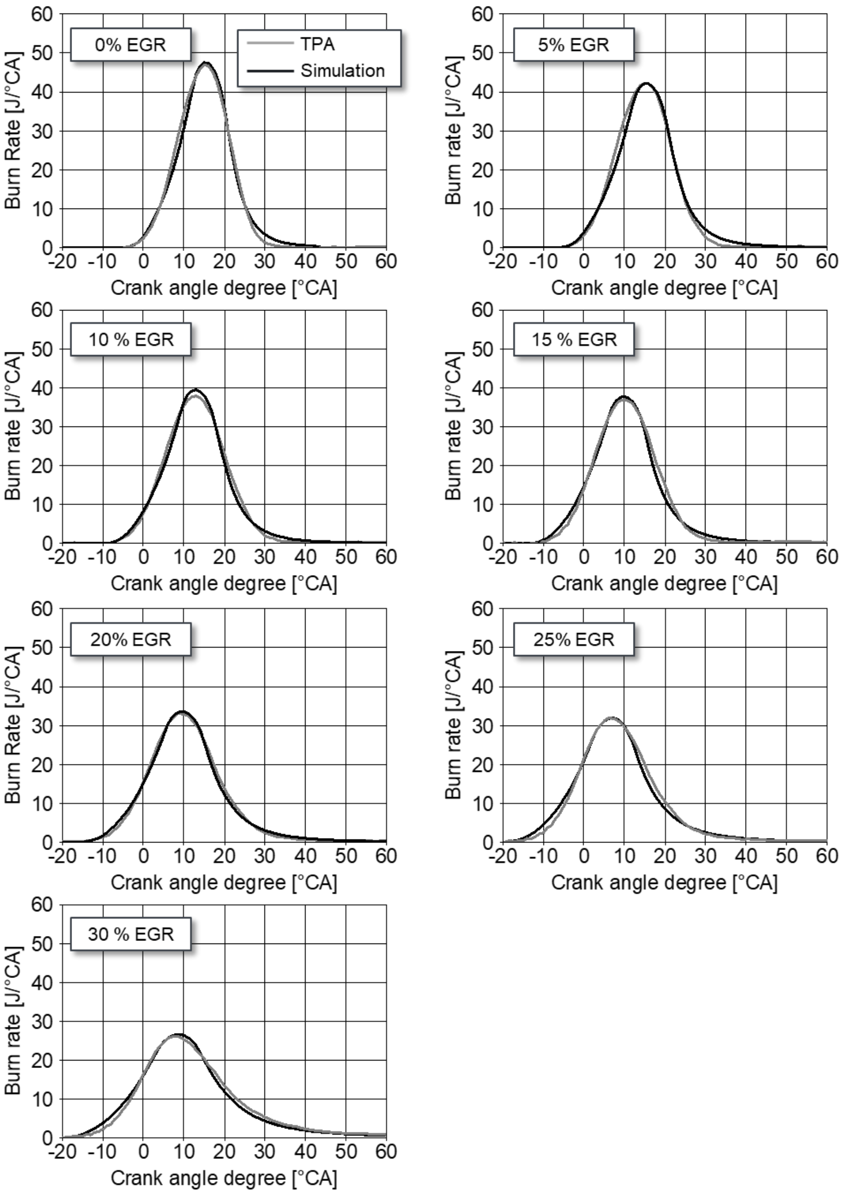

Figure 3.9. Burn rates with TPA and simulation for an EGR variation at 2000 RPM, 11 bar IMEP with the engine layout B

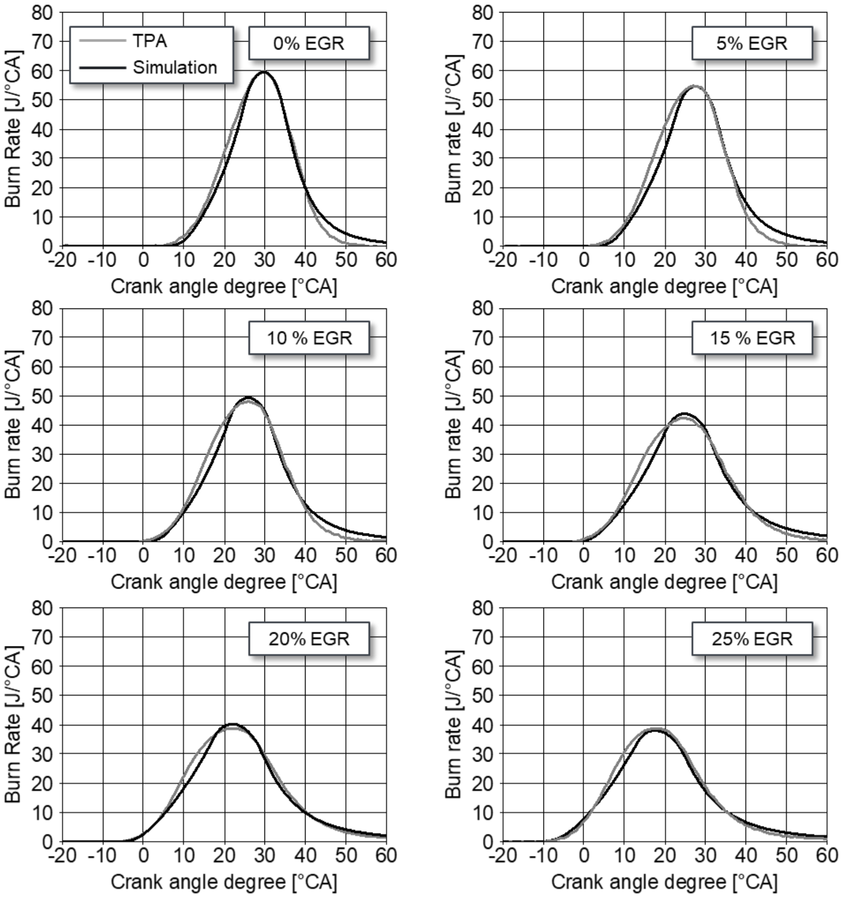

Figure 3.10. Burn rates with TPA and simulation for an EGR variation at 2500 RPM, 16 bar IMEP with the engine layout B

At the lowest load, no calibration of C_u is necessary. At the two other operating points, the uncalibrated combustion model tends to underestimate the influence of EGR on burn rate, and therefore an adjustment of the model parameter C_u is necessary. A linear correction of C_u as a function of EGR rate yields the good agreement shown in the diagrams, with C_u being reduced by around 20% for the maximum EGR rate.

EGR variation with closed tumble flap

With the engine layout C which uses a closed tumble flap in contrast to the engine layout B, the burn rate is increased significantly. In the model, C_u is increased to simulate this effect. The comparison of TPA and simulated burn rates are shown in Figure 3.11. Here too, the correction of model parameter C_u is necessary (%15 correction for 30% EGR rate) and consistent to the necessary correction in the previous case with EGR rate variation with open tumble flaps.

As a result of the investigations with EGR, it is decided that the full engine models should also have a correction for the model parameter C_u proportional to the EGR rate.

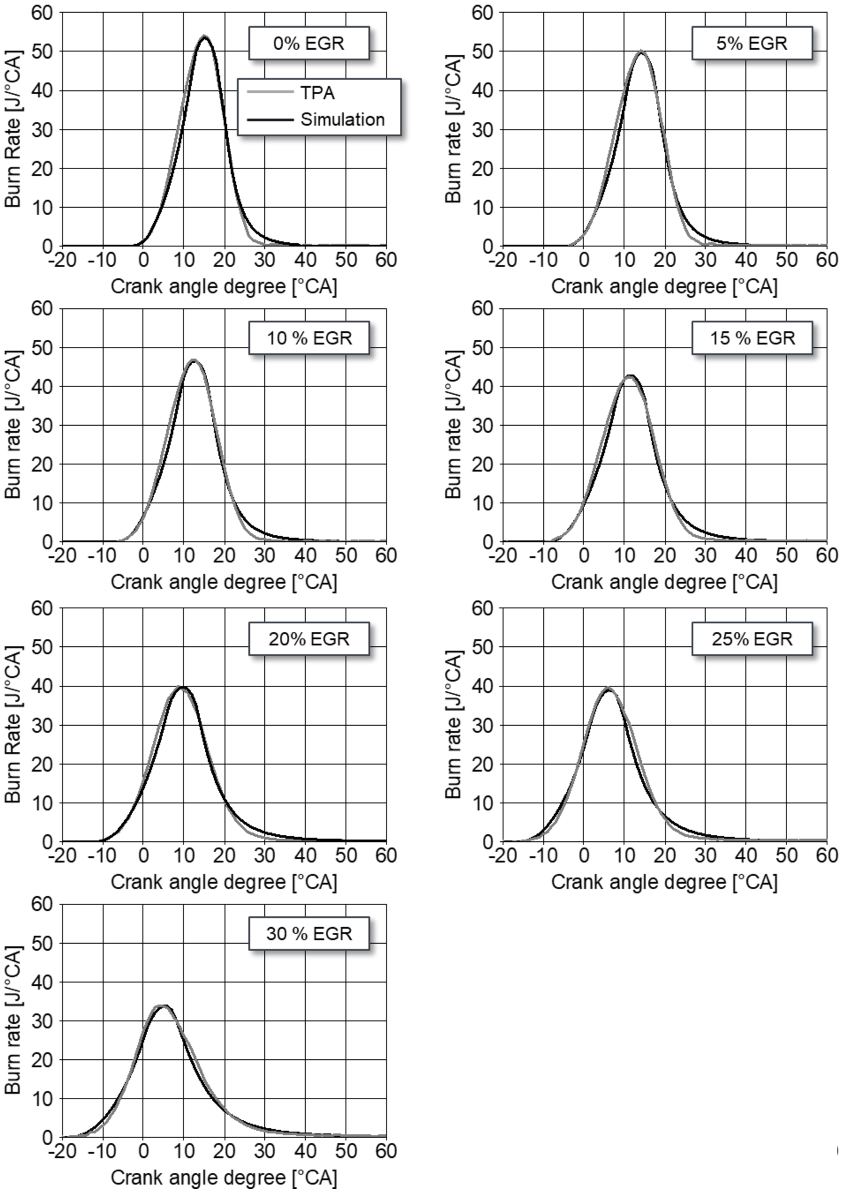

Figure 3.11. Burn rates with TPA and simulation for an EGR variation at 2000 RPM, 11 bar IMEP with closed tumble flap (engine layout C)

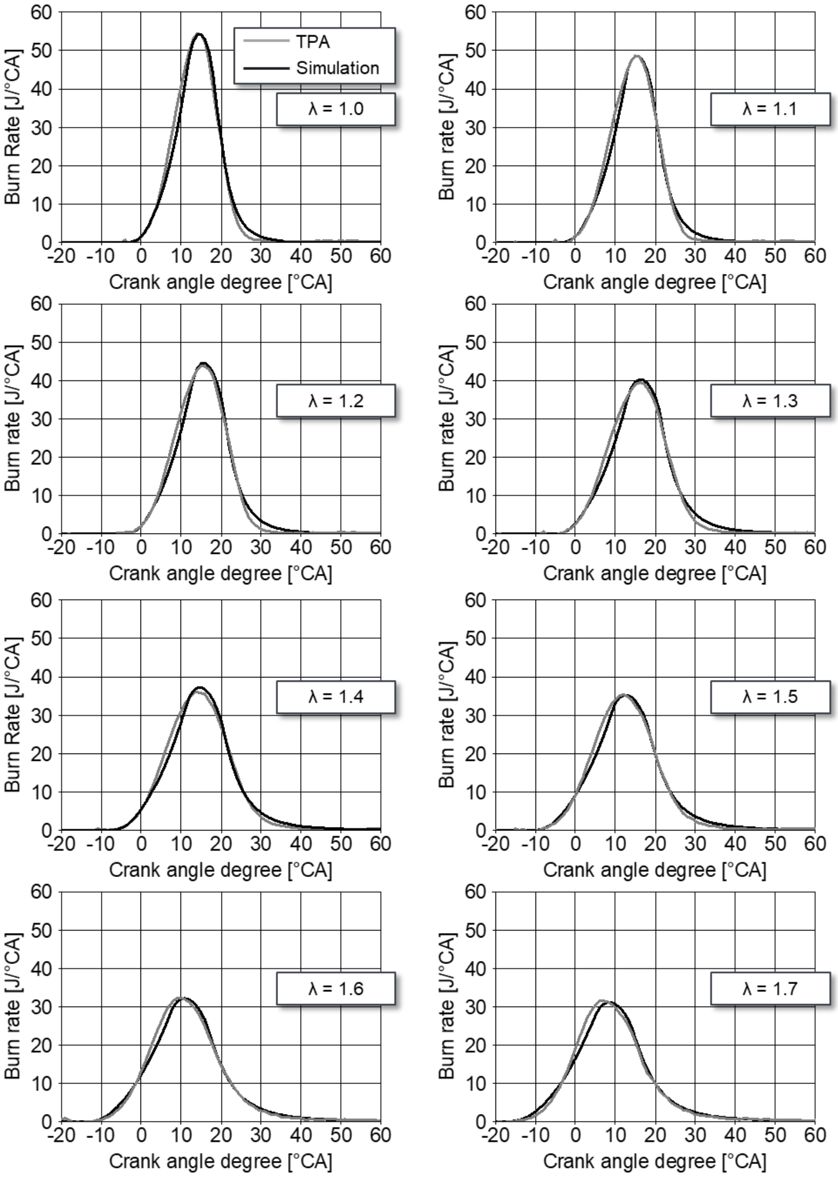

Figure 3.12. Burn rates with TPA and simulation for an air-fuel-ratio variation at 2000 RPM, 11 bar IMEP, tumble flap closed (engine layout C)

Lean combustion

For the model calibration of lean combustion, only the cases with closed tumble flap are considered (i.e. engine layout C), since a high turbulence level is essential for a reasonable application of lean combustion with high enough air-fuel ratios and acceptable NO_X raw emission levels.

The calibration of the lean combustion model is conducted through an air-fuel equivalence ratio λ variation first at the operating point 2000 RPM 11 bar IMEP. The experiments are conducted with the same engine configuration as with the EGR variation. The comparison of TPA and simulated burn rates are shown in Figure 3.12 for values between $\lambda=1.0$ and $\lambda=1.7$ with steps of 0.1.

For the good agreement shown in Figure 3.12, the model parameter needs to be calibrated. Similar to the EGR, the change of the combustion duration is underestimated by the uncalibrated model with increasing λ. Also, the necessary correction is linear. However, a more significant correction was necessary for the maximum investigated air-fuel equivalence ratio of $\lambda=1.7$ than for the maximum investigated EGR rate of 30%: C_u needs to be reduced by 25% for $\lambda=1.7$.

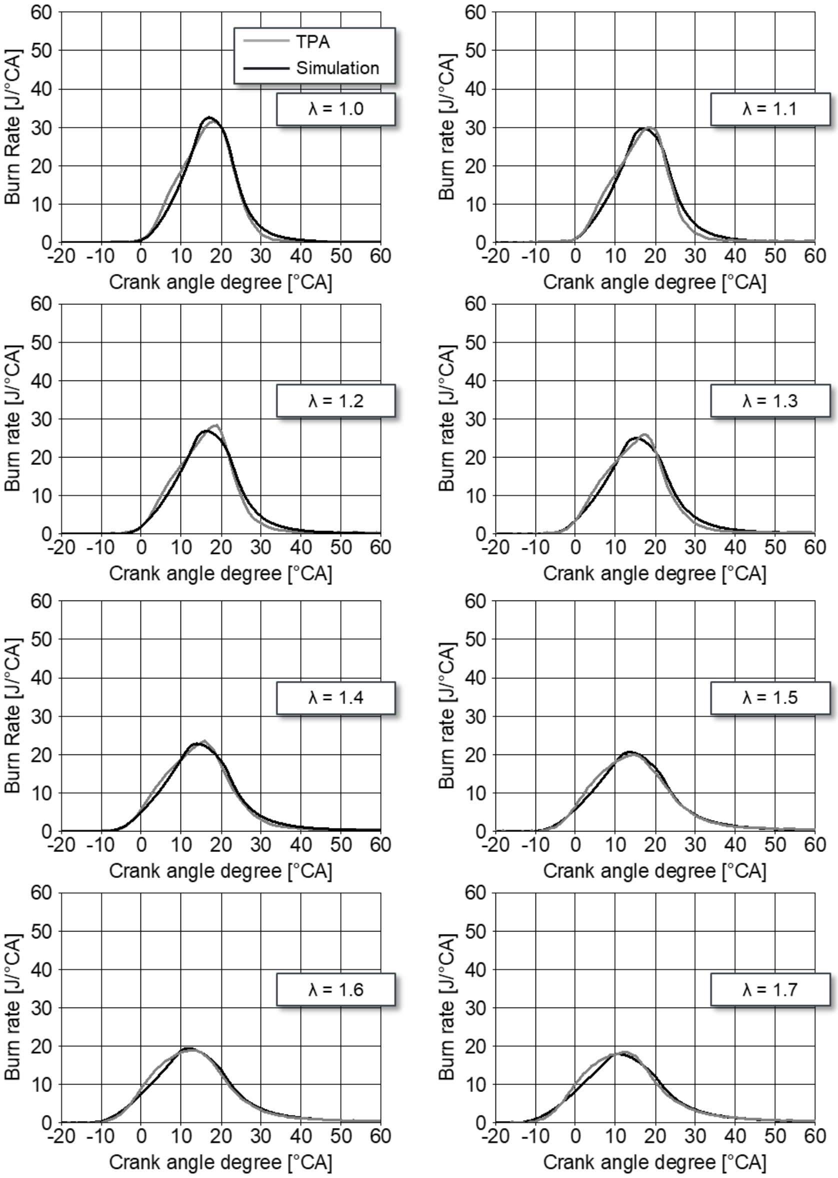

Figure 3.13. Burn rates with TPA and simulation for an air-fuel-ratio variation at 2000 RPM, 8 bar IMEP with the engine layout D

A further λ-variation is also conducted with the engine layout D with an increased compression ratio of 18. Since 11 bar IMEP would be too high for the chosen compression ratio, the investigation is conducted at the operating point 2000 RPM and 8 bar IMEP instead. The comparison of TPA and simulated burn rates is shown in Figure 3.13. Here too, a linear correction of C_u is used that reaches 25% at $\lambda=1.7$.

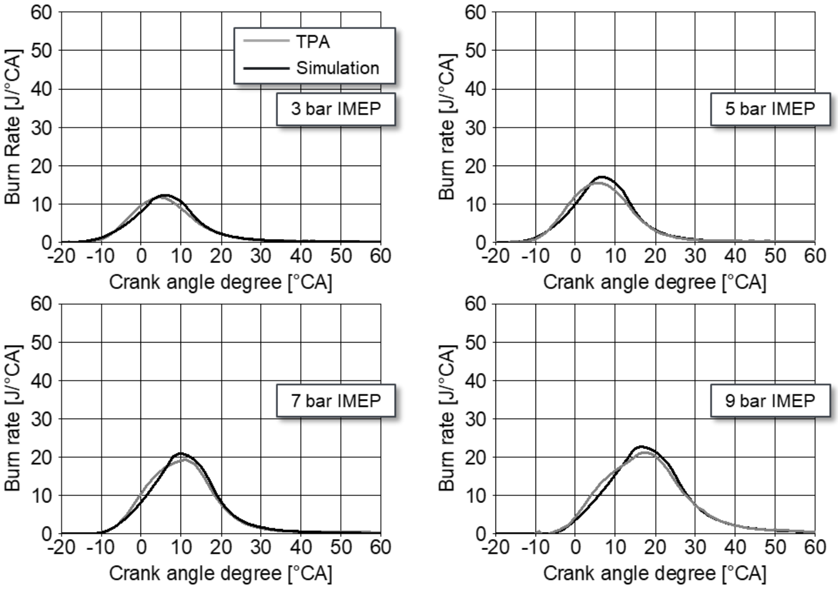

Figure 3.14. Burn rates with TPA and simulation for a load variation at 2000 RPM, lean combustion with $\lambda=1.5$ with the engine layout D

Another comparison of the TPA and simulation results is made for a load variation with the *engine layout D* at a constant λ of 1.5. The load is varied between 3 bar and 9 bar IMEP with 2 bar steps and results are shown in Figure 3.14. The model is calibrated for this investigation according to the two previously shown cases. At all loads, the simulation shows good agreement with the burn rates from the measurement.

3.2.2 Knock model

Load variation

For the prediction of mfb50%, the knock model is calibrated with the help of the load variation at 2000 RPM conducted with the engine layout A. According to the mfb50% during the load variation that are shown in Figure 3.15, there is a very good agreement between the measured and simulated values. For the shown behavior, the knock model parameter x_{ub} is calibrated only at a single operating point and no further correction of this parameter for different loads is necessary.

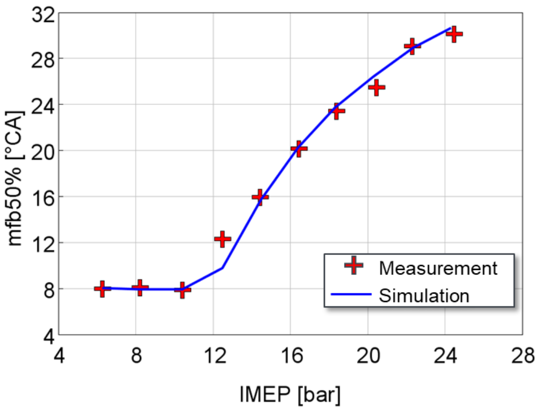

Figure 3.15. The measured and simulated center of combustion for a load variation at 2000 RPM, engine layout A

Water injection

The same load variation with the engine layout A with 100% water injection is used for the knock model calibration with water injection. In Figure 3.16, the measured and simulated mfb50% are compared. As in the previous case, the knock model parameter x_{ub} is constant throughout the load variation. However, the knock model underestimated knock behavior improvement with water injection and an adjustment of x_{ub} is found to be necessary. A similar adjustment is also applied later to the full engine models.

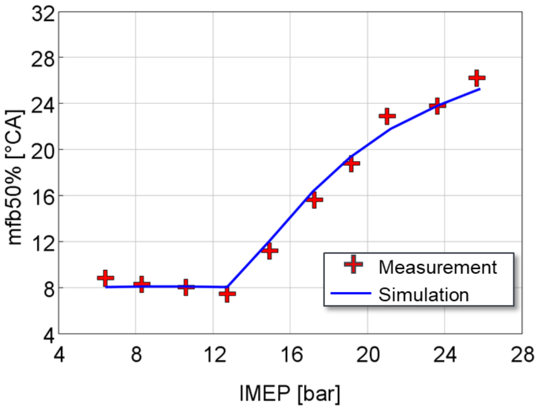

Figure 3.16. The measured and simulated center of combustion for a load variation at 2000 RPM with 100% water injection, engine layout A

EGR variation

Three operating points are considered for the calibration: 2000 RPM, 11 bar IMEP with tumble flap open (engine layout B) and closed (engine layout C) and 2500 RPM 16 bar IMEP (engine layout B). The previously mentioned operating point with 2250 RPM and 6.5 bar is not used, because no knock occurs at that load.

It is found that fitting x_{ub} values differ for different operating points and EGR rates considerably. At 2000 RPM 11 bar, a linear dependency of x_{ub} on the EGR rate is suitable whereas at 2500 RPM 16 bar IMEP the dependency somewhat resembles of an exponential trend. In this operating point, the knock reduction capability of EGR is strongly underestimated by the uncalibrated model, so a very strong correction is necessary. A possible explanation for this behavior might be that the knock model overestimates the influence of increased pressure on knock sensitivity, if the pressure in combustion chamber is already high, as is the case for higher loads.

Nevertheless, the knock model calibration for EGR is conducted for each operating point separately and the mfb50% for 2500 RPM 16 bar IMEP and 2000 RPM 11 bar IMEP, both with open tumble flaps are shown in Figure

3.17. However, it should be noted that such a calibration is not useful for the following studies with the full engine model.

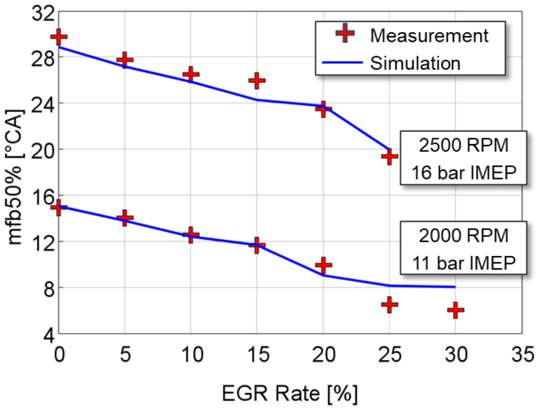

Figure 3.17. The measured and simulated center of combustion for an EGR variation for two operating points: 2500 RPM 16 bar IMEP (above), 2000 RPM 11 bar IMEP (below)

Since the conventional model calibration is not possible, a more pragmatic approach is necessary: Here, two points are considered:

1. Experimental data suggest that mfb50% improves by around 8°CA with around 25% EGR rate.
2. The predictive capabilities of Fandakov knock model for EGR get worse with increasing loads.

It is found that for the full engine models, a knock model calibration for lower and medium loads is possible while satisfying the first point. Also, the full engine models have very few operating points with EGR at higher loads. Therefore, the knock model is calibrated by only considering lower and medium loads and higher loads are simply omitted. With this approach, the usage of the Fandakov knock model is still possible while not causing any significant error during the further investigations.

At this point it should be explored, why the calibration of the knock model for EGR is proven to be challenging and why predicting the knock behavior with increasing EGR rates with 0D/1D simulation methods is overall a difficult task. The 0D/1D methods mainly only consider the average working cycle, i.e. quantities such as temperature, pressure are calculated for the average cycle and those values are processed further in other sub-models – in this case, in the knock model which determines the knock behavior. Therefore, the predictive capabilities of the models decrease with increasing cycle-to-cycle variations, because the conditions during an extreme cycle deviate more significantly than from the conditions at the average cycle. This is illustrated schematically in Figure 3.18. The knocking cycle is mostly the one with the earliest mfb50%, because at this cycle the temperature and pressure are the highest. For 0% EGR, the cycle-to-cycle variations are relatively low and the knocking cycle is very close to the average cycle. Therefore, the knock model can predict the knock behavior adequately even by considering the average cycle. However, with a higher EGR rate, the cycle-to-cycle variations increase and the knocking cycle is very different than the average cycle. As a result, if the knock model considers solely the average cycle in this case, it is natural that the prediction would not be accurate.

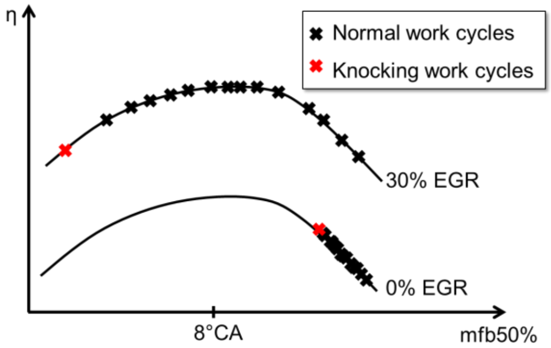

Figure 3.18. The effect of cycle-to-cycle variations on the distribution on working cycles and knock behavior

Lean combustion

The calibration of the knock model for lean combustion is challenging similar to the case with EGR with the difficulties grow with increasing λ. Therefore, it is decided that Fandakov knock model should not be used at all and another approach should be chosen.

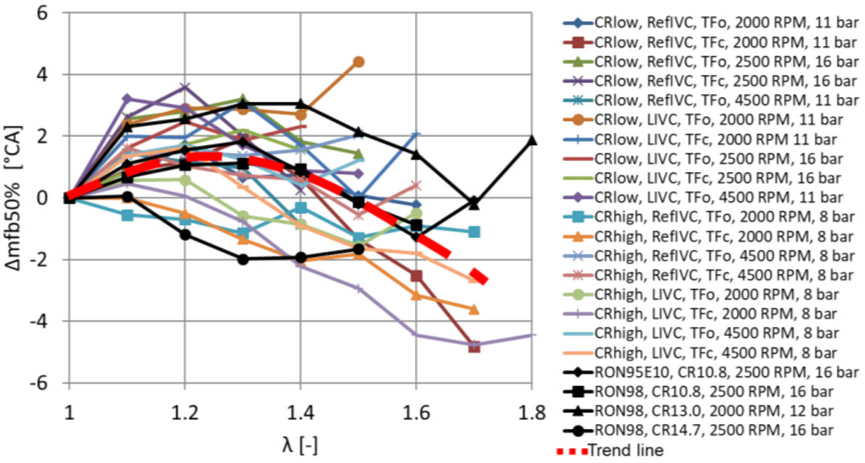

Figure 3.19. The change of center of combustion with increasing air-fuel equivalence ratio. Black solid lines are measurements VKA, the other solid lines from IVB. Red dashed line is the trend line that approximately shows the average observed knock behavior. CRlow = compression ratio of 12.42, CRhigh = compression ratio of 18, RefIVC = Reference intake valve closure, LIVC = Late intake valve closure, TFo = tumble flap open, TFc = tumble flap closed, fuel is RON95E10 if not stated otherwise, the value in bar is IMEP, the value following CR is the compression ratio.

In Figure 3.19, the behavior of mfb50% throughout λ variations for several configurations (including engine layouts apart from the engine layouts A-F) measured by IVB and VKA are summarized. Negative values indicate an earlier mfb50% in comparison to the mfb50% measured at $\lambda=1.0$, positive values a later mfb50%. Although the knock behavior varies considerably from configuration to configuration, a general trend can be observed, which is marked by the thick red dashed line. The results suggest that the knock tendency on average first increases then decreases with increasing λ.

For the prediction of the mfb50% at the full engine models for lean combustion, the following approach is used: An operating point is first simulated with $\lambda=1.0$ and the mfb50% is predicted with the help of the calibrated knock model. Then for the lean concept, the mfb50% is corrected. If for instance, the operating point has to be operated with $\lambda = 1.7$, the mfb50% should be around 2.5°CA better than the predicted mfb50% for $\lambda=1.0$.

3.2.3 Model calibration for alternative fuels

Methanol

For model calibration of methanol, a more direct approach is used and burn duration 10-90% are compared between measurement and simulation. Since the measurements are done with the engine of the VKA, which has different attributes and as a result very different burn durations, it should be determined in the first step, how the burn durations differ for gasoline and methanol. In Figure 3.20, the burn durations from the measurement with the engine layout E for gasoline and the engine layout F for methanol and model are shown. The turbulence level in the model is matched for gasoline so that the measured and simulated burn durations are very similar. Then methanol is also simulated with the same turbulence level, and it is found that a slight adjustment for an exact match of the methanol's burn durations is necessary.

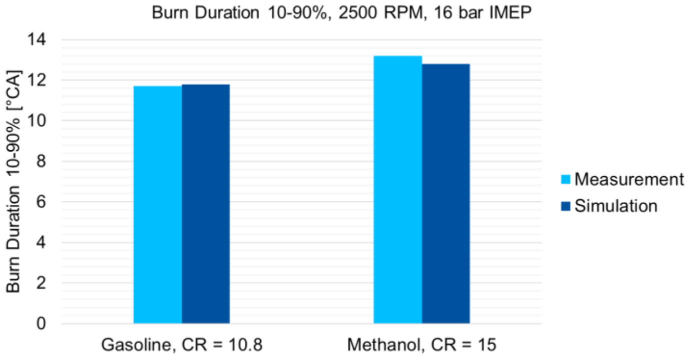

Figure 3.20. Measured and simulated burn durations for gasoline and methanol, 2500 RPM, 16 bar IMEP, gasoline with the engine layout E, methanol with the engine layout F

A more detailed model calibration for methanol is done through a λ variation in the operating point 2500 RPM 16 bar IMEP with the engine layout F. The comparison of the measured burn durations and burn durations acquired from the simulation are shown in Figure 3.21. For the good agreement shown in the diagram, both a slight model calibration for $\lambda=1$ for methanol as fuel (15% slowed down combustion) and a slight correction of the model parameters for increasing λ (15% quicker combustion for $\lambda=1.7$) is necessary. The correction with increasing λ is linear. The full engine models for the methanol are adjusted accordingly.

Due to lack of measurements with methanol with knock, no knock model is calibrated for methanol. However, the measurement data suggests, under what circumstances methanol can be operated knock-free. This information can be used to determine, what load-compression ratio combinations can be operated knock-free with methanol. Then a methanol engine model can be designed accordingly, which is then operated with 8°CA mfb50% all the times.

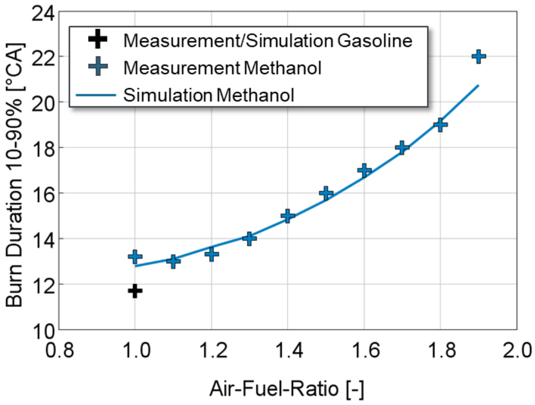

Figure 3.21. Measured and simulated burn durations for methanol for an air-fuel ratio variation, 2500 RPM, 16 bar IMEP with the engine layout F. The shown point for gasoline is at the same operating point with the measured and simulated with the engine layout E.

Blend G70M15E15

In this work, aside from gasoline and methanol, a blend fuel, which is a mixture of 70%v/v gasoline, 15%v/v methanol and 15%v/v ethanol -hence the name G70M15E15- is considered in a short study. For this short study, a quick and simple model calibration is conducted, which is to be described briefly. It is found that blend can be simulated well as gasoline in the model, but with slower burn durations and a higher knock resistance. For the calibration of the burn rate and knock models, the load variation at 2500 RPM is used, where the blend fuel is investigated with the engine layout F. The burn duration of the blend is around 25% higher than of the gasoline and its mfb50% increases around half the rate with the increasing loads even though the compression ratio during the investigation with the blend is by 4 units higher, as shown in Figure 3.22. The model parameters C_u and x_{ub} are matched to catch those similar trends. In fact, suitable model parameters could be found and a correction neither for burn rate nor for knock model for changing loads are necessary.

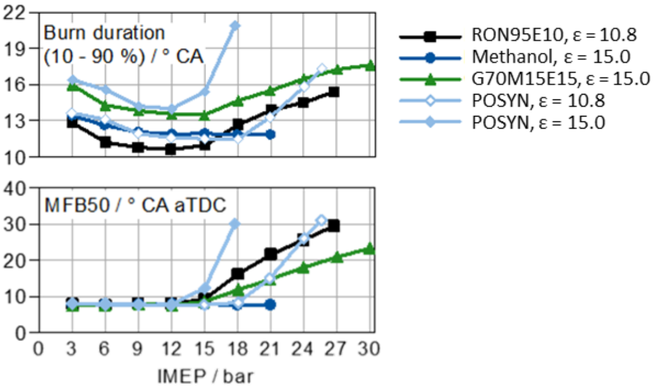

Figure 3.22. Measured burn durations and mfb50% for the blend fuel G70M15E15 with the engine layout F in comparison to other fuels for a load variation at 2500 RPM [29]

3.3 Full Engine Modeling and Calibration

The calibration of the remaining sub-models is conducted on a full engine model. In the following, the used methods should be described.

The full engine model is created based on the engine VW EA211 TSI evo [17]. It is a four-cylinder, 1.5-liter engine with a rated power of 96 kW and a maximum torque of 200 Nm. The engine has a compression ratio of 12.5, which can be considered as high for a SI engine. In order compensate for the high compression ratio and keep knocking under control, the engine is operated with a Miller strategy with a 150°CA opening event (>1mm valve lift) and variable valve timings. The engine also has cylinder deactivation so that two of the cylinders can be deactivated at lower loads. The stroke-to-bore ratio chosen for this engine is 1.15, which is above average and therefore worth mentioning. A further noteworthy feature is that due to an integrated water-cooled exhaust manifold, no enrichment at full load is necessary to lower exhaust gas temperatures, although the engine is equipped with a variable geometry turbocharger. The BSFC map of the engine is shown in Figure 3.23. This engine map should be used to calibrate the sub-models of the full engine model. The aim is to create a full engine model of VW EA211 TSI evo that delivers a stationary BSFC map that closely resembles this published BSFC map. The criterium here is good agreement for the three shown operating points as well as along the 240 g/kWh contour line.

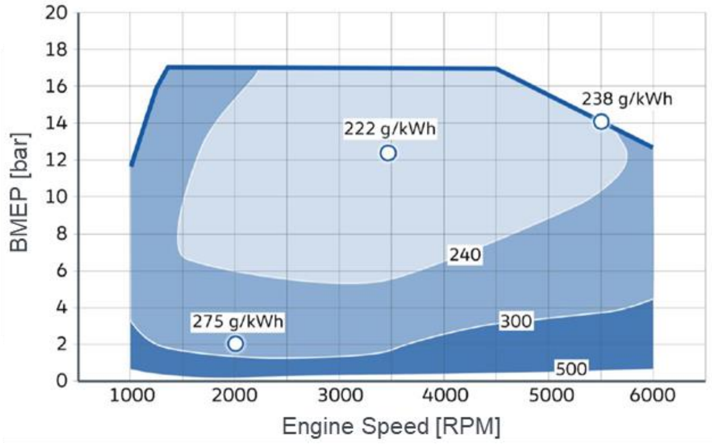

Figure 3.23. BSFC map of the Reference Engine VW EA211 TSI evo [17]

In the first step, the engine model is built in accordance to the features of the engine that are described in [17]. Then, the sub-models for the burn rate and knock are implemented according to the findings in the previous Chapter 3.2. Since the burn rate for this engine is unknown, a plausible value for the turbulence fluctuation C_u is assumed. Furthermore, for the knock model, a plausible initial value for x_{ub} is assigned which is to be calibrated in a later step. The FMEP map is generated with the help of two supporting points in accordance to the Fischer method that is built in in GT-Power. Then, the turbocharger matching is done in a way so that the full load points at 1300 RPM, 4500 RPM and 5500 RPM can be realized.

The following step is the optimization of the valve timings. The choice of the valve opening and closure timings, several criterions should be considered: The intake valve timing should be late enough to allow the necessary amount of intake air into the cylinder. It should also be as early as necessary in order to minimize the load exchange losses at lower loads (i.e. intake pressure should get as close to the atmospheric pressure as possible) and to maximize the knock resistance at higher loads (i.e. the mfb50% should get as close to 8°CA as possible). Also, the intake valve timings at very low loads should not be chosen as too early, in order to prevent an excessive amount of valve overlap, because otherwise the high amount of residual gas trapped in the cylinder will have a detrimental effect of the combustion and causing even misfires. Adjustments to the exhaust valve timings at these loads are also effective for decreasing the valve overlap and the amount of the residual gas in cylinder. Exhaust valve timings throughout the engine map is also to be optimized, however the effects on the efficiency are rather negligible and usually a moderate exhaust valve timing should be should be chosen.

The following step is the calibration of the wall heat model for the cylinder. For this, several operating points at lower loads are considered that are not knocking and the BSFC values of the model are compared with the published BSFC map of the engine, and a suitable multiplier for the wall heat losses is determined, which is assumed to be constant throughout the engine map.

The last step is the calibration of the knock model. Since the knock behavior of every engine is different, the determined knock model parameter x_{ub} values throughout the single cylinder engine calibration may or may not be suitable for the currently discussed engine and its full engine model. The knock model of the full engine model is calibrated at higher loads where the engine is certainly knocking by comparing the BSFC values from the simulations and from the published BSFC map. As a result of this comparison, a suitable x_{ub} value is determined that is assumed to be constant throughout the engine map.

It should be noted that despite of a step by step description of the model generation, optimization and calibration processes, in reality an iterative process is necessary. For example, knock model influences the knock behavior and thus the mfb50%, which influences the exhaust temperature which affects the turbocharger in a way that the size of the turbocharger must be adjusted in order to realize the low-end-torque. But then, some of the valve timings must be readjusted for optimal efficiency, which then in turn affects the knock behavior etc.. The stationary BSFC map of the resulting engine model is shown in Figure 3.24.

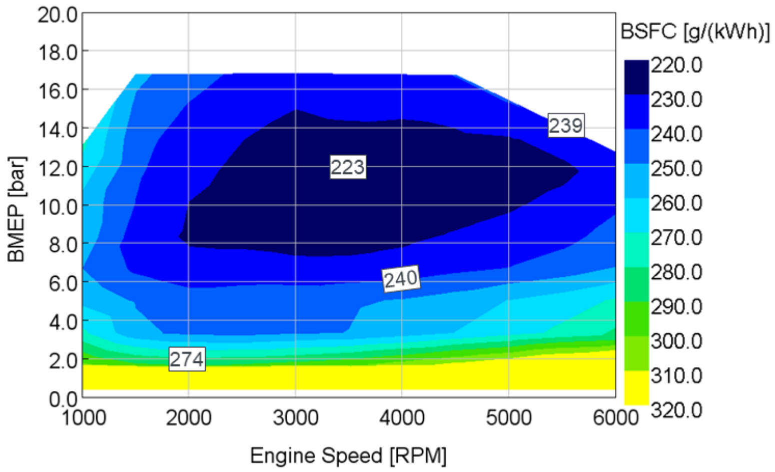

Figure 3.24. Simulated BSFC map of the VW EA211 TSI evo model

A comparison of the published BSFC map in Figure 3.23 and the simulated BSFC map in Figure 3.24 shows an excellent agreement. The model can predict the fuel consumption of the three shown operating points (low load, best BSFC and rated power) on the with a precision of ±1 g/kWh. There is also a very good agreement along the 240 g/kWh contour.

This engine model serves as a starting point for the generation of further models of highly advanced, highly efficient engines, which are equipped with further technologies. In the case of these models, the model parameters are kept same, but expanded if necessary in case of EGR, lean combustion or water injection in accordance to the investigations with the single cylinder engine models. The wall heat losses are also slightly adjusted in case of EGR and lean combustion in order to reflect the expected efficiency increase better. A high turbulence concept in the models is realized by a further increase of turbulence level and a simultaneous decrease of the discharge coefficient of the intake valves in order to simulate the effects of the adjusted geometries of the intake ports. The friction model calibration remains unchanged as the specific loads and the engine speeds of the two supporting points are stays the same. In accordance to the considerations in Chapter 3.1.2, the friction model is neither affected by downsizing nor by changing stroke-to-bore ratios. The turbocharger is also to be fitted for changing boost pressure demands of different engines. Especially in case of downsizing, a higher boost pressure is necessary for the same air mass flow and therefore a smaller turbocharger becomes more suitable to avoid the pumping limit. Also, the efficiencies of the turbochargers for the highly technological engines is increased in accordance to the discussion in Chapter 3.1.2.

The process of optimization of the valve timings is different due to the presence of EGR or lean concept as well as a variable compression ratio. The optimal trio of the compression ratio, variable valve timing and EGR rate must be determined for each operating point by an iterative process. Here, it is recommended starting with the variable valve timings and continuing with the EGR. In the case of lean concept, no optimal air-fuel-ratio is determined since the air-fuel-ratio is very limited by NOx emissions from below and flame stability from above. Here, the first necessary step is to determine, up to which loads an operation with lean concept is possible before proceeding with the optimization process. Also, since the knock model for the lean concept cannot be used, the mfb50% values must be determined in a separate stoichiometric engine model, which then are corrected and adapted in the lean engine model in accordance to the discussion in Chapter 3.2.2.

4 Investigations of Engine Concepts

Over the course of this research project, a number of full engine models are created. The most significant of those are listed below:

- The “Reference Engine” model is modeled after the state-of-the-art VW EA211 TSI evo engine. It serves mainly as a basis for comparisons. It is suitable for C-segment vehicles.
- The “High Efficiency Engine” (HEE) is equipped with various technologies for enhancing the efficiency. It has the same rated power and maximum torque as the Reference Engine.
- The “A-Segment Engine” is a smaller version of the High Efficiency Engine with lower rated power.
- The “J-Segment Engine” is a larger version of the High Efficiency Engine with higher rated power.
- The “Methanol Engine” has the same technologies as the High Efficiency Engine, but uses methanol instead of RON95E10.
- The “Blend Engine” has the same technologies as the High Efficiency Engine, but uses G70M15E15 as fuel. It is only optimized along 2500 RPM for a short study.
- The “Full Load Water Injection Engine” (FLWI Engine) substitutes the complex and costly technology of variable compression ratio at the High Efficiency Engine with water injection at full load.
- The “Lean High Efficiency Engine” is similar to the High Efficiency Engine, but is operated at lower loads under lean conditions and does not have EGR.
- The “Lean Full Load Water Injection Engine” is similar to the Full Load Water Injection Engine, but is operated under lean conditions at lower loads and does not have EGR.

- The “Lean Methanol Engine” is similar to the Methanol Engine, but is operated under lean conditions for the most part of its engine map and does not have EGR.

A more detailed overview of these engine models along with the present technologies are shown in Table 4.1 and Table 4.2. In the following subchapters, the listed engine models are introduced, the potential of achievable benefits are illustrated. Furthermore, the individual technologies as well as their combinations that leads to those efficiency advantages are assessed with the help of these engines.

The development of the engine concepts was accompanied by Kuznik et al. from VKM of the University of Darmstadt during the FVV research project “ICE2025+: Ultimate System Efficiency”. Their task was to use efficiency maps generated during this work and to run certain maneuvers and driving cycles with full vehicle simulations, while testing and comparing different hybrid architectures. Their feedback, what the power and the low-end torque requirements are and in which engine map regions the efficiencies must be prioritized, supported decision making processes throughout this work. Their methods and results in detail can be found in the end report of the research project [29].

Table 4.1. Overview of the engine models. The present technologies are marked with the symbol "x".

Engine	VW EA211 TSI evo	High Efficiency Engine	A-Segment Engine	J-Segment Engine	Methanol Engine
Fuel	RON95 E10	RON95 E10	RON95 E10	RON95 E10	Methanol
Displacement [cm^3]	1500	1000	700	1500	1000
Number of cylinders	4	4	3	4	4
Torque [Nm]	200	200	140	300	200
Power [kW]	96	96	67	144	144
Stroke [mm]	85.9	75.1	73.2	95.5	75.1
Bore [mm]	74.5	65.1	63.7	70.1	65.1
s/b	1.15	1.15	1.15	1.35	1.15
CR	12.5	8…19	8…19	8…19	12.7…19
Cylinder deactivation	x	x	x	x	x
Variable valve timings + Miller	x	x	x	x	x
High turbulence concept		x	x	x	x
Aggressive downsizing		x	x	x	x
Variable compression ratio		x	x	x	x
EGR		x	x	x	x
Lean concept					
Water injection					

Table 4.2. Continuation of Table 4.1: Overview of the engine models. The present features are marked with the symbol "x".

Engine	Blend Engine	FLWI Engine	Lean High Eff. Engine	Lean FLWI Engine	Lean Methanol Engine
Fuel	G70E15 M15	RON95 E10	RON95 E10	RON95 E10	Methanol
Displacement [cm^3]	1000	1000	1000	1000	1000
Number of cylinders	4	4	4	4	4
Torque [Nm]	200	200	200	200	200
Power [kW]	96	96	96	96	96
Stroke [mm]	75.1	75.1	75.1	75.1	75.1
Bore [mm]	65.1	65.1	65.1	65.1	65.1
s/b	1.15	1.15	1.15	1.15	1.15
CR	12.7…19	13.5	8…19	13.5	12.7…19
Cylinder deactivation	x	x	x	x	x
Variable valve timings + Miller	x	x	x	x	x
High turbulence concept	x	x	x	x	x
Aggressive downsizing	x	x	x	x	x
Variable compression ratio	x		x		x
EGR	x	x			
Lean concept			x	x	x
Water injection		x		x	

4.1 Reference Engine

The Reference Engine chosen for the studies is VW EA211 TSI evo [17]. The engine as well as how it is modeled are already described in Chapter 3.3. Due to its many modern features the engine is considered state-of-the-art and can achieve very good efficiencies. The engine model is used to generate the efficiency map, which is shown in Figure 4.1. The operating points which are used to generate the map are also shown in the same figure. The choice of operating points remains similar throughout this work: Equidistant 10% load and 500 RPM speed steps. Further maps for different quantities such as intake pressure, maximum pressure, mfb50%, burn duration etc. can be found in Appendix (for the Reference Engine as well as for the other engines).

According to the efficiency map, the engine reaches a peak efficiency of 38.4%. One noteworthy feature that is recognizable at the map is the relatively high efficiencies along the 40 Nm load, which has a similar level to the efficiencies at 60 Nm. This is due to application of the cylinder deactivation at 40 Nm and below.

The model of the Reference Engine and its efficiency map serve as starting point for the numerous investigations as well as for several engine models. In the following, these investigations will be presented.

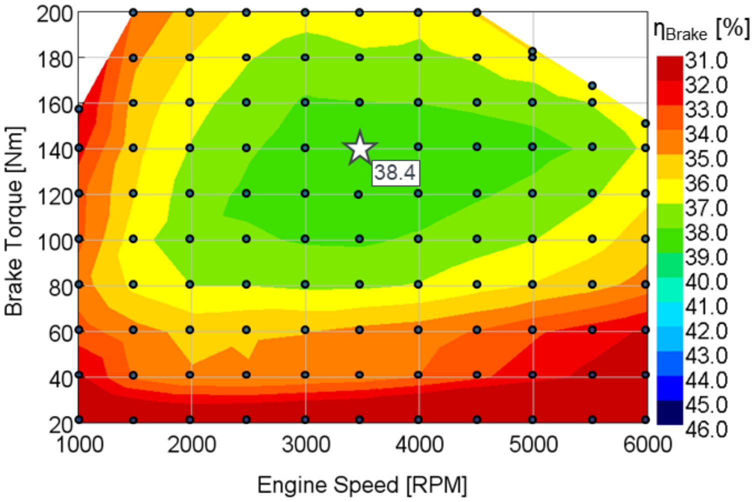

Figure 4.1. Simulated brake efficiency map of VW EA211 TSI evo. The dark blue dots represent the operating points that are simulated to generate the map.

Investigations with the Reference Engine

In this step, some of the previously introduced technologies should be assessed using the Reference Engine model. This objective of this assessment is not only to demonstrate how much a full engine would benefit from these technologies but also to figure out what measures should be used for designing engines with higher efficiencies.

Cylinder deactivation

For the investigation of the benefits through cylinder activation, operation with cylinder deactivation is compared at low loads with the operation without cylinder deactivation. For the operation without cylinder deactivation, an earlier intake valve closure timing is chosen in order to minimize the throttling losses. In other words, the best efficiencies achievable with and without cylinder deactivation are compared with each other. This comparison can be seen in Figure 4.2.

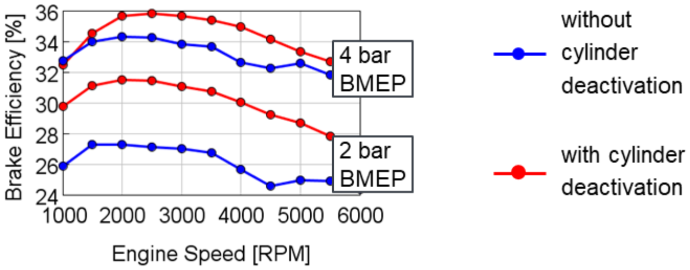

Figure 4.2. The effect of cylinder deactivation on efficiency at two different loads

Cylinder deactivation is found to be desirable at loads lower than around 4 bar BMEP (approx. 25% load) for this engine. In Figure 4.2, the benefits through cylinder deactivation for 2 bar BMEP and 4 bar BMEP are shown. The efficiency benefit at 2 bar BMEP is approximately 15%[1]. At 4 bar BMEP, the cylinder deactivation leads to around 5% better efficiency at engine speeds greater than 2000 RPM.

Miller strategy, variable valve timings

For demonstrating the benefits of Miller strategy with variable valve timings, optimal valve timings are compared with a valve timing where the intake valve is opened around the TDC and closed around BDC enabling the maximal air flow during the intake (i.e. the reference valve timing). For this investigation, two operating points are chosen at 2000 RPM with 60 Nm and 200 Nm loads. At the low load point, no knocking is present, so the benefits are through lower throttling losses. Here, the intake valve is opened and closed 45°CA before the reference valve timing. At higher load, the knock reduction potential through Miller strategy is demonstrated. Here, the intake valve is opened and closed 35°CA before the reference valve timing. The results are shown in Figure 4.3. At the operating point with 60 Nm, the optimal valve timing enables an efficiency increase of almost 6%. At 200 Nm, the improvement is 10%, which is a result of a 9°CA earlier mfb50%.

---

[1] All efficiency changes, improvements, comparisons etc. in this work -unless mentioned otherwise- are given in relative values.

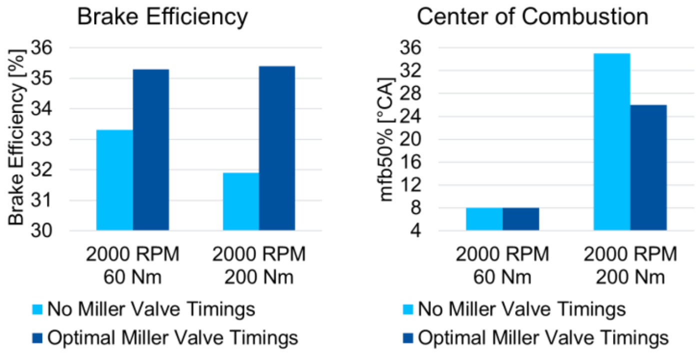

Figure 4.3. The effect of early intake valve closure on efficiency and knock resistance at two different operating points

Downsizing

For the investigation of downsizing, the displacement volume of the engine is reduced from 1.5 liters to 1.0 liter, while keeping the stroke-to-bore ratio, the maximum torque and nominal power constant. In this case, the downsizing leads to a very high power density with a maximum BMEP of greater than 25 bar. However, it is found that this would not be achievable because of the knock limitations. For argument's sake, the compression ratio at higher loads (>120 Nm) is lowered as a temporary solution in order to keep knocking under control and an efficiency map is generated. The efficiency map of this hypothetical downsized engine model is shown in Figure 4.4.

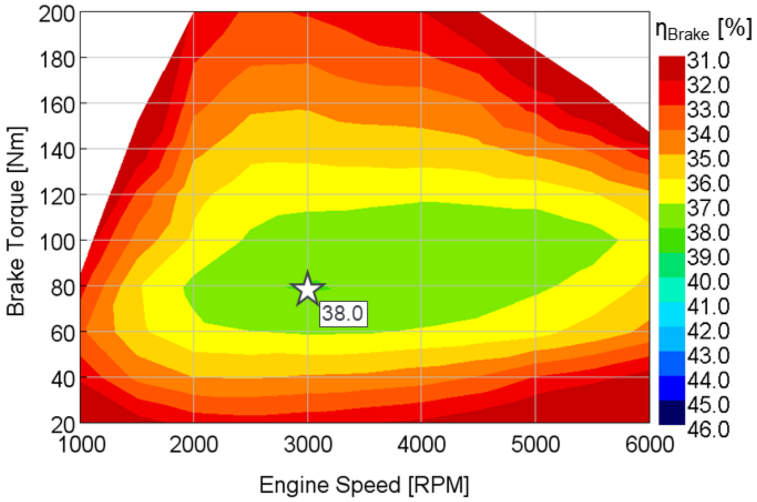

Figure 4.4. The efficiency map of the hypothetical downsized engine

In comparison to the Reference Engine model, the peak efficiency drops slightly by around 1%. However, as the high efficiency window shifts from 120-140 Nm to 80-100 Nm, the efficiency at lower loads becomes significantly better as well. For example, the efficiency increases at 2000 RPM 60 Nm by 4% and at 2000 RPM 20 Nm by 9%. According to the distribution of operating points shown in Figure 2.4, it is expected that the overall efficiency of the engine should profit from this downsizing. The assessment of VKM could also confirm that the proposed downsizing would lead to a better overall efficiency during a WLTC cycle. This result suggest that downsizing would be a step in the right direction. Furthermore, it shows that the emphasis should be put on increasing the efficiencies at lower loads. However, it should be noted that such an aggressive downsizing is only possible if combined with an additional measure such as variable compression ratio.

A further question is the optimal number of the cylinders for the downsized engine. For this, a three-cylinder version of the same downsized engine is also modeled. For a fair comparison, the stroke of the cylinders is kept constant. That way, the average piston speed remains constant and the total area of the intake valves is very similar so that a similar Miller strategy can be used throughout the entire engine map. The three-cylinder engine has slightly less wall heat losses due to decreased wall area and as a result slightly better efficiencies for some portions of the engine map. On the other hand, the cylinder deactivation strategy becomes less beneficial, since it is assumed that the three-cylinder engine should also run with two cylinders in case of a cylinder activation. As an example, the efficiency at 2500 RPM for both four-cylinder and the three-cylinder engines are shown in Figure 4.5.

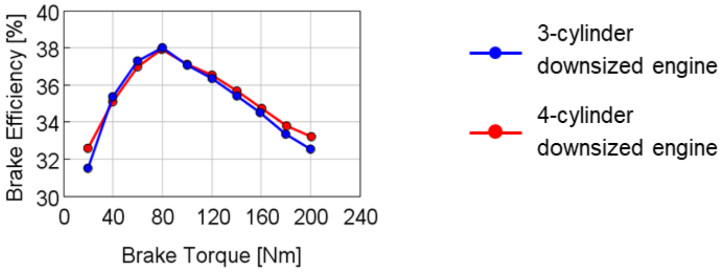

Figure 4.5. Comparison of efficiencies of for three and four-cylinder downsized engines at 2500 RPM

The efficiency of four-cylinder version is significantly higher at loads lower than 40 Nm due to the more efficient cylinder deactivation strategy. Between 40 and 80 Nm, the three-cylinder version has better efficiencies, but the benefit is less than 1%. For higher loads, the four-cylinder version is slightly better again, due to a slightly better knock behavior, but it is likely that the better knock behavior is a result of an expected inaccuracy of the model rather than of an actual improvement of knock resistance. The studies with WLTC simulations at VKM also showed that the four-cylinder version is efficiency-wise better, although the difference is rather negligible. Therefore, it can be concluded that in case of a downsizing, a reduction of number of cylinders is not necessary.

4.2 High Efficiency Engine

In the next step, it should be demonstrated, how much the efficiency of an engine can be improved, if it would be equipped with more advanced features. Therefore, the High Efficiency Engine model is created. The High Efficiency Engine must prove better efficiencies and also must have a better overlapping of the high efficiency window and the operating window in comparison to the Reference Engine. For a fair comparison of the Reference Engine and the High Efficiency Engine, both engines must have the same rated power and same maximum torque. Also, the same fuel (RON95E10) must be used.

For the development of the High Efficiency Engine, the Reference Engine model serves as a starting point. As shown above, the technologies that are already present in the Reference Engine prove to have significant advantages and therefore retained in the High Efficiency Engine. Also, downsizing is applied and the displacement volume is reduced to 1.0 liter and the number of cylinders is kept at four. As discussed, the downsizing is complemented by the technology of variable compression ratio. Furthermore, the engine is equipped with the high turbulence concept for better knock resistance, which enables burn durations comparable to the values observed during the measurements of VKA of the RWTH Aachen University. An external, cooled, high pressure EGR is also used for further enhancement of the efficiency. In the following steps, the turbocharger is matched and the valve timings, the EGR rates and compression ratios for each operating point are optimized for best efficiency. The resulting efficiency map of the High Efficiency Engine is shown in Figure 4.6.

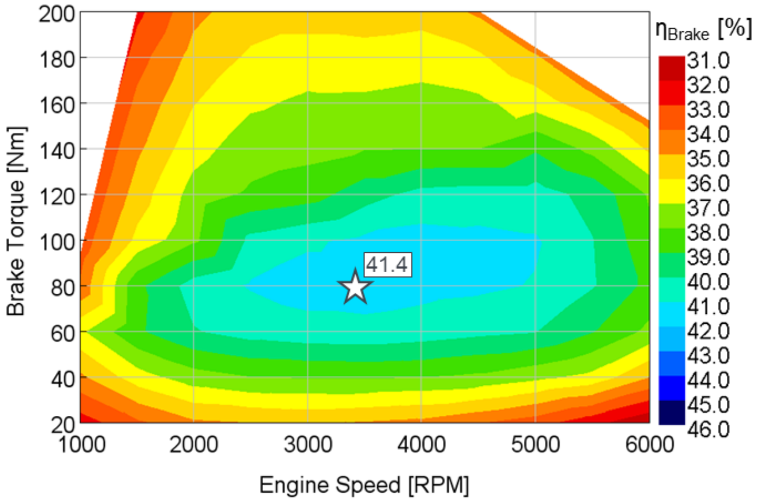

Figure 4.6. The efficiency map of the High Efficiency Engine model

As a result of the improvements, the peak efficiency of the High Efficiency Engine reaches the value of 41.4%, which is an approx. 7% relative increase in comparison to the Reference Engine. Also, the high efficiency zones of the engine map are shifted towards lower loads as a result of the downsizing. In Figure 4.7, the relative change of efficiency going from the Reference Engine to the High Efficiency Engine is shown. At low to middle loads and low to middle engine speeds, where the engine would be generally operated most of the time, the efficiency is approximately 10% higher on average. At higher loads, the efficiency gets slightly worse, because variable compression ratio and high turbulence concept cannot totally compensate for the aggressive downsizing and thus increasing knock tendency at higher loads.

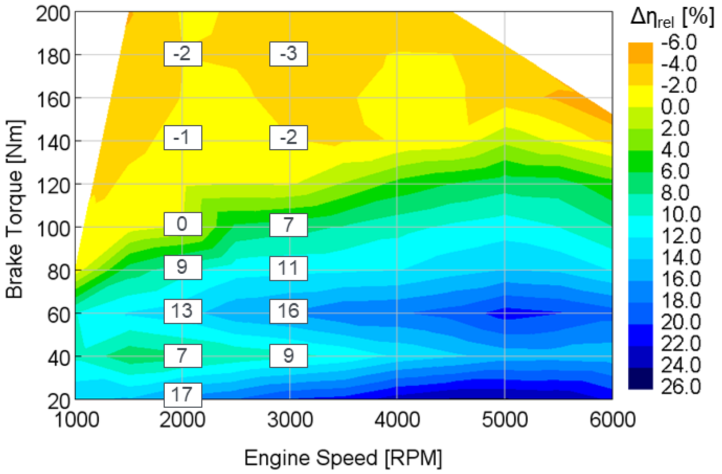

Figure 4.7. The relative difference in brake efficiency of the High Efficiency Engine in comparison to the Reference Engine (VW EA211 TSI evo). Green and blue indicate, that the High Efficiency Engine is better. Yellow and orange indicate that the Reference Engine is better.

The EGR map of the High Efficiency Engine is shown in Figure 4.8. At higher loads, EGR is not possible due to intake pressure being higher than the exhaust pressure. At lower loads, EGR is found to be advantageous and therefore utilized. However, the trade-off between EGR and Miller strategy is worth mentioning: If EGR were not present in the engine, a more aggressive Miller strategy could have been used, i.e. the intake valves could have been closed earlier. At a given operating point, the intake mass increases with increasing EGR rate and therefore a milder Miller strategy must be chosen. Otherwise it is not possible to reach the necessary air mass during the intake and the desired load cannot be realized. Therefore, usually a compromise between Miller strategy and EGR rates has to be found for optimal efficiencies. The optimal values for EGR rate in this given engine mostly lie between 20% and 30% and it is usually combined with a moderate Miller strategy.

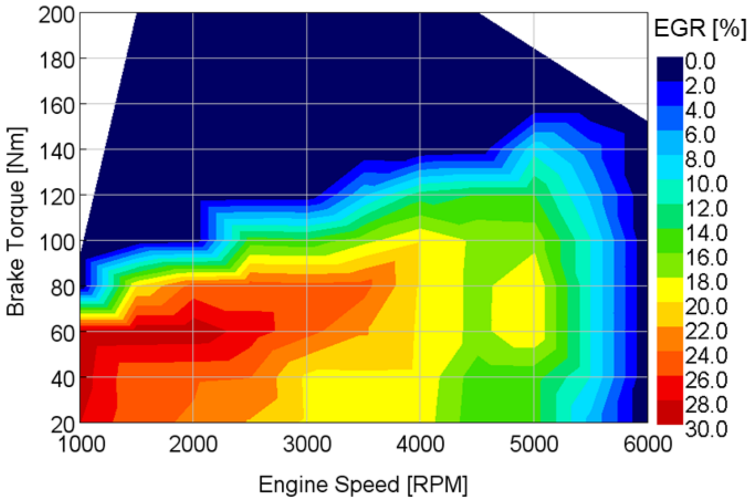

Figure 4.8. EGR rate map of the High Efficiency Engine

The map of the compression ratios of the High Efficiency Engine in Figure 4.9 shows the optimal compression ratios for each operating point. In general, the higher the knock tendency is, the lower the compression ratio should be. In other words, with decreasing loads and increasing engine speeds, the compression ratio is increased. The exception is at very low loads. A high compression ratio leads to higher friction losses, which plays a more significant role at lower loads. Therefore, at lower loads a more moderate compression ratio is more suitable. The compression ratios of the High Efficiency Engine vary between 8 and 19 throughout the engine map. At low-end torque, the value as low as 8 is optimal, because of the high knock tendency. Values higher than 19 could have been desirable at some regions of the engine map from a thermodynamic point of view, however would not be possible due to the collision of the piston with the spark plug and/or valves.

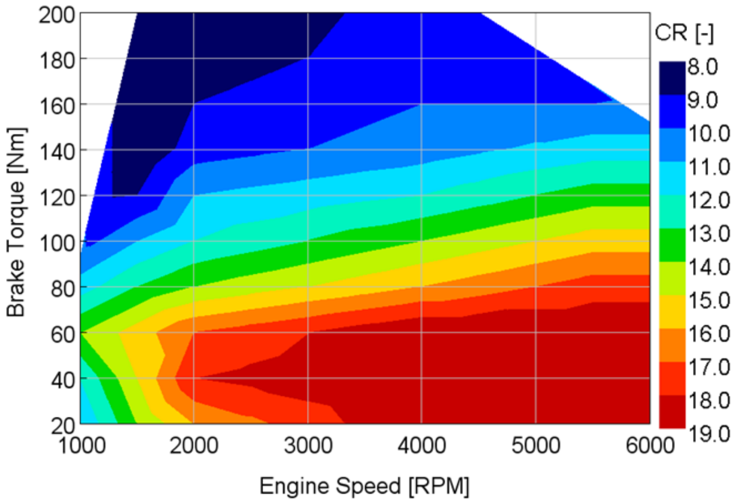

Figure 4.9. Compression ratio map of the High Efficiency Engine

Investigations with the High Efficiency Engine

The remaining technologies that have been introduced previously will be investigated with the help of the High Efficiency Engine.

Friction losses

There is no measure to directly decrease the friction losses in the High Efficiency Engine. However, the friction losses differ from the Reference Engine and this is mainly due to two factors: The downsizing and the (variable) compression ratio. The downsizing leads to a decrease of the friction losses despite an increase in FMEP in individual operating points. The variable compression ratio system itself is assumed not to influence the friction losses, but with increasing compression ratio, the friction losses increase as well.

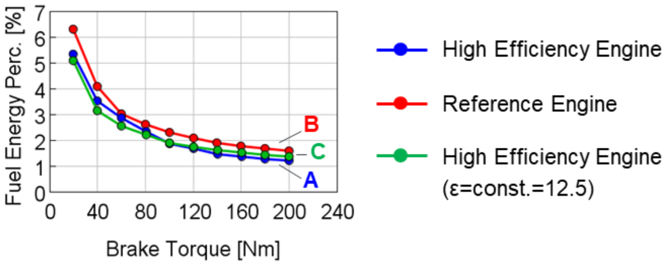

Figure 4.10. Friction losses as the percentage of fuel energy, for the Reference Engine, the High Efficiency Engine and for the High Efficiency Engine with a constant compression ratio of 12.5 (same as the Reference Engine)

The influence of the downsizing and the different compression ratios on friction losses is illustrated in Figure 4.10, where the friction losses are shown as the percentage of the fuel energy along the 2000 RPM. Line A shows the friction losses of the High Efficiency Engine and Line B of the Reference Engine. Furthermore, Line C shows the friction losses of the High Efficiency Engine, if it had a constant compression ratio of 12.5 - same as the Reference Engine. The comparison of lines B and C reveals the influence of downsizing, whereas the comparison between A and C demonstrates the influence of different compression ratios. Overall, the High Efficiency Engine has lower friction losses than the Reference Engine, with benefits increasing towards lower loads.

High turbulence concept

For demonstration of the effects of the turbulence level, a load variation is performed on the engine model at 2000 RPM. In order to be able to evaluate the high turbulence concept in isolation, the compression ratio is kept constant at 12.5 and no EGR is used. A comparison of the results of high turbulence concept and normal turbulence level is shown in Figure 4.11, where diagrams for burn durations (BD 10-90%), mfb50%, and efficiency are illustrated.

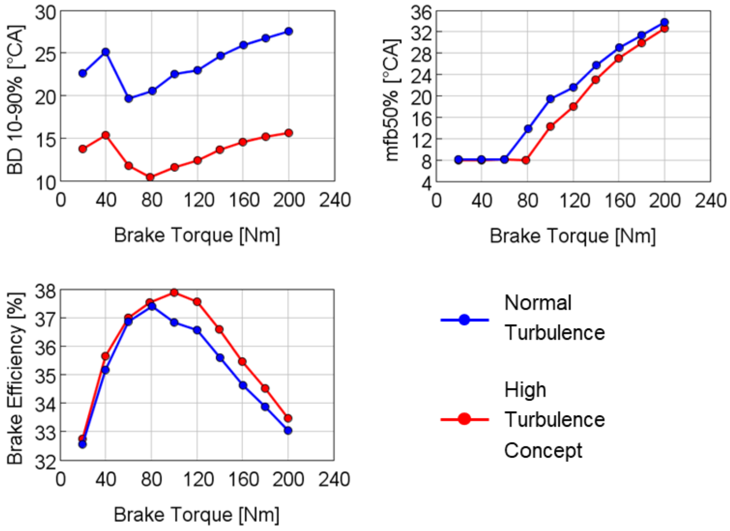

Figure 4.11. Effects of the high turbulence concept on burn durations, center of combustion and brake efficiency

The shorter burn duration leads to almost no efficiency advantage at lower loads as long as no knocking occurs. Some advantage is evident, if mfb50% can be improved by the high turbulence concept. In this case, the efficiency can be improved by approx. 2%. Overall, the benefits through the high turbulence concept alone are modest.

High turbulence concept in combination with variable compression ratio and EGR

The true advantages of the high turbulence concept are revealed, only when it is combined with other technologies.

The first synergy effect can be observed during the combination with the variable compression ratio. In Figure 4.12, mfb50% and efficiency are shown as a function of compression ratio for two different turbulence levels at the operating point of 2000 RPM and 60 Nm. With a normal turbulence level, efficiency can be increased by 2%, if the compression ratio would be increased from the reference value of 12.5 to the optimal value of 15. With the high turbulence concept, the compression ratio can be increased up to 17 for optimal efficiency due to better knock resistance. In this case, the efficiency is increased by 4%.

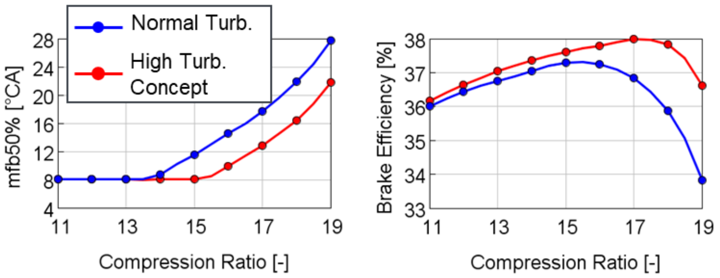

Figure 4.12. Effect of compression ratio on knock behavior and efficiency for two different turbulence levels

A second synergy effect becomes apparent during the combination of the high turbulence concept and EGR. Typically, with increasing EGR rates, problems arise such as increased burn durations which results in incomplete and instable combustion. Also, a too long burn duration means that the combustion takes a form which resembles a nearly isobaric heat addition, which has a further detrimental effect on efficiency. These effects can be counteracted very effectively with a higher turbulence level. In Figure 4.13, BD 10-90%, mfb50% and efficiency are shown as a function of EGR rate for two different turbulent levels at the same operating point of 2000 RPM and 60 Nm. The valve timings are kept constant with changing EGR rates and represent a mild Miller strategy. The compression ratio is chosen optimally and is 15 for normal turbulence and 17 for high turbulence concept. Due to the described effects above, increasing the EGR rate above 25% for the normal turbulence proves to be counterproductive. The higher EGR tolerance with the high turbulence concept makes EGR rates up to 34% desirable, which leads to an almost 10% increase in efficiency, contrary to a more modest 5% increase with the normal turbulence.

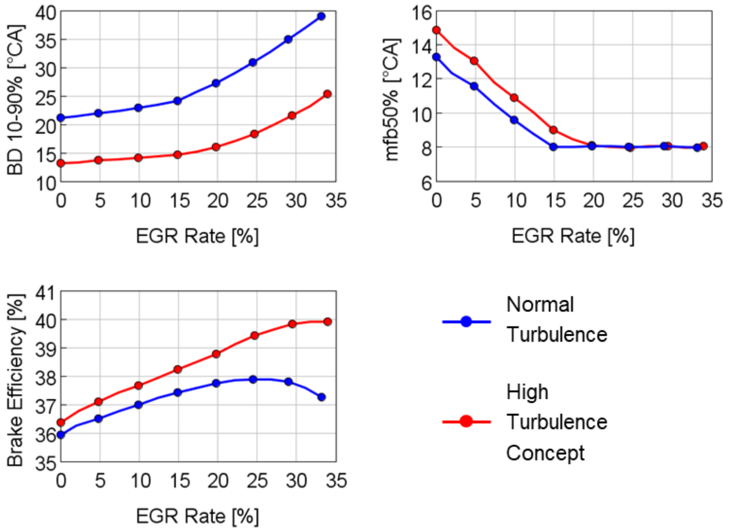

Figure 4.13. Effect of EGR on burn duration, knock behavior and efficiency for two different turbulence levels

In summary, the advantages of variable compression ratio and EGR are approximately doubled, if the high turbulence concept is used.

Trade-off between EGR and Miller

Although Figure 4.13 suggest an almost 10% improvement with EGR, this result does not reflect the real benefit through EGR at the considered engine, since many of the benefits of EGR can also be achieved with variable valve timings, i.e. Miller strategy. For a correct assessment of the benefits with the EGR, it is more appropriate to vary the EGR rate and the valve timing simultaneously -in contrary to the previous study, where the valve timing is kept constant and the EGR rate is the only value that is varied. The point is, a lower EGR rate allows an earlier closure of the intake valve. The results for a simultaneous variation of EGR and the valve timing an investigation is shown in Figure 4.14. The results with the constant valve timings from Figure 4.13 are also plotted as dashed lines for a comparison.

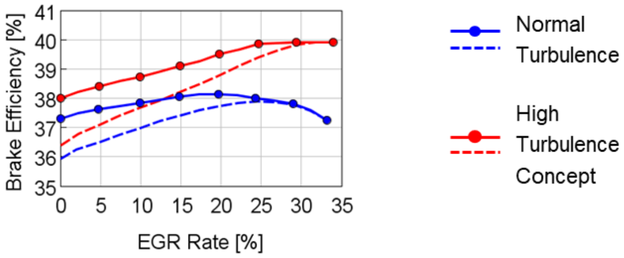

Figure 4.14. Effect of EGR on efficiency, if optimal valve timings are chosen for each EGR rate (solid lines) and if the valve timings are kept constant throughout the EGR variation (dashed lines).

The results suggest that at 0% EGR rate, the aggressive Miller strategy already allows a significant improvement of the efficiency. In fact, for the normal turbulence level, the benefits with the Miller strategy almost matches the benefits through EGR, which makes EGR in this given case almost superfluous. For a high turbulence concept, the benefits through EGR are around 5% and still significant. In other words, EGR is a very good addition for an engine with a high turbulence level, but not necessarily for an engine with a normal turbulence level, especially if this engine is fitted with variable valve timings.

Stroke-to-bore ratio

For the dimensioning of the High Efficiency Engine, one important question is, how the stroke-to-bore ratio should be chosen or more specifically why a higher stroke-to-bore ratio than in the Reference Engine would not be suitable. This is illustrated in Figure 4.15 with the help of a stroke-to-bore variation at two operating points. During this variation, the displacement volume is kept constant.

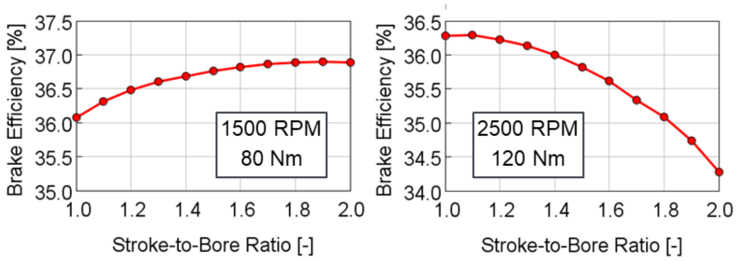

Figure 4.15. Effect of stroke-to-bore ratio on efficiency at two different operating points

At the operating point 1500 RPM and 80 Nm, the efficiency increases with increasing stroke-to-bore ratio as expected, since both the knock tendency and the wall heat losses are decreased as predicted. More interesting is the operating point with a somewhat higher engine speed of 2500 RPM and a somewhat higher load of 120 Nm, where the trend is reversed and does not conform with the expectations anymore. Therefore, a more detailed discussion of the results is necessary: With increasing stroke-to-bore ratio and a constant displacement volume, the bore gets smaller. As a result, the valves must be dimensioned smaller as well. This leads to a more challenging gas exchange. The direct drawback is therefore the increased pumping losses. A secondary effect is that it is no longer be possible to operate the engine with an aggressive Miller strategy because the required charge air mass can no longer be reached. A milder Miller strategy leads however to an increased knock tendency. The described effect (i.e. trade-off between a more aggressive Miller strategy and a higher stroke-to-bore ratio) is present at both operating points, but the effects are rather uncritical at 1500 rpm and 80 Nm due to lower air requirement and increased time for the gas change. The higher the engine speeds and the loads are, the more problematic a high stroke-to-bore ratio becomes. For similar reasons, the power density of the engine has to be decreased with increasing stroke-to-bore ratio, because the boost pressure has to be too high in order achieve the same load with smaller valves. For the reasons described, it is not advantageous to choose stroke-to-bore ratio much greater than unity for the High Efficiency Engine. In fact, the value of 1.15 as in the Reference Engine yielded the optimal results.

In conclusion, the investigations with the High Efficiency Engine suggest that with additional technologies and an aggressive downsizing a significant improvement in comparison to state-of-the-art engines is possible. Next, alternative solutions and additional ways for further efficiency improvement should be discussed with the help of various engine models.

4.3 A-Segment Engine

The A-Segment Engine has the same technologies as High Efficiency Engine for the C-Segment, but has a smaller displacement volume, lower rated power and maximum torque. The chosen dimensions for this engine are 700 ccm and the engine has three cylinders instead of four. The rated power is 64 kW and the maximum torque is 140 Nm, therefore the power density of the engine is same as the High Efficiency Engine. The turbocharger is also fitted to match lower mass flows and has a smaller diameter. The cooling of the exhaust manifold is adapted to become weaker, otherwise the exhaust gas enthalpy would be too low for the turbocharger. The reason is the thinner pipes in the smaller engine has a higher surface-to-volume proportion and the heat is therefore transferred more quickly away from the exhaust gas. A further change is the cylinder deactivation strategy, where only one cylinder is deactivated. Further changes include the optimization of valve timings, compression ratios and EGR rates for the new engine dimensions and boundary conditions. The stroke-to-bore ratio is kept constant at 1.15.

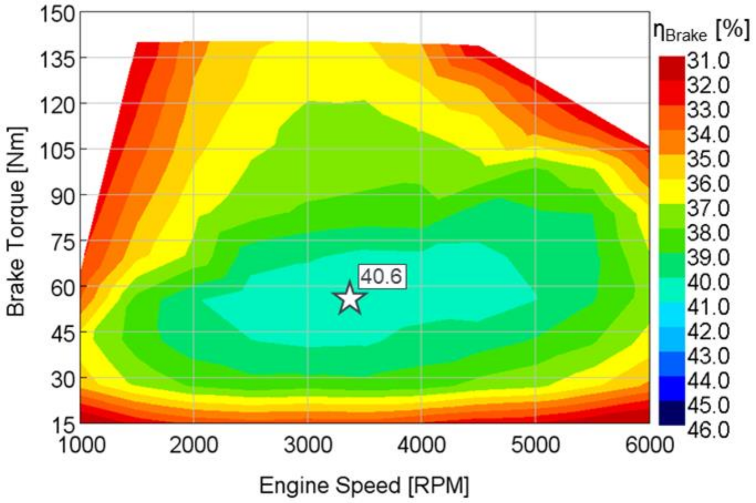

Figure 4.16. The efficiency map of the A-Segment Engine model

The efficiency map of the engine is presented in Figure 4.16Figure 4.16. Qualitatively, the efficiency maps of the C-Segment and A-Segment engines with same technologies are very similar. This applies for other quantities such as EGR rate and compression ratio distribution. A noteworthy difference is the efficiencies of the A-Segment Engine being slightly lower than the C-Segment High Efficiency Engine.

4.4 J-Segment Engine

The J-Segment engine is also equipped with the same technologies as the High Efficiency Engine. It has a displacement volume of 1.5 Liters, a larger turbocharger, a maximum torque of 300 Nm and a rated power of 144 kW. As a result, this engine too has the same power density as the High Efficiency Engine.

There are two questions regarding the dimensions of the engine: The number of cylinders and the stroke-to-bore ratio. In the first step, an inline-six engine, a V6-engine and an inline-four engine models are created and compared. The main advantage of the six-cylinder configuration is more flexibility during cylinder deactivation. The drawback is the higher wall heat losses. In this case, the flexibility during cylinder deactivation (i.e. deactivating up-to four cylinders at very low loads) brings rather insignificant benefits and does not compensate for the increased wall heat losses. The four- cylinder configuration has better overall efficiencies than both six-cylinder engines.

In the second step, the stroke-to-bore ratio should be determined. The increased displacement volume of the J-Segment engine allows a greater flexibility regarding to stroke-to-bore ratio. The increased stroke-to-bore ratio leads to better efficiencies at lower loads and engine speeds but lower efficiencies at higher loads and engine speeds. Since having good efficiencies at lower loads is considered to be a priority, the stroke-to-bore ratio for the J-Segment engine is chosen as 1.35 which is higher than of the High Efficiency Engine for the C-Segment. Further increasing the stroke-to-bore ratio up to 1.45 is also possible, without compromising the power density, but the efficiency gain at lower loads in this case is negligible and efficiency drops steeply at medium and lower loads. As an example, the efficiencies for different stroke-to-bore ratios are demonstrated along the 2500 RPM Figure 4.17.

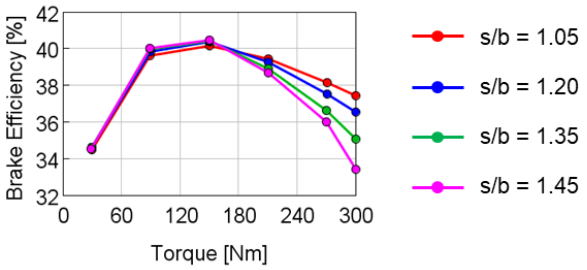

Figure 4.17. The efficiencies of the J-Segment Engine with different stroke-to-bore ratios at 2500 RPM

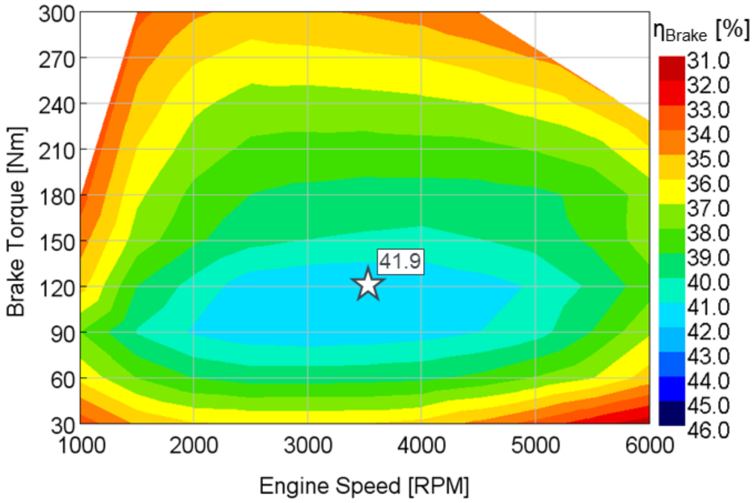

Figure 4.18. The efficiency map of the J-Segment Engine model

After the number of cylinders and optimal stroke-to-bore ratio is determined and the engine model is dimensioned, the compression ratios, the valve timings and the EGR rates are optimized as in the previously created models. The efficiency map of the J-Segment engine is shown in Figure 4.18. As in the case with the A-Segment Engine, the efficiency map of the J-Segment Engine is also qualitatively similar to the High Efficiency Engine for the C-Segment. The efficiencies of the J-Segment engine are slightly higher. There are also no noteworthy differences for quantities such as EGR rates and compression ratios.

The investigations with the A and J-Segment Engines reveal that, as long as engines have the same technology level and the same power density, their efficiency maps look very similar qualitatively, just scaled up and down by their respective sizes.

4.5 Methanol Engine

Here it should be demonstrated, how much the efficiency of a high technology engine can be improved, if an alternative fuel -namely methanol- is used instead of gasoline. The Methanol Engine modeled for this investigation has the same engine dimensions, maximum torque and rated power as the High Efficiency Engine. It is also equipped with the same technologies as the High Efficiency Engine, but quantities like valve timings, compression ratios and EGR rates are needed to be adjusted for methanol, for optimizing the efficiencies. Here, the most notable change is the significant increase of the compression ratios, which is possible due to excellent knock resistance of methanol. Further notable adjustments are the re-matching of the turbocharger and optimization to the cylinder deactivation strategy.

After the required optimizations, the simulations are undertaken in a similar manner to the High Efficiency Engine and the efficiency map is created which is shown in Figure 4.19. With the help of the technologies and methanol as fuel, a peak efficiency of 45.3% is achieved. This is an 18% improvement in comparison to the Reference Engine.

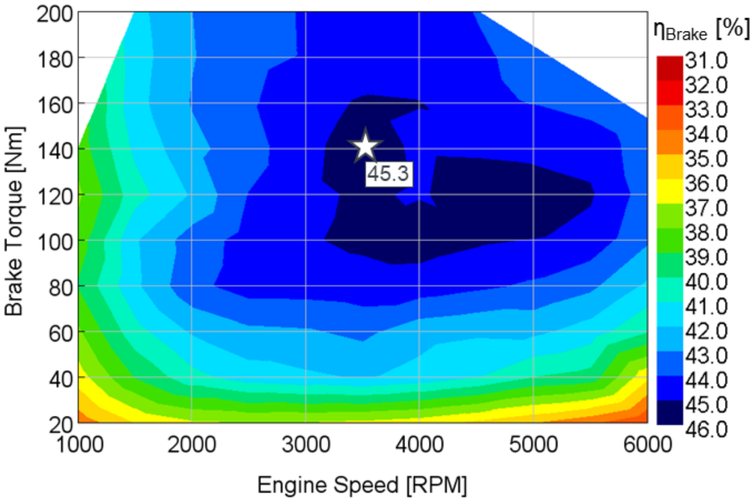

Figure 4.19. The efficiency map of the Methanol Engine

The high knock resistance of the methanol enables an increase of compression ratio throughout the engine map by around 4 units while maintaining a knock-free operation, i.e. mfb50% is at its optimal value of 8°CA. Also, no Miller strategy is necessary for decreasing knock resistance. In fact, Miller strategy is only used for decreasing the throttling losses. Furthermore, to knock-free operation makes the cylinder deactivation strategy advantageous at somewhat higher loads and adaptations are made accordingly.

Figure 4.20Figure 4.20 shows the comparison map for efficiencies of the Methanol Engine with the High Efficiency Engine which reveals the efficiency improvement potential with methanol. For lower loads (≤50% load), efficiency benefits around 8% are evident. With increasing loads, the efficiency benefit increases as well. At full load, up to 25% benefits are observed. It should also be added that with the implementation of suitable technologies and by using methanol as fuel, an efficiency increase of 15-20% through most of the engine map is possible which can be revealed by comparing the efficiency maps of the Reference Engine and the Methanol Engine.

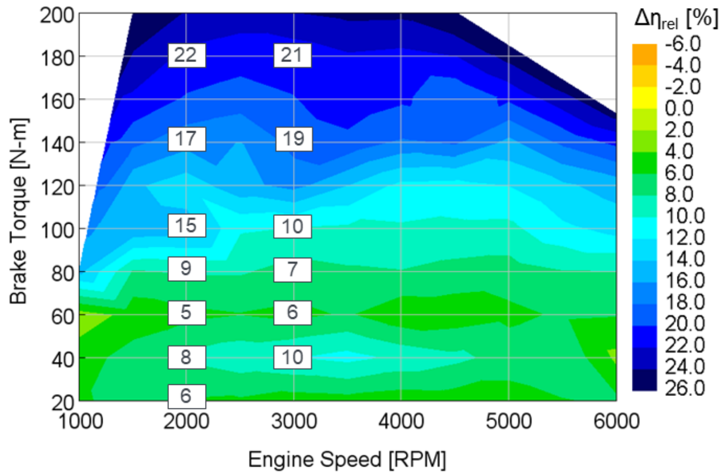

Figure 4.20. The relative difference in brake efficiency of Methanol Engine in comparison to the High Efficiency Engine. Green and blue indicate, that the Methanol Engine is better. Yellow and orange indicate, that the High Efficiency Engine is better.

Investigations with the Methanol Engine

It is found that methanol has many properties, which are advantageous in terms of efficiency. These advantages apply for both higher and lower loads and should be discussed and investigated further.

Methanol has an evaporation energy about three times higher than gasoline and its lower heat value is around half of gasoline. The latter can initially be considered as a drawback for a fuel, because for the same amount of fuel energy, the injected mass must be doubled, making its application more challenging. However, it simultaneously means that heat of evaporation of direct injection methanol engine is around six times higher than of a direct injection gasoline engine at a similar operating point. That leads to a much greater cooling effect with methanol. As a result, the temperatures during the compression and combustion are significantly reduced. This is one of the main contributors to the excellent knock resistance of methanol. Furthermore, with lower temperatures the wall heat losses, losses due to dissociation and losses through exhaust energy tend to decrease.

A further characteristic of methanol is that the heat value of the stoichiometric methanol-air mixture is higher than the heat value of the stoichiometric gasoline-air mixture. In other words, the required air mass is significantly less (approx. 10%) for realizing the same fuel energy with methanol. Also, the lower combustion temperatures with methanol -which is resulted by the higher evaporation enthalpy as mentioned above- lead to lower temperatures at the cylinder head and intake ports as well. Therefore, the temperature of the intake air tends to be lower for methanol than for gasoline. Combination of lower air mass requirement and lower intake temperatures leads to a significantly lower intake pressure requirement at any given operating point for methanol. However, this cannot be strictly considered as an advantage. On one hand, at higher engine loads, the required compression power of the turbocharger is decreased, which translates into a lower exhaust backpressure and a higher engine efficiency. On the other hand, at low loads, the throttling losses are increased. Overall, the effects are found to be rather minor. Benefits due to decreased boost pressure requirement with methanol would be more relevant, if this effect is complemented by another efficiency increasing measure: For increasing efficiency at lower loads further, downsizing can be considered. Or, a higher stroke-to-bore ratio can become attractive, since valve diameters can be decreased. Also, cylinder deactivation is useful for a wider range of operation window.

At this point, it is worth investigating, what portion of the benefits come through the superior knock resistance of methanol and what portion through the other aforementioned effects.

Advantages through higher knock resistance

For demonstrating the advantages through superior knock resistance of methanol, a simulative investigation is conducted with the help of four different fuels: Gasoline, Gasoline+, Gasoline++ and Methanol. Gasoline is the standard RON95E10 used for the High Efficiency Engine. Gasoline+ and Gasoline++ are two hypothetical, more knock resistant versions of gasoline. Gasoline+ enables a knock-free operation (i.e. optimal mfb50%) at the High Efficiency Engine. Gasoline++ enables a knock-free operation at the High Efficiency Engine, even if the compression ratio of the engine would be increased to a level of the Methanol Engine. In other words, Gasoline++ and Methanol show an identical knock behavior.

In Figure 4.21, the achievable efficiencies of Gasoline, Gasoline+, Gasoline++ at the High Efficiency Engine as well as methanol at the Methanol Engine are shown for two operating points at 2500 RPM with 100 Nm and 200 Nm. The center of combustion mfb50% as well as the compression ratio for each configuration are also denoted above respective columns on the diagram.

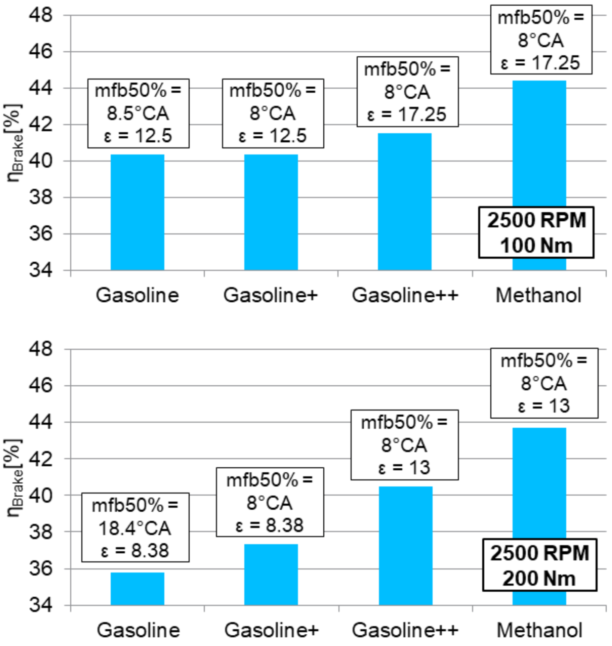

Figure 4.21. Comparison of achievable efficiencies with RON95E10 (Gasoline), with more knock-resistant, hypothetical versions of gasoline (Gasoline+, Gasoline++) as well as with methanol at two different operating points. The center of combustion (mfb50%) and compression ratio (ε) of each configuration is denoted above the respective column.

At full load (200 Nm), significant benefits could have been achieved, if gasoline had the same knock behavior as methanol, since the mfb50% and compression ratio can be improved. At part load (100 Nm), the efficiency benefits through a knock-resistant gasoline is more modest, since mfb50% is already almost optimal. However, at both operating points, methanol is still significantly superior to Gasoline or even to Gasoline++. In fact, only around half of the methanol’s efficiency advantage comes through its high knock resistance.

Advantages through other effects

In order to analyze, why methanol is still superior to gasoline, even if it was as knock-resistant as methanol (Gasoline++), the conversion of the fuel energy into the mechanical energy as well as the distribution of the mechanical losses, losses through the exhaust energy, wall heat losses, pumping losses and losses due to incomplete combustion are illustrated in Figure 4.22 for the same operating points and the same fuels with the same configurations.

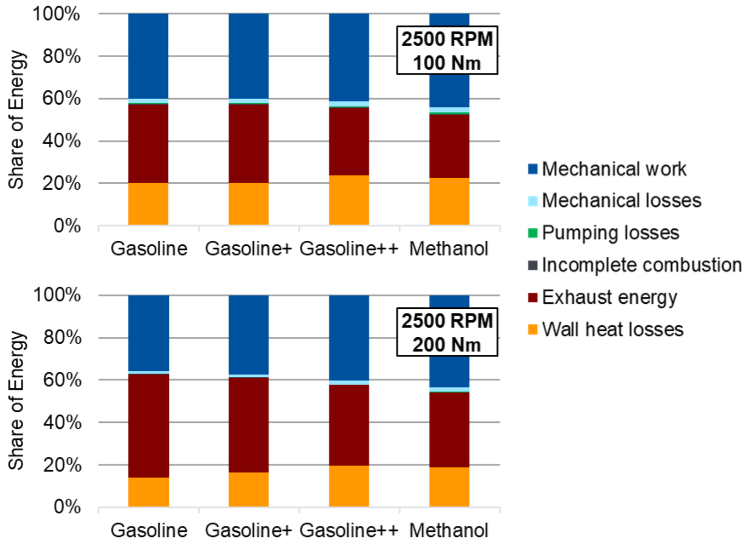

Figure 4.22. Share of energy of the mechanical output and various losses at two different loads for the four configurations with different fuels.

For all fuels and for all operating points the friction losses, pumping losses and losses due to incomplete combustion are similar and the differences result through wall heat losses and losses through the exhaust energy. A comparison between Gasoline, Gasoline+ and Gasoline++ shows that earlier mfb50% and increasing compression ratios cause the wall heat losses to increase and exhaust losses to decrease, whereas the effect of the latter is the dominant one. Here, even though the efficiency increases overall, the increasing wall heat losses with increasing combustion temperatures should not be underestimated.

The comparison between Gasoline++ and Methanol reveal that both the wall heat losses and the losses through exhaust energy losses get lower. Here, the lower combustion temperatures play the main role. In fact, the maximum combustion temperature of Methanol is around 200 K lower than of Gasoline++, which translates into a 7-8% efficiency increase in both operating points.

These studies suggest that an alternative fuel suitable for highly efficient direct injection SI internal combustion engines should have two properties: A high knock resistance and a high evaporation energy. In this case, significantly higher efficiencies can be achieved than with gasoline.

4.6 Short study: Blend Engine with G70M15E15

The blend fuel G70M15E15 offers itself as an alternative both to gasoline and methanol. It has better efficiencies than gasoline and has less concerns than methanol in terms of aspects such as toxicity or corrosivity. In addition, it is suggested that the high evaporation energy of pure methanol fuel can become a liability regarding the cold start behavior [50].

For the evaluation of the potential of the blend fuel G70M15E15, only a short study is conducted. For this study, instead of the laborious optimization of the entire engine, only the operating points along the 2500 RPM are optimized, which is the most commonly used engine speed throughout the different engines and hybridization levels according to the results from VKM [29].

For this study, the High Efficiency Engine serves as a starting point, which is to modified for the operation with the blend fuel. Since the blend is more knock resistant, the compression ratios of the engine can be increased significantly and suitable values are close to the ones which are adopted at the Methanol Engine. Together with the compression ratios, valve timings and EGR rates are optimized for best efficiency, and the results are compared along the engine speed of 2500. The results are shown in Figure 4.23Figure 4.23.

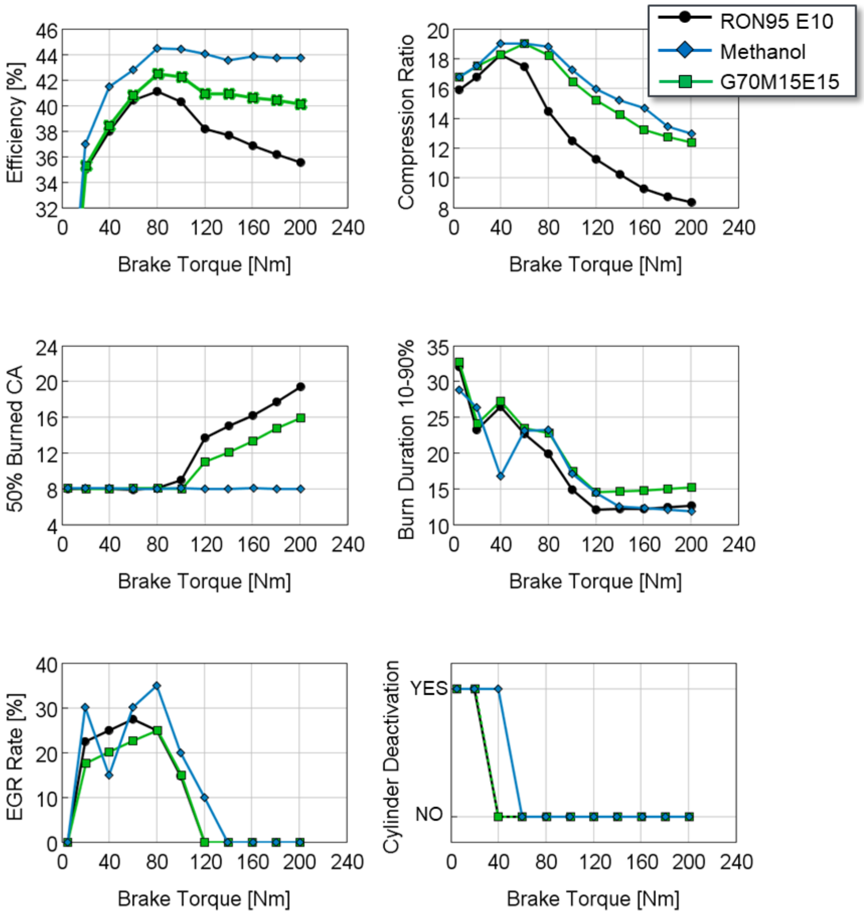

Figure 4.23. Brake Efficiencies, compression ratio, center of combustions, burn durations, EGR rates and loads when cylinder deactivation is active for High Efficiency Engine, Methanol Engine and Blend Engine along the engine speed 2500 RPM

All engines are operated similarly up to the 60 Nm load (regarding compression ratio and mfb50%) with efficiencies of blend and gasoline being similar and methanol's efficiency being better. At 40 Nm, methanol is especially more efficient because the Methanol Engine can be operated with cylinder deactivation efficiently due to methanol's lower air mass and boost pressure requirements as discussed in the previous chapter. But at the same operating point, the blend and gasoline can be operated with higher EGR rates and a more aggressive Miller strategy and the throttling losses can be kept under control that way as well.

The differences between blend and gasoline are more pronounced at loads equal or greater than 80 Nm. Due to greater knock resistance of the blend, the compression ratio of the Blend Engine is much closer to the compression ratios of the Methanol Engine and still the mfb50% of the blend is significantly better than gasoline. As a result, blend as fuel proves better efficiencies for higher loads than gasoline does.

It can be concluded that even with a moderate amount of admixture of methanol and ethanol to the gasoline, significant efficiency improvements can be achieved and the blend fuel in fact can be considered as a good compromise between gasoline and pure methanol fuels.

4.7 Full Load Water Injection Engine

The High Efficiency Engine demonstrates the best achievable efficiencies at every operating point due the optimal combination of the compression ratio, EGR rate and valve timing. The main drawback of such an engine is, however, the complexity and cost of a variable compression ratio system. Therefore, an alternative with a constant compression ratio should also be investigated. In order to keep the power density and the compression ratio high at the same time, an additional technology for managing knock is necessary. This additional technology is the water injection and used for knock reduction along the full load curve.

The optimal compression ratio for this configuration is found to be 13.5. This comes with a slight drawback that the 1500 RPM 200 NM (full load) is no longer achievable due to knock limitations, even with water injection. To enable the operation at this point, a compression ratio of 12.5 would be necessary, however, this would be disadvantageous regarding the engine efficiency. On the other hand, increasing the compression ratio further -for instance to 14.5- is also not recommended, because in this case even the 2000 RPM 200 Nm would not be achievable. Also, increasing the compression ratio from 13.5 to 14.5 would not lead to a significant change in overall engine efficiency, because the efficiency increase at lower loads are modest and the increased knock tendency even at moderate loads should not be underestimated. The compression ratio map from the Figure 4.9 as well as the diagram shown for the compression ratio variation in Figure 4.12 serve together as a good guideline, what the optimal compression ratio for each operating point is, and how much the chosen constant compression ratio deviates from the optimum.

As a result of these considerations, the model of the Full Load Water Injection Engine is created. The engine geometries, the maximum torque and the nominal power of the engine are same as the High Efficiency Engine. The Full Load Water Injection Engine also has EGR and high turbulence concept. The main difference to the High Efficiency Engine is therefore a constant compression ratio of 13.5 and water injection at the full load instead.

The efficiency map of the Full Load Water Injection Engine is shown in Figure 4.24. The water injection is used along the full load curve between 1000 and 2000 RPM as well as between 5000 and 6000 RPM, here, the mass of injected water is equal to the mass of injected fuel. The peak efficiency of 41.2% is very similar to the value from the High Efficiency Engine. The Full Load Water Injection Engine also proves to have comparable efficiency at lower loads, as a compression ratio of 13.5 leads to decent efficiencies.

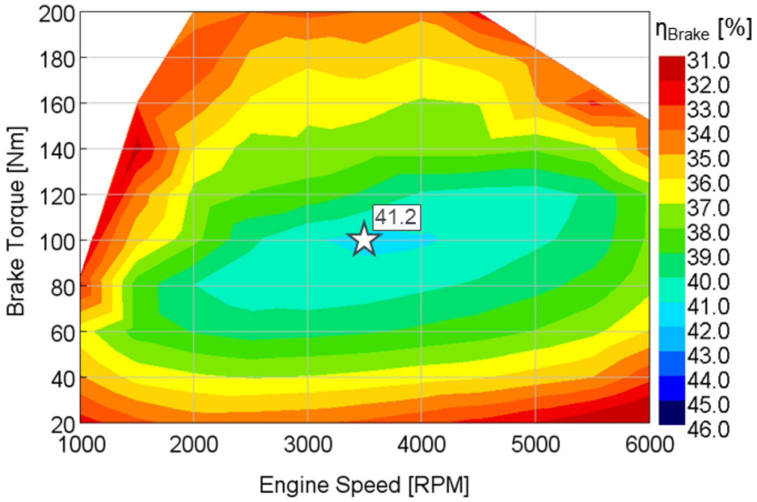

Figure 4.24. The efficiency map of the Full Load Water Injection Engine model

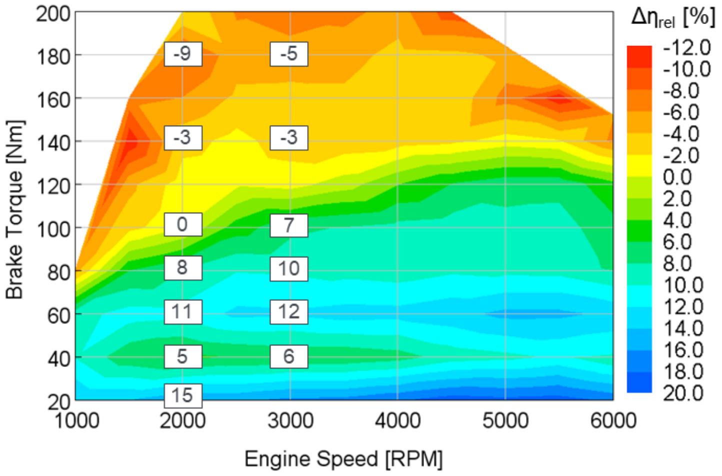

Figure 4.25. The relative difference in brake efficiency of the Full Load Water Injection Engine in comparison to the Reference Engine (VW EA211 TSI evo). Green and blue indicate, that the Full Load Water Injection Engine is better. Yellow and orange indicate, that the Reference Engine is better.

In Figure 4.25, the efficiencies of the Full Load Water Injection Engine are compared with the efficiencies of the Reference Engine. Up to middle loads, the Full Load Water Injection Engine has significantly better efficiencies. However, as a result of the heavy downsizing and increased compression ratio, its efficiency is significantly worse at higher loads. A comparison of the Full Load Water Injection Engine with the High Efficiency Engine is also shown in Figure 4.26. Here, it becomes evident that by leaving the variable compression ratio out and implementing water injection instead, the efficiency gets only slightly worse for the most parts of the engine map. As long as high loads are avoided, the Full Load Water Injection Engine is expected to have 2% lower efficiencies than the High Efficiency Engine.

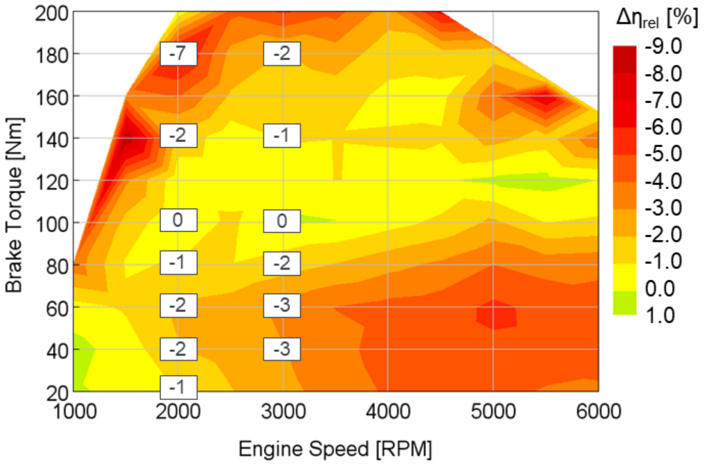

Figure 4.26. The relative difference in brake efficiency of the Full Load Water Injection Engine in comparison to the High Efficiency Engine. Light green and yellow indicate that both engines have similar efficiencies, red indicates that the High Efficiency Engine is better.

It can be concluded that a variable compression ratio is not a must for a highly efficient engine and water injection at full load offers itself as an interesting alternative for enabling high compression ratios and an aggressive downsizing simultaneously. As a result, efficiency improvements comparable to the ones at the High Efficiency Engine are observed. However, it should be added that these improvements are mainly at lower loads.

4.8 Lean High Efficiency Engine

The lean concept is very promising from the efficiency point of view. For the evaluation of its potential a modified version of the High Efficiency Engine is used.

The application of lean concept has two main challenges. The first challenge is high raw NO_X emissions. The NO_X production is favored heavily by simultaneous high temperatures and a lean air-fuel mixture. Therefore, to keep the NO_X emissions in control, only a high air-fuel equivalence ratio (λ) is should be considered. For example, $\lambda=1.3$ can prove to be beneficial efficiency-wise but not acceptable from a NO_X emissions point of view. According to the measurement results during the research project ICE2025+: Ultimate System Efficiency, the value of $\lambda=1.7$ offers itself as the most suitable option [29]. Lower values tend to increase NO_X production significantly, while higher values cause heavy cycle-to-cycle variations, which leads to decreased efficiency.

The second challenge is the difficulties with turbocharging. With increasing air-fuel ratio, the necessary charge air mass and boost pressure to realize any given operating point increase proportionally. Simultaneously, the exhaust temperatures decrease, i.e. the available energy for the turbine decreases. Therefore, it is not possible to realize the desired $\lambda=1.7$ throughout the entire engine map. Similarly, an aggressive Miller strategy is not compatible with lean combustion, because of the additional difficulty during the gas exchange. The exception to this is very low loads, where both strategies should be applied to minimize throttling losses.

The Lean High Efficiency Engine has the same dimensions, rated power and maximum torque as the stoichiometric High Efficiency Engine. It is also fitted with the same features, except for EGR. EGR and lean concept have similar advantages and problems, while latter being the more efficient one. Therefore, EGR is superfluous, when lean concept is present. The compression ratios of the Lean High Efficiency Engine are also kept the same as in the stoichiometric High Efficiency Engine. The high turbulence strategy is also essential for flame stability at values around $\lambda=1.7$. Furthermore, the valve timings are adjusted, if beneficial or necessary.

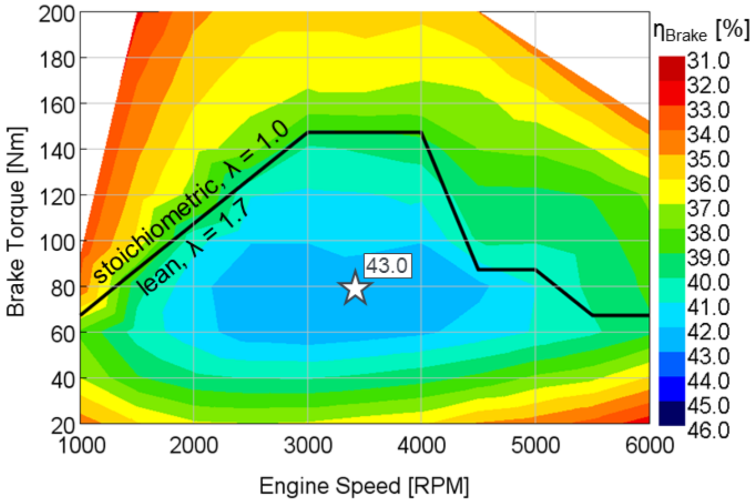

Figure 4.27. The efficiency map of the Lean High Efficiency Engine model with black solid line representing the border between stoichiometric and lean operation

The development of the Lean High Efficiency Engine is carried on in two steps. In the first step, it should be investigated, at which operating zone lean combustion can be realized. For this investigation, no Miller valve timings are utilized and the lean full load curve is determined. In the second step, the operating points below the determined loads are operated with $\lambda=1.7$ and their valve timings are optimized. The remaining operating points at higher loads remain identical to the stoichiometric High Efficiency Engine. A few exceptions are the operating points, where they are operated with EGR at the stoichiometric engine, but cannot be operated with $\lambda=1.7$ at the lean version. Since the Lean High Efficiency Engine does not have EGR, those operating points are operated with a more aggressive Miller strategy instead.

The efficiency map of the Lean High Efficiency Engine is shown in Figure 4.27. The black line represents the border between stoichiometric and lean operated zones.

To quantify the advantages through lean concept, the efficiency comparison map of the stoichiometric and lean versions of the High Efficiency Engine is shown in Figure 4.28. The highest benefits through lean are evident at loads up to around 25%. Here, an efficiency increase of around 5% is achieved, marked as the zone A in Figure 4.28. With increasing loads, the efficiency benefits get lower. This is due to the lack of EGR and Miller at those operating zones, which lead to a worse knock resistance and therefore a later mfb50%. In fact, at the zone B, the achievable efficiency with Miller and EGR is similar than the efficiency with lean combustion. This is both due to later mfb50%, and the increased pumping losses. Towards the zone C, on contrary, the efficiency advantage once again increases. This is due to absence of EGR at the stoichiometric High Efficiency Engine at this operating zone which is reasoned by exhaust pressure being lower than the intake pressure. In other words, in the zone C the lean operation is possible but operation with EGR is not. As a result, the lean concept brings substantial advantages in the zone C. Above the black line, the both the stoichiometric and lean engines are operated identically, therefore the efficiency is identical and the difference is due to numerical error. The exception is the zone D, where the stoichiometric engine is operated with EGR and the lean engine is operated instead with a more aggressive Miller strategy.

The results suggest that lean concept is a respectable addition for a high efficiency engine. However, it should be noted that with a suitable set of technologies, stoichiometric engines can also have high efficiencies and the leap from stoichiometric engine to a lean engine would be in this case not that substantial.

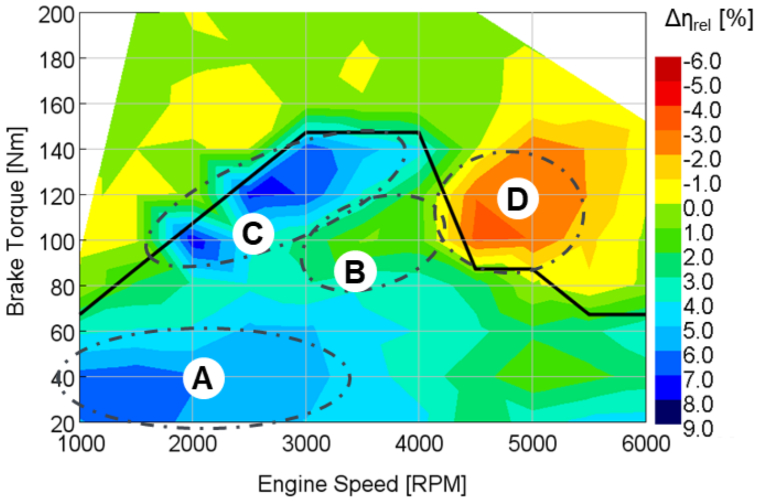

Figure 4.28. The comparison of stoichiometric and lean versions of the High Efficiency Engine. Green and blue indicate that the lean version is better. Yellow and orange indicate that the stoichiometric version is better.

4.9 Lean Full Load Water Injection Engine

The lean version of the Full Load Water Injection Engine is modeled analogous to the Lean High Efficiency Engine. The technology of EGR is replaced with lean concept while the remaining technologies are kept. The engine dimensions, the rated power, the maximum torque and the compression ratio remain unchanged.

The main difference determining the efficiency between Lean Full Load Water Injection Engine and Lean High Efficiency Engine is the compression ratio. As already discussed, the lean concept has overall a lower knock resistance. Therefore, the engine with lower compression ratios should profit more from the lean concept.

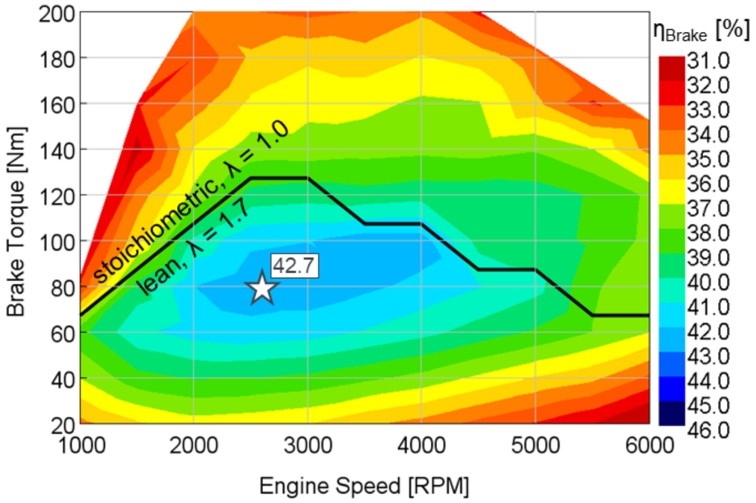

Figure 4.29. The efficiency map of the Lean Full Load Water Injection Engine model with black solid line representing the border between stoichiometric and lean operation

In Figure 4.29 the efficiency map of the Lean Full Load Water Injection Engine is shown. The engine profits from the lean concept at the lower half of the engine map and the peak efficiency is increased to 42.7%. In Figure 4.30, the efficiencies of stoichiometric and lean variants are compared. The black line represents the border between stoichiometric and lean operated zones. The grey dashed line shows the upper limit of the possible lean operation. In other words, in region between dashed and solid lines (zone B) lean operation is possible but not desired, since both the pumping losses would be high and the absence of Miller would cause heavy knocking, due to Full Load Water Injection Engine having higher compression ratios in those regions. The regions A, C, D are similar to those discussed in Lean High Efficiency Engine. It should be noted however, that the region A with ca. 5% higher efficiencies in the Lean Full Load Water Injection Engine is broader, reaching up to around 40% load. This is due to the more moderate compression ratios of the Lean Full Load Water Injection Engine in this region in comparison to Lean High Efficiency Engine.

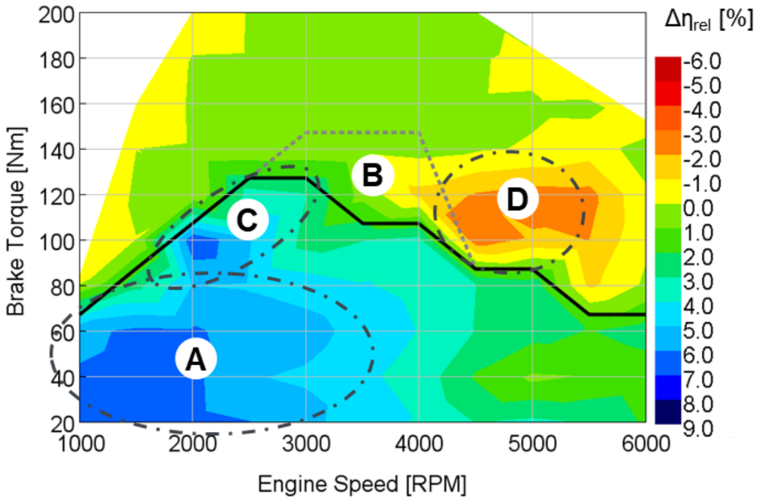

Figure 4.30. The comparison of stoichiometric and lean versions of the Full Load Water Injection Engine. Green and blue indicate that the lean version is better. Yellow and orange indicate that the stoichiometric version is better. The dashed grey line represents the maximum possible reachable load with λ = 1.7.

According to the results, the benefits of lean concept change depending on whether the engine has constant or variable compression ratios, and the engine with the constant compression ratio profits more from the lean concept, if lower loads are considered as more important.

4.10 Lean Methanol Engine

The Lean Methanol Engine is created in a similar manner based on the stoichiometric Methanol Engine. The lean concept with methanol has two significant advantages over lean concept with gasoline: The first advantage is a larger operation window with lean combustion with methanol. This is due to lower boost pressure requirement with methanol. As a result, lean operation at higher loads becomes possible. The second advantage comes through the higher knock resistance of methanol. The stoichiometric gasoline engines presented previously are operated with Miller strategy to keep knocking under control and secure a good mfb50%. The lean gasoline engines however are operated with a milder or even without Miller, which leads to lower knock resistance. Therefore, some of the efficiency benefit through lean concept is lost, because of the comparatively worse mfb50%. The Methanol Engine, on the other hand, is operated knock-free and without Miller at higher loads regardless of lean or stoichiometric operation. Therefore, the full advantage of the lean concept can be exploited at the Methanol Engine.

The efficiency map of the Lean Methanol Engine is shown in Figure 4.31. The white solid line represents the border between stoichiometric operation and the operation with *λ=1.7*. Between 2500 RPM and 4000 RPM a stoichiometric operation even at full load possible and a peak efficiency of 46.8% and an efficiency of more than 45% for a wide operation range are achieved.

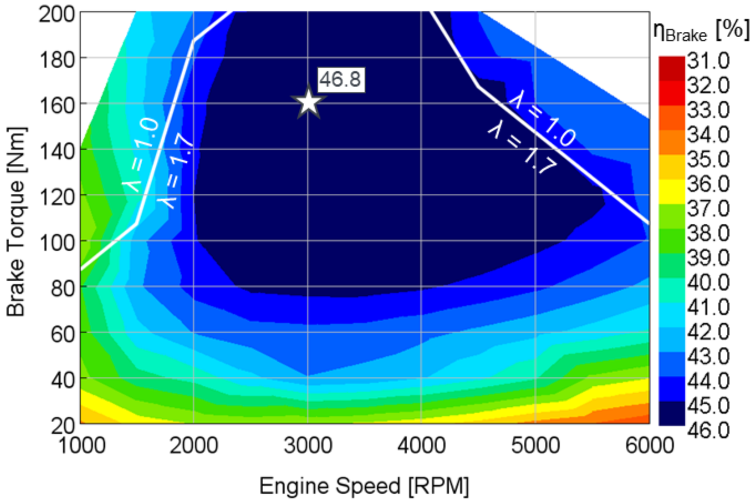

Figure 4.31. The efficiency map of the Lean Methanol Engine model with white solid line representing the border between stoichiometric and lean operation

The efficiency benefit through lean concept is shown in Figure 4.32 by a comparison of the lean and stoichiometric variants of the Methanol Engine. At the bottom half of the engine map, efficiency benefits through lean concept are lower to the previously discussed lean gasoline engines. In fact, at the operating point 2000 RPM 40 Nm, the efficiency benefit with cylinder deactivation, Miller strategy and EGR with $\lambda=1$ is equal to the efficiency benefit with lean concept. In contrary to the gasoline engines, however, the benefits with lean concept gets greater with increasing loads.

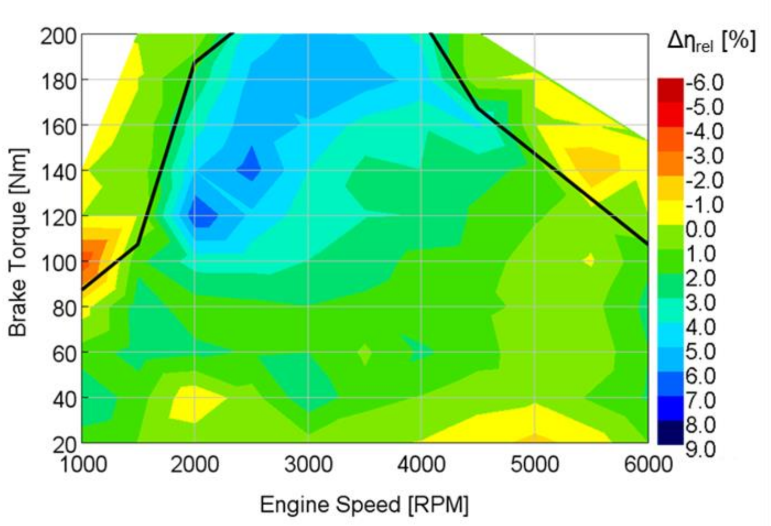

Figure 4.32. The comparison of stoichiometric and lean versions of the Methanol Engine. Green and blue indicate that the lean version is better. Yellow and orange indicate that the stoichiometric version is better.

The studies with the Lean Methanol Engine reveal that in addition to its previously discussed advantages, methanol also proves to have noteworthy synergy effects with the lean concept, making it attractive for stoichiometric and lean applications alike.

4.11 Discussion of the Results with the Help of Overall Powertrain Efficiencies during WLTC cycles

In this chapter, the benefits of a more efficient engine in a hybridized powertrain should be discussed in the light of the follow-up investigations and results of VKM of University of Stuttgart within the framework of the project ICE2025+: Ultimate System Efficiency [29]. With the help of the efficiency maps, they simulated WLTC cycles and determined the overall efficiency of the vehicles with the engine models that are presented so far, while considering a variety of hybrid architectures. The considered hybrid configurations are: P1, 48V (low voltage) P2 (LV P2), 400 V (high voltage) P2 (HV P2) and power split (PS). For determining the efficiency, the distribution of the operating points along the efficiency or a BSFC map is considered. An example is shown in

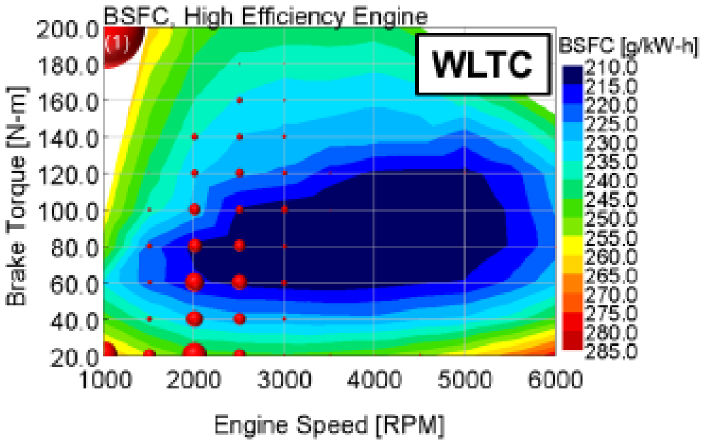

Figure 4.33. Distribution of operating points through the engine map during a WLTC cycle for the High Efficiency Engine with P2 LV hybrid architecture, according to investigations of VKM [29]

Figure 4.33 for a C-Segment vehicle operated with the High Efficiency Engine with a P2 LV configuration. The area of the red circles represents the spent time in the vicinity of an operating point. The red circle on the upper left corner represents the time spent during pure electric drive, i.e. the internal combustion engine is not running.

The overall efficiencies are for different engines with different hybrid configurations are shown in Table 4.3. Please note that all the configurations are equipped with start-stop and while the vehicle is not moving the engine is turned off and no fuel is consumed.

Table 4.3. Mean powertrain efficiencies for different engines combined with different hybrid architectures during the WLTC cycle [29]

	w/o Hybrid	P1	P2 LV	P2 HV	PS
VW EA211 TSI evo	28.2%	-	-	-	-
HEE	-	38.1%	39.3%	40.6%	40.4%
FLWI	-	37.7%	39.0%	39.7%	40.0%
Methanol	-	41.1%	42.7%	44.6%	44.1%
HEE lean	-	39.5%	40.8%	41.6%	41.7%
FLWI lean	-	39.3%	39.9%	41.3%	41.8%
Methanol lean	-	41.1%	44.3%	44.7%	44.4%

According to the results, the state-of-the-art VW EA211 TSI evo without any hybridization reaches an overall efficiency of 28.2%. In comparison, the more technologically advanced and efficient gasoline engines with hybridization reach efficiencies between 38.1% and 41.8%. With methanol, efficiencies up to 44.7% is achieved. Unfortunately, no investigation with either reference engine with hybridization or with the efficient engines without hybridization is conducted. Therefore, it is not possible to directly know how much of the benefits are through technologically advanced engines and how much of the benefits are through the hybridization. However, an estimation is possible by analyzing the energy flows through the powertrain.

First, the powertrain of the reference engine VW EA211 TSI evo is considered which is schematically shown in Figure 4.34. For completing the WLTC cycle, the vehicle requires 3.00 kWh of drive energy. With a differential efficiency of 98% and a gearbox efficiency of 95%, the internal combustion engine must deliver 3.22 kWh of mechanical energy, which requires a 10.60 kWh of fuel energy with an average efficiency of 30.3%.

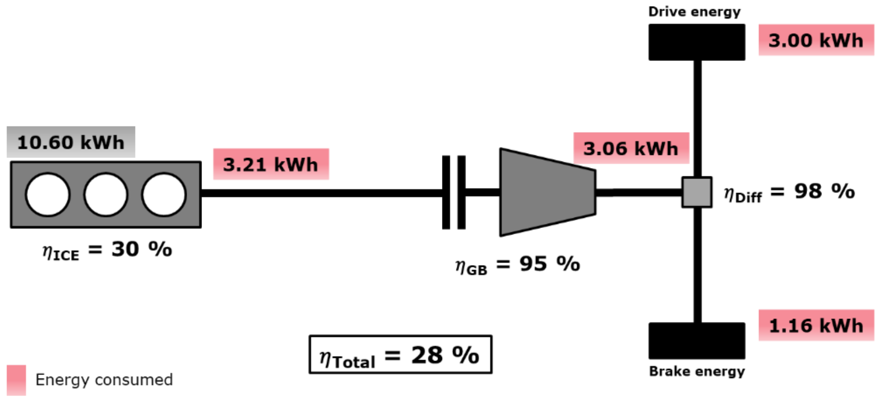
Drive energy
3.00 kWh
10.60 kWh
3.21 kWh
3.06 kWh
η_{Diff} = 98 %
η_{ICE} = 30 %
η_{GB} = 95 %
1.16 kWh
η_{Total} = 28 %
Brake energy
🟥 Energy consumed

Figure 4.34. Powertrain and energy flows for the Reference Engine VW EA211 TSI evo without hybridization [29]

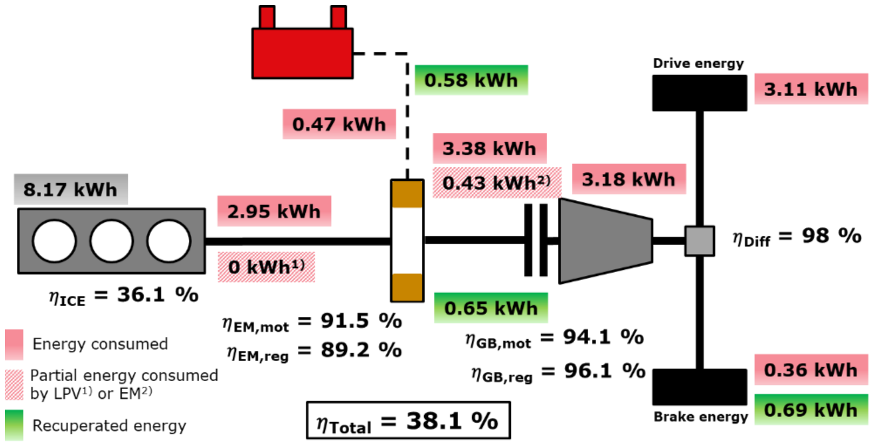
0.58 kWh
Drive energy
3.11 kWh
0.47 kWh
3.38 kWh
0.43 kWh$^{2)}$
3.18 kWh
8.17 kWh
2.95 kWh
η_{Diff} = 98 %
0 kWh$^{1)}$
η_{ICE} = 36.1 %
0.65 kWh
$\eta_{EM,mot}$ = 91.5 %
$\eta_{EM,reg}$ = 89.2 %
$\eta_{GB,mot}$ = 94.1 %
$\eta_{GB,reg}$ = 96.1 %
0.36 kWh
0.69 kWh
Brake energy
η_{Total} = 38.1 %
🟥 Energy consumed
▨ Partial energy consumed by LPV$^{1)}$ or EM$^{2)}$
🟩 Recuperated energy

Figure 4.35. Powertrain and energy flows for the High Efficiency Engine with the P1 hybrid architecture [29]

In Figure 4.35, the energy flows through the powertrain for P1 hybrid architecture with the High Efficiency Engine are shown. Here, a drive energy of 3.11 kWh for a WLTC cycle is necessary. Of this drive energy, a certain fraction is the result of braking. Of this brake energy, 0.69 kWh can be recuperated and converted into 0.58 kWh electrical energy charging the battery and 0.36 kWh is lost permanently. 0.47 kWh of electrical energy from the battery is used for supporting the internal combustion engine during high load phases. It is important to note that no load lifting is utilized because the recuperated energy is sufficient to charge the battery. In this configuration, the internal combustion engine consumes 8.17 kWh worth of fuel energy and delivers 2.95 kWh of mechanical energy, which translates into an efficiency of 36.1%. The overall efficiency of the vehicle is 38.1%.

For estimating the benefits of hybridization two extreme scenarios for the P1 architecture are considered: In the first scenario, it is assumed that the load point shifting for avoiding high loads does not contribute to the efficiency of the internal combustion engine at all. In other words, the efficiency of the internal combustion engine is assumed to be 36.1% even without hybridization. In the second scenario, it is assumed that hybridization enables a very effective load point shifting so that the internal combustion engines efficiency is significantly worse without hybridization. An example of a very effective load point shifting can be found between operating points 2000 Nm 80 Nm and 2000 RPM 100 Nm, as can be seen in the efficiency map of the High Efficiency Engine in Figure 4.6. The 80 Nm operating point has an efficiency higher than 40% while the 100 Nm operating point has an efficiency lower than 38%. By supporting the engine with about 4.3 kW electric energy the operating point with 100 Nm can be avoided. Assuming the 0.47 kWh electric power is used solely for this purpose, the efficiency of the non-hybrid High Efficiency Engine which is operated more often with 100 Nm would be 35.0% (The associated calculations can be found in Appendix.) In other words, the High Efficiency Engine without hybridization must have an efficiency between 36.1% and 35.0%. This translates into a vehicle efficiency between 33.6% and 32.6% assuming a differential efficiency of 98% and a gearbox efficiency of 95%.

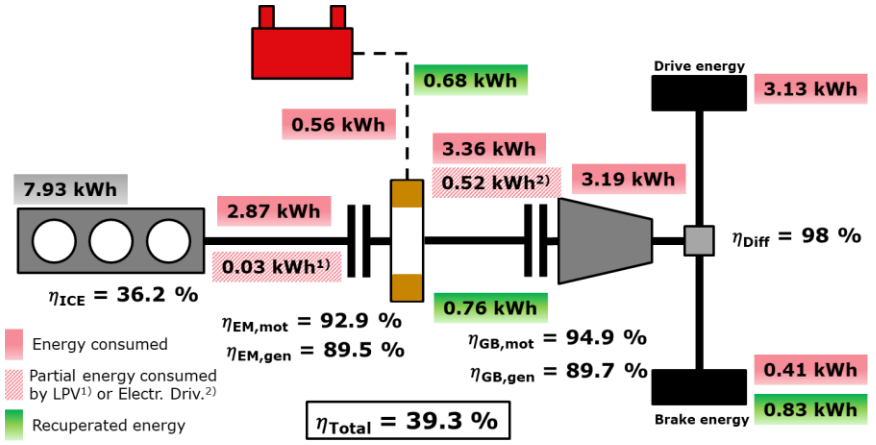
Drive energy
3.13 kWh
0.68 kWh
0.56 kWh
3.36 kWh
0.52 kWh²⁾
3.19 kWh
7.93 kWh
2.87 kWh
0.03 kWh¹⁾
ηDiff = 98 %
ηICE = 36.2 %
0.76 kWh
ηEM,mot = 92.9 %
ηEM,gen = 89.5 %
ηGB,mot = 94.9 %
ηGB,gen = 89.7 %
0.41 kWh
0.83 kWh
Brake energy
Energy consumed
Partial energy consumed by LPV¹⁾ or Electr. Driv.²⁾
Recuperated energy
ηTotal = 39.3 %

Figure 4.36. Powertrain and energy flows for the High Efficiency Engine with the P2 LV hybrid architecture [29]

The P2 configuration allows pure electric drive, thus leading to better overall efficiencies. The high voltage variant equipped with more powerful electric machine and a higher battery capacity, which allow greater flexibility regarding the operation of the powertrain. However, it also increases the vehicle weight so that some of the efficiency benefits are cancelled out.

The energy flows through the powertrain for the P2 LV configuration equipped with the High Efficiency Engine is shown in Figure 4.36. The disadvantage of the low voltage configuration becomes apparent during the load point lifting phase: Due to the limited capacity of the battery, only 0.03 kWh of mechanical energy can be used to generate electrical energy with load point lifting. Also, the internal engine efficiency remains at the same level (36.2% instead of 36.1%), despite the ability of pure electric driving. The reason for this is once again the very limited battery capacity that does not allow well-timed engine shut-offs for avoiding operating points with poor efficiencies. Still, the P2 LV enables a higher amount of the brake energy to be recuperated and reaches a vehicle efficiency of 39.3%. In contrast, in the P2 HV configuration 0.79 kWh of the mechanical output of the internal combustion engine is used to generate electric energy due to load point shifting, thus achieving an internal combustion efficiency of 37.6% and a vehicle efficiency of 40.6% [75].

The comparison of the efficiencies might be misleading, since the weight of the vehicle changes for different hybrid architectures. Since the task of the vehicle, i.e. completing the WLTC cycle, is always the same, the most reliable way of comparison different configurations is comparing the consumed fuel energy. Such a comparison for the Reference Engine and the High Efficiency Engine, including the estimated worst- and best-case scenarios is shown in Figure 4.37.

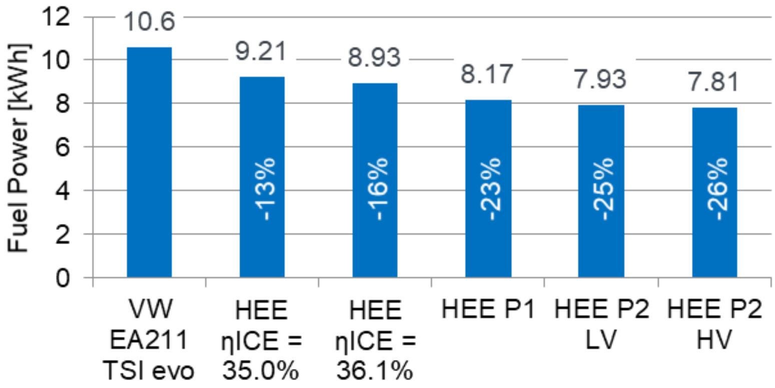

Figure 4.37. Consumed fuel energy for different powertrain configurations [75]

According to results, 26% reduction of the fuel consumption is possible with the High Efficiency Engine and with a high degree of hybridization. Also, estimations show that 13% at the worst 16% at the best fuel consumption is due to the better internal combustion engine. This is equivalent to 15-19% efficiency improvement. The value of 15-19% is significantly higher than the previously estimated efficiency increase of 10% with the efficiency comparison map in Figure 4.7. This once again stresses the importance of higher efficiencies at the lowest loads and thus the importance of an aggressive downsizing.

The diagram in Figure 4.37 also show that the rather modest P1 hybrid enables a 7-10% fuel consumption reduction, despite its shortcomings. Other more ambitious variants with P2 enable only a few percent of additional fuel consumption reduction, despite using the advantages of hybridization to its full extent and increasing the powertrain efficiency significantly. In other words, the weight increase of the vehicle with higher degrees of hybridization should not be underestimated.

Finally, it can be concluded that the fuel consumption of a vehicle can be decreased by around one-fourth (which is equivalent to an efficiency increase by one-third) with by substituting the state-of-the-art internal combustion engine with a more advanced one and by implementing hybridization. In this case, slightly more than the half of the overall fuel consumption reduction is due to improved internal combustion engine while slightly less than the half is due to hybridization. Naturally, the amount and the proportion of the benefits would be less, if a less efficient engine than the High Efficiency Engine would be used, for example if some of the technologies would be taken out from the High Efficiency Engine or the Full Load Water Injection Engine would be used instead. On the other hand, higher benefits should be expected, if the lean version of the High Efficiency Engine or the Methanol Engine would be used.

5 Summary and Outlook

In order to demonstrate the potential of efficiency increase of SI engines, 0D/1D investigations are conducted and benefits through various technologies are assessed and the potential of alternative fuels is investigated.

Starting from the state-of-the-art Reference Engine, two challenges were to overcome: Shifting the high efficiency regions of the engine map towards more relevant operating window and increasing the efficiency of the engine in general.

The better overlapping between high efficiency zone and the most relevant operating window is achieved with an aggressive downsizing. However, this downsizing should be combined with a technology such as variable compression ratio or water injection in order to keep knocking at full load under control and enable high power densities. For achieving highest efficiencies for a stoichiometric concept, the technologies of EGR, variable compression ratio and high turbulence concept in addition to the already present technologies in the Reference Engine such as Miller cycle and cylinder deactivation are recommended. Here, the high turbulence concept demonstrates especially interesting synergy effects: The decrease in burn duration increases the tolerance of the engine for high EGR rates, thus boosting the benefits with the EGR. Also, the increased knock resistance with the high turbulence concept makes higher compression ratios more desirable, increasing the engine efficiency at lower and higher loads alike. On the other hand, an increase of stroke-to-bore ratio, although being promising in theory, proves to be unsuitable and counterproductive for some of the considered configurations: The smaller valve sizes caused by a high stroke-to-bore ratio makes the gas exchange more challenging. This leads to increased pumping losses, prevents aggressive Miller strategy thus increasing the knock tendency and does not allow the desirable level of downsizing. A particularly attractive technology is the variable compression ratio which enables a free choice of the compression ratio – higher values at lower loads, lower values at higher loads. It can be considered as a key technology for achieving best possible efficiencies throughout the entire engine map as well as for enabling an aggressive downsizing.

Results show that with the aforementioned measures the peak efficiency of the internal combustion engine can be increased to 41.4% as demonstrated with the help of the High Efficiency Engine in comparison to the peak efficiency of the state-of-the-art Reference Engine of 38.4%. More importantly, greater efficiency benefits are evident at lower loads. The analysis of the overall powertrain efficiencies and energy flows indicate that the High Efficiency Engine should allow a 13-16% fuel consumption reduction during a WLTC cycle in comparison to the Reference Engine. This is equivalent to a 15-19% efficiency increase. The combination of a suitable hybrid architecture and the High Efficiency Engine can enable a fuel consumption reduction by one-fourth in comparison to the conventional powertrains.

The investigations with smaller and larger engines with lower and higher rated powers respectively showed that the engine efficiency maps are qualitatively very similar regardless of the size, if same technologies are implemented. Only the overall efficiencies tend to increase slightly with increasing engine dimensions.

If a variable compression ratio is not desired for reasons such as complexity and cost, water injection at full load combined with a moderate to high compression ratio presents itself as a decent alternative. In this case, the optimal efficiency window without the variable compression ratio is smaller and overall efficiencies are slightly worse despite a similar peak efficiency. Without the variable compression ratio and with the water injection, about 2% higher fuel consumption in comparison to the High Efficiency Engine is expected.

Additional efficiency benefits can be achieved with the lean concept. However, the benefits are limited up to medium loads due to high boost pressure requirements. Also, with the implementation of lean concept, EGR and partially the Miller strategy must be abandoned, resulting in an increased knock tendency at the affected operation range of the engine. Yet still, with lean concept, the efficiency at the more relevant operating window can be increased by a further 4-5% in comparison to a high efficiency stoichiometric concept, while the peak efficiency is pushed to 43.0%.

Using methanol as fuel brings advantages over gasoline, thanks to its high knock resistance and high evaporation enthalpy. The high knock resistance enables an increase of the compression ratios by around 4 units and the engine could still be operated with the optimal mfb50% of 8°CA at all times. However, even at lower loads, where knock is not a problem for a gasoline engine and both engines have similar compression ratios, the methanol still proves to be remarkably superior to gasoline. This is due to high evaporation energy of the methanol which leads to lower combustion temperatures, thus resulting in lower losses both through the exhaust gas energy and the wall heat transfer. By using methanol as fuel instead of gasoline, on average an 8% efficiency increase at lower loads is achieved. With increasing loads, the benefits get higher, reaching around 25% at full load. Also, this engine reaches a peak efficiency of 45.3%.

Furthermore, methanol is an especially suitable fuel for the lean concept. Due to a lower boost pressure requirement, the methanol engine can be operated under lean conditions for a much larger operation range and thus profits from a lean concept particularly. With the combination of methanol and lean concept a peak efficiency of 46.8% is reached.

The blend G70M15E15 presents itself also as an interesting compromise between gasoline and methanol. Due to its high knock resistance, an operation with compression ratios similar to those with methanol is possible, without heavily retarding the center of combustion. Blend enables significantly higher efficiencies than gasoline at medium and high loads, but its efficiency is still significantly worse than of methanol.

As an overview, the peak efficiencies of the designed engine models for the C-Segment along with the relative improvement are shown in Figure 5.1. Please note that, considering the emphasis put on the efficiency improvement at lower loads, the actual overall efficiency improvement of the engine is greater than the values seen in the diagram. The estimated benefits for a WLTC cycle are also shown in Figure 5.2.

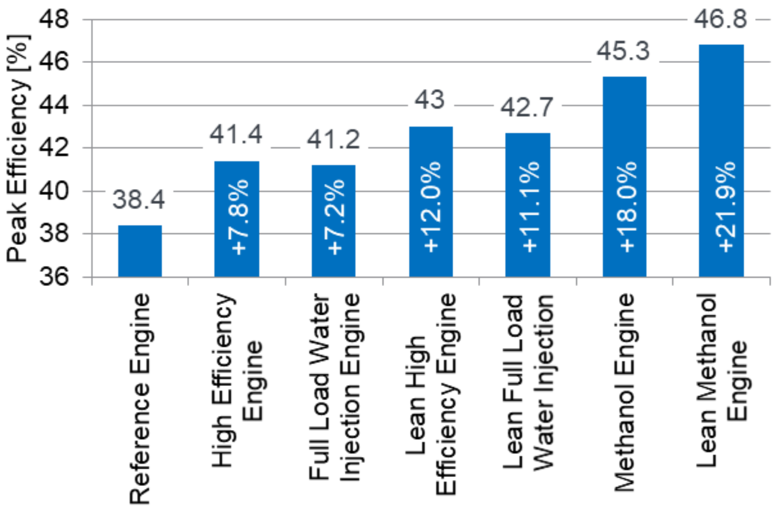

Figure 5.1. Overview of the peak efficiencies for different engine models

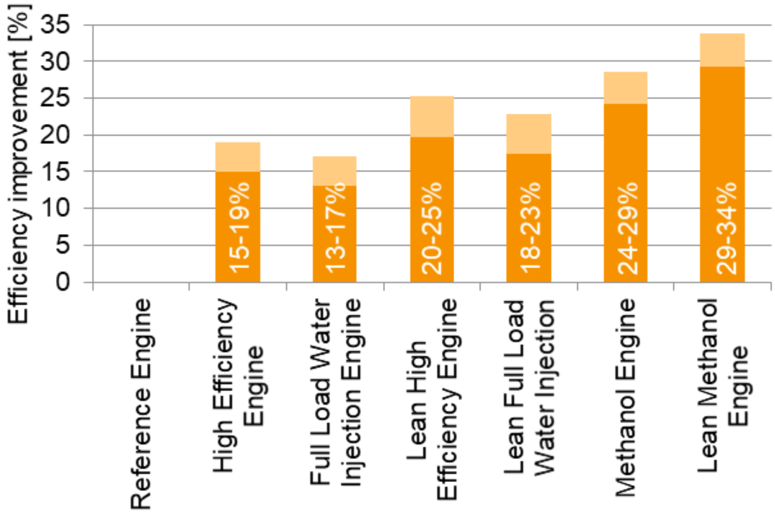

Figure 5.2. Overview of the estimated efficiency benefits for different engine models, dark orange for the worst-case, light orange for the best-case scenarios

In conclusion, this work shows that the internal combustion engine still has a significant potential for an efficiency increase. The efficiency improvement arises mainly from an increased knock resistance, decreased throttling losses, decreased losses through wall heat transfer and improvements to the thermodynamic combustion cycle as well as to the caloric. The higher knock resistance is achieved by high turbulence concept, Miller, EGR and with alternative fuels. Lower wall heat losses and a better caloric are achieved with the EGR, lean concept, high evaporation energy of the chosen fuel. The lower throttling losses are achieved with cylinder deactivation, Miller, EGR or downsizing. The technologies of variable compression ratio or water injection rounds the engine up well, as they enable an aggressive downsizing, without compromising the compression ratio. On the other hand, a high stroke-to-bore ratio, despite being initially promising, is not always recommended, since it interferes with downsizing and Miller and might become counterproductive. Furthermore, the lean concept can be considered for further efficiency improvement. Moreover, a significant leap in efficiency is possible by using methanol as an alternative fuel.

The results of this work also suggest that putting further effort both on engine development and modeling approaches is necessary. The current models underestimated the effects of water injection, EGR and lean combustion on the burn durations of gasoline slightly, but consistently. Therefore, a refinement or an expansion of the entrainment model might improve the predictive capabilities of the simulations. One such good addition to the models might be consideration of the inhomogeneities in the combustion chamber which is currently investigated by Mir et al. during their FVV research project “Gemischhomogenisierung Otto II”. Also, improvements to the knock model are necessary in case of the EGR and especially of the lean combustion. Although Hess et al. managed develop a new knock model during his FVV research project “Engine Knock Model” with enhanced predictive capabilities [76], unfortunately, their knock model could not be utilized during this work, since their project and this project were run more or less simultaneously. Furthermore, since alternative fuels show promising results and offer a sustainable solution to the mobility in the future, it is also recommended to expand current laminar flame speed and knock models for the up-and-coming alternative fuels and fuel mixtures in order to support the developments in the following years.

Since methanol proved itself as a very attractive candidate, the development of an actual methanol engine as quickly as possible is strongly recommended. Therefore, intensive research should be conducted that addresses the challenges and concerns of methanol fuel - cold start behavior, toxicity, corrosivity to name a few. Equally important is investing effort in the development of further alternative fuels with desirable characteristics. Here, a high knock resistance and a high evaporation enthalpy are the two most important attributes for achieving high efficiencies. Here, the work of Wagner et al. is worth mentioning in which the alternative fuel DMC+ (a mixture of Dimethyl carbonate and methyl formate) is investigated as an attractive alternative fuel [77].

During this work, the equivalence air-fuel ratio was limited to 1.7 due to the limitations to the flame stability and burn duration. If these aspects can be kept under control and the air-fuel ratio can be increased further, the full potential of the lean concept can be exploited. That means, not only the efficiency gains with the lean concept can be increased, but also the raw NO_X emissions can be reduced due to decreasing combustion temperatures, making the lean concept even more desirable. One possibility for increasing the flame stability and the burn rate is the usage of hydrogen. Since the laminar flame speed of hydrogen is an order of magnitude higher than of gasoline and of other liquid fuels, even with a slight hydrogen admixture, significant improvements can be expected. In order to be able to evaluate these potential benefits, it is recommended to conduct extensive research, both experimentally and simulatively. A project addressing this topic is already started as the FVV research project “ICE2030”.

In conclusion, despite the statement at the beginning, arguing that the internal combustion engine is a more than 150 years old and thus nearly perfected technology, this work has demonstrated that it still has remarkable potential for improvement as long as research, development and engineering effort is invested.

6 References

[1] Lešnik, L., Kegl, B., Torres-Jiménez, E., and Cruz-Peragón, F. 2020. Why we should invest further in the development of internal combustion engines for road applications. *Oil Gas Sci. Technol. – Rev. IFP Energies nouvelles* 75, 56.

[2] 2022. *Global Internal Combustion Engine Market (2020 to 2028) - Surging Adoption of Gas Powered IC Engines in Developing Countries Presents Opportunities - ResearchAndMarkets.com*. https://www.businesswire.com/news/home/20210712005390/en/. Accessed 26 January 2022.

[3] Nakata, K., Nogawa S., Takahashi, D., Yoshihara, Y. 2016. *Engine technologies for achieving 45% thermal efficiency of SI engine*. *SAE International Journal of Engines Vol. 9, No. 1 (April 2016), pp. 179-192*.

[4] Heywood, J. B. 1988. *Internal Combustion Engine Fundamentals*. McGraw-Hill, New York.

[5] Merker, G. P. and Teichmann, R., Eds. 2014. *Grundlagen Verbrennungsmotoren*. *Funktionsweise, Simulation, Messtechnik*. ATZ/MTZ-Fachbuch. Springer Vieweg, Wiesbaden.

[6] Huß, M. 2013. *Übertragung von Motoreigenschaften mit Hilfe charakteristischer Skalierfunktionen zur Simulation verschiedener Varianten von Ottomotoren*. *Dissertation*.

[7] McBride, B. J. 1993. *Coefficients for Calculating Thermodynamic and Transport Properties of Individual Species*. NASA Langley Research Center.

[8] Grill, M. 2006. *Objektorientierte Prozessrechnung von Verbrennungsmotoren*. *Dissertation. DOI*=10.18419/opus-4076.

[9] Bargende, M. *Grundlagen der Fahrzeugantriebe*. *Vorlesungsskript*.

[10] European Parliament and the Council. 2009. *Regulation (EC) No 443/2009 of the European Parliament and of the Council of 23 April 2009 setting emission performance standards for new passenger cars as part of the Community's integrated approach to reduce CO2 emissions from light-duty vehicles (Text with EEA relevance)*.

[11] Spicher, U. 2017. Downsizing und Downspeeding. In *Ottomotor mit Direkteinspritzung und Direkteinblasung*. Springer Vieweg, Wiesbaden, 235–242. DOI=10.1007/978-3-658-12215-7_8.

[12] Fraser, N., Blaxill, H., Lumsden, G., and Bassett, M. 2009. Challenges for Increased Efficiency through Gasoline Engine Downsizing. *SAE Int. J. Engines* 2, 1, 991–1008.

[13] Hancock, D., Fraser, N., Jeremy, M., Sykes, R., and Blaxill, H. 2008. *A New 3 Cylinder 1.2l Advanced Downsizing Technology Demonstrator Engine*. SAE Technical Paper 2008-01-0611. DOI=10.4271/2008-01-0611.

[14] Schmid, A. and Bargende, M. 2011. Wirkungsgradoptimierter Ottomotor. *MTZ Motortech Z* 72, 12, 980–987.

[15] C. Ternel, A. Pagot, P. Anselmi, and X. Gautrot. 2008. *A new approach for variable displacement: The OVaLiD® concept* 3.

[16] Inside Mazda. 2017. *Mazda's New Technology Makes SKYACTIV-G Even Better | Inside Mazda*. https://insidemazda.mazdausa.com/the-mazda-way/technology/mazdas-new-cylinder-deactivation/. Accessed 3 August 2021.

[17] Eichler, F., Demmelbauer-Ebner, W., Theobald, J., Stiebels, B., Hoffmeyer, H., and Kreft, M. 2016. *Der neue EA211 TSI® evo von Volkswagen*. 37. Internationales Wiener Motorensymposium.

[18] Küpper, K., Linsel, J., Pingen, B., and Weber, C. 2016. Zylinderabschaltung beim Dreizylindermotor. *MTZ Motortech Z* 77, 12, 48–55.

[19] Tabata, M., Yamamoto, T., and Fukube, T. 1995. Improving NOx and Fuel Economy for Mixture Injected SI Engine with EGR. In *SAE Technical Paper Series*. SAE International, 400 Commonwealth Drive, Warrendale, PA, United States. DOI=10.4271/950684.

[20] Grandin, B. and Ångström, H.-E. 1999. *Replacing Fuel Enrichment in a Turbo Charged SI Engine: Lean Burn or Cooled EGR*. SAE Technical Paper 1999-01-3505. DOI=10.4271/1999-01-3505.

[21] Ganser, J., Blaxill, H., and Cairns, A. 2007. Hochlast-AGR am turboaufgeladenen Ottomotor. *MTZ Motortech Z* 68, 7-8, 564–569.

[22] Kapus, P., Prevedel, K., Wolkerstorfer, J., and Neubauer, M. 2013. *200 g/kW h–can the stoichiometric gasoline engine beat the diesel*. 22nd Aachen Colloquium Automobile and engine Technology, pp.

[23] Bozza, F., Bellis, V. de, Gimelli, A., and Muccillo, M. 2014. Strategies for Improving Fuel Consumption at Part-Load in a Downsized Turbocharged SI Engine: a Comparative Study. *SAE Int. J. Engines* 7, 1, 60–71.

[24] Kiga, S., Moteki, K., and Kojima, S. 2017. Der neue Nissan VC-Turbo mit variablem Verdichtungsverhältnis. *MTZ Motortech Z* 78, 11, 44–53.

[25] INFINITI. 2021. *VC-Turbo Engine Technology | Infiniti USA*. https://www.infinitiusa.com/infiniti-news/technology/vc-turbo-engine.html. Accessed 3 August 2021.

[26] Weinowski, R., Wittek, K., Dieterich, C., and Seibel, J. 2012. Zweistufige Variable Verdichtung für Ottomotoren. *MTZ Motortech Z* 73, 5, 388–392.

[27] 2016. *Variable Compression Ratio-in a Technology Competition?*

[28] Berntsson, A. W., Josefsson, G., Ekdahl, R., Ogink, R., and Grandin, B. 2011. The Effect of Tumble Flow on Efficiency for a Direct Injected Turbocharged Downsized Gasoline Engine. *SAE Int. J. Engines* 4, 2, 2298–2311.

[29] *ICE2025+: Ultimate System Efficiency*. FVV Final Report, Project no. 1307, 2021, Frankfurt am Main.

[30] Filipi, Z. S. and Assanis, D. N. 2000. The effect of the stroke-to-bore ratio on combustion, heat transfer and efficiency of a homogeneous charge spark ignition engine of given displacement. *International Journal of Engine Research* 1, 2, 191–208.

[31] Vacca, A., Bargende, M., Chiodi, M., Franken, T., Netzer, C., Gern, M. S., Kauf, M., and Kulzer, A. C. 2019. *Analysis of Water Injection Strategies to Exploit the Thermodynamic Effects of Water in Gasoline Engines by Means of a 3D-CFD Virtual Test Bench*. SAE Technical Paper 2019-24-0102. DOI=10.4271/2019-24-0102.

[32] Hunger, M., Böcking, T., Walther, U., Günther, M., Freisinger, N., and Karl, G. 2017. Potential of Direct Water Injection to Reduce Knocking and Increase the Efficiency of Gasoline Engines. In . Springer, Cham, 338–359. DOI=10.1007/978-3-319-69760-4_20.

[33] Vacca, A., Cupo, F., Chiodi, M., Bargende, M., Khosravi, M., and Berkemeier, O. 2021. The Virtual Engine Development for Enhancing the Compression Ratio of DISI-Engines Combining Water Injection,

Turbulence Increase and Miller Strategy. *SAE Int. J. Adv. & Curr. Prac. in Mobility* 3, 1, 685–701.

[34] Böhm, M., Durst, B., Unterweger, G., and Rubbert, S. 2016. Ansätze zur Onboard-Wassergewinnung für eine Wassereinspritzung. *ATZ Automobiltech Z* 118, 1, 54–59.

[35] Franzke, B., Voßhall, T., Adomeit, P., and Müller, A. 2019. Wassereinspritzung zur Erfüllung zukünftiger RDE-Anforderungen für Turbo-Ottomotoren. *MTZ Motortech Z* 80, 3, 32–41.

[36] Yi, M., He, J., Huang, B., and Zhou, H. 1999. Friction and wear behaviour and abradability of abradable seal coating. *Wear* 231, 1, 47–53.

[37] Arnold, S., Calta, D., Dullack, K., Judd, C., and Thompson, G. 2005. Development of an Ultra-High Pressure Ratio Turbocharger. In *SAE Technical Paper Series*. SAE International, 400 Commonwealth Drive, Warrendale, PA, United States. DOI=10.4271/2005-01-1546.

[38] Zeppei, D., Koch, S., and Rohi, A. 2016. Wälzlagerungstechnologie für Pkw-Turbolader. *MTZ Motortech Z* 77, 11, 28–35.

[39] Al-Hasan, N., Böning, R., Kraus, D., and Sandor, I. 2018. Otto-Turbolader mit variabler Turbinentechnologie. *MTZ Motortech Z* 79, 1, 40–43.

[40] Chen, W. F., Chang, J. T., and Su, J. H. 2014. Researches on the Measurement Rebuilding and Multi-Axis Flank Milling NC Machining of the Compressor Impeller. *Precision Engineering and Nanotechnology V* 625, 241–246.

[41] Feneley, A. J., Pesiridis, A., and Andwari, A. M. 2017. Variable Geometry Turbocharger Technologies for Exhaust Energy Recovery and Boosting-A Review. *Renewable and Sustainable Energy Reviews* 71, 959–975.

[42] Whitfield, A., Doyle, M. D. C., and Firth, M. R. 1993. Design and Performance of a High-Pressure Ratio Turbocharger Compressor Part 2: Experimental Performance. *Proceedings of the Institution of Mechanical Engineers, Part A: Journal of Power and Energy* 207, 2, 125–131.

[43] Whitfield, A. and Sutton, A. J. 1989. The Effect of Vaneless Diffuser Geometry on the Surge Margin of Turbocharger Compressors.

Proceedings of the Institution of Mechanical Engineers, Part D: Journal of Automobile Engineering 203, 2, 91–98.

[44] Steglich, T., Vogt, M., and Weiss, M. 2020. Alternative Bypassregelung für Turbolader. *MTZ Motortech Z* 81, 9, 50–55.

[45] Matsumoto, K., Tojo, M., Jinnai, Y., Hayashi, N., and Ibaraki, S. 2008. *Development of compact and high-performance turbocharger for 1,050 C exhaust gas*. Mitsubishi Heavy Industries, Ltd.Technical Review Vol. 45 No. 3 (Sep. 2008).

[46] Baumgarten, H., Görgen, M., Balasz, A., Nijs, M., Lehn, H., Claßen, J., Sterlepper, S., Ackermann, J., and Wittler, M. 2018. *New lambda= 1 gasoline powertrains new technologies and their interaction with connected and autonomous driving*. 30th International AVL Conference “Engine & Environment”, June 7 th - 8th, 2018, Graz, Austria.

[47] Morand, N., Agnew, G., Bontemps, N., and Jeckel, D. 2017. Turbolader mit variabler Turbinengeometrie für Miller-Ottomotoren. *MTZ Motortech Z* 78, 1, 44–49.

[48] Taylor, J., Fraser, N., and Wieske, P. 2010. Water Cooled Exhaust Manifold and Full Load EGR Technology Applied to a Downsized Direct Injection Spark Ignition Engine. *SAE Int. J. Engines* 3, 1, 225–240.

[49] 2021. *Boosting Technologies - BorgWarner*. https://www.borgwarner.com/technologies/boosting-technologies. Accessed 2 September 2021.

[50] Wouters, C., Lehrheuer, B., Heuser, B., and Pischinger, S. 2020. Ottomischkraftstoffe mit Methanol, Ethanol und Butanol. *MTZ Motortech Z* 81, 3, 16–23.

[51] Rossi, E., Hummel, S., Cupo, F., Vacca, A., Chiodi, M., Bargende, M., Villforth, J., Kulzer, A. C., and Deeg, H.-P. 2021. *Experimental and Numerical Investigation for Improved Mixture Formation of an eFuel Compared to Standard Gasoline*. SAE Technical Paper 2021-24-0019. DOI=10.4271/2021-24-0019.

[52] Villforth, J., Kulzer, A. C., Deeg, H.-P., Vacca, A., Rossi, E., Cupo, F., Chiodi, M., and Bargende, M. 2021. *Methods to Investigate the Importance of eFuel Properties for Enhanced Emission and Mixture*

Formation. SAE Technical Paper 2021-24-0017. DOI=10.4271/2021-24-0017.

[53] Crönert Sebastian. 2022. *A complete methodology for the predictive simulation of novel, single- and multi-component fuel combustion*. *Dissertation*. Submitted for publication.

[54] The European Union and the Council. 2009. *DIRECTIVE 2009/30/EC*.

[55] *GT-Power*. Gamma Technologies.

[56] *FKFS UserCylinder*. FKFS.

[57] Wenig, M., Grill, M., and Bargende, M. 2013. A New Approach for Modeling Cycle-to-Cycle Variations within the Framework of a Real Working-Process Simulation. *SAE Int. J. Engines* 6, 2, 1099–1115.

[58] Gülder, Ö. L. 1984. *Correlations of Laminar Combustion Data for Alternative S.I. Engine Fuels*. SAE Technical Paper 841000. DOI=10.4271/841000.

[59] Grill, M., Fandakov, A., Hann, S., Keskin, M.-T., Urban, L., and Bargende, M. 2018. Lean combustion, EGR or gHCCI at high-load: challenging tasks in the 0D / 1D engine simulation. In *Internationaler Motorenkongress 2018*. Springer Vieweg, Wiesbaden, 149–174. DOI=10.1007/978-3-658-21015-1_11.

[60] Hann, S., Urban, L., Grill, M., and Bargende, M. 2017. Influence of Binary CNG Substitute Composition on the Prediction of Burn Rate, Engine Knock and Cycle-to-Cycle Variations. *SAE Int. J. Engines* 10, 2, 501–511.

[61] Hann, S., Grill, M., Bargende, M., and Altenschmidt, F. 2020. *A Quasi-Dimensional SI Burn Rate Model for Predicting the Effects of Changing Fuel, Air-Fuel-Ratio, EGR and Water Injection*. SAE Technical Paper 2020-01-0574. DOI=10.4271/2020-01-0574.

[62] Launder, B. E. and Spalding, D. B. 1974. The numerical computation of turbulent flows. *Computer Methods in Applied Mechanics and Engineering* 3, 2, 269–289.

[63] Bossung, C., Grill, M., Bargende, M., and Dingel, O. 2015. A quasi-dimensional charge motion and turbulence model for engine process calculations. In *15. Internationales Stuttgarter Symposium*. Springer Vieweg, Wiesbaden, 1001–1019. DOI=10.1007/978-3-658-08844-6_68.

[64] 2020. *Turbulenzmodellierung II*. FVV Abschlussbericht, Vorhaben Nr. 1233, Frankfurt am Main.

[65] 1998. *Turbulence modeling for CFD*.

[66] Tippelmann, G. 1977. A New Method of Investigation of Swirl Ports. In *SAE Technical Paper Series*. SAE International, 400 Commonwealth Drive, Warrendale, PA, United States. DOI=10.4271/770404.

[67] Fritsch, S., Grill, M., Bargende, M., and Dingel, O. 2020. *A Phenomenological Homogenization Model Considering Direct Fuel Injection and EGR for SI Engines*. SAE Technical Paper 2020-01-0576. DOI=10.4271/2020-01-0576.

[68] Fandakov, A., Bargende, M., Grill, M., Mally, M., and Kulzer, A. C. 2018. A New Model for Predicting the Knock Boundary with EGR at Full Load (Ein neues Modell zur Vorhersage der Klopfgrenze bei Volllast-AGR). In *Ladungswechsel im Verbrennungsmotor 2017*. Springer Vieweg, Wiesbaden, 47–72. DOI=10.1007/978-3-658-22671-8_3.

[69] Livengood, J. C. and Wu, P. C. 1955. *Correlation of autoignition phenomena in internal combustion engines and rapid compression machines* 5.

[70] Fandakov, A., Grill, M., Bargende, M., and Kulzer, A. C. 2017. Two-Stage Ignition Occurrence in the End Gas and Modeling Its Influence on Engine Knock. *SAE Int. J. Engines* 10, 4, 2109–2128.

[71] 1981. *Beitrag zur Ermittlung eines Klopfkriteriums der ottomotorischen Verbrennung und zur Vorausberechnung der Klopfgrenze*.

[72] Worret, R., Bernhardt, S., Schwarz, F., and Spicher, U. 2002. Application of Different Cylinder Pressure Based Knock Detection Methods in Spark Ignition Engines. In *SAE Technical Paper Series*. SAE International, 400 Commonwealth Drive, Warrendale, PA, United States. DOI=10.4271/2002-01-1668.

[73] Woschni, G. 1967. A Universally Applicable Equation for the Instantaneous Heat Transfer Coefficient in the Internal Combustion Engine. In *SAE Technical Paper Series*. SAE International, 400 Commonwealth Drive, Warrendale, PA, United States. DOI=10.4271/670931.

[74] Fischer, G. 1999. *Ermittlung einer Formel zur Vorausberechnung des Reibmitteldrucks von Ottomotoren - Abschlussbericht*. Reibmitteldruck - Ottomotor Vorhaben Nr. 629, Frankfurt am Main.

[75] Kuznik, A. 2022. *personal communication*.

[76] 2021. *Engine Knock Model - Final Report*. FVV Research Project #1313, Frankfurt am Main.

[77] Wagner, C., Keskin, M.-T., Grill, M., Bargende, M., Cai, L., Pitsch, H., and Blochum, S. 2020. Potential analysis and virtual development of SI Engines operated with DMC+. In *20. Internationales Stuttgarter Symposium*. Springer Vieweg, Wiesbaden, 49–74. DOI=10.1007/978-3-658-30995-4_9.

Appendix

A1. Model parameter C_u for experimental setups

Load variation 2000 RPM

Here, C_u is 6.25 and constant throughout the load variation.

Load variation with water injection 2000 RPM

With 50% water injection, the fitting value for C_u is 5.4. With 100% water injection the fitting value for C_u is 5.0.

EGR variations

Here, the C_u values are chosen as shown below:

EGR Rate:	**0%**	**5%**	**10%**	**15%**	**20%**	**25%**	**30%**
2250 RPM 6.5 bar	4.25	4.25	4.25	4.25	4.25	4.25	
2000 RPM 11 bar	4.60	4.45	4.30	4.15	4.00	3.85	3.70
2000 RPM 11 bar closed tumble flap	5.4	5.3	5.2	5.1	5.0	4.9	4.8
2500 RPM 16 bar	4.90	4.72	4.54	4.36	4.18	4.00	

Air-fuel equivalence ratio variations

Here, the C_u values are chosen as shown below:

λ:	**1.0**	**1.1**	**1.2**	**1.3**	**1.4**	**1.5**	**1.6**	**1.7**
2000 RPM 11 bar closed tumble flap	5.4	5.2	5.0	4.8	4.6	4.4	4.2	4
2000 RPM 8 bar closed tumble flap ε = 18	5.2	5.0	4.8	4.6	4.4	4.2	4.0	3.8

Load variation, lean, ε = 18

Here, the C_u has a constant value of 4.4 throughout the load variation.

Methanol, air-fuel equivalence ratio variation, 2500 RPM, 16 bar IMEP

The C_u values fitting for lean methanol combustion are chosen as follows. The value for stoichiometric gasoline combustion at the same engine at the same operating point is also shown:

λ:	**1.0**	**1.1**	**1.2**	**1.3**	**1.4**	**1.5**	**1.6**	**1.7**	**1.8**	**1.9**
Methanol	5.2	5.3	5.4	5.5	5.6	5.7	5.8	5.9	6.0	6.1
Gasoline	6.0									

A2. Model parameter x_{ub} for experimental setups

Load variation 2000 RPM

Here, the fitting value for x_{ub} is 0.16.

Load variation 2000 RPM, 100% water injection

Here, the fitting value for x_{ub} is 0.1.

EGR variations

The suitable values for x_{ub} are as shown below:

EGR Rate:	**0%**	**5%**	**10%**	**15%**	**20%**	**25%**	**30%**
2000 RPM 11 bar	0.120	0.108	0.096	0.084	0.072	0.060	0.048
2000 RPM 11 bar closed tumble flap	0.110	0.102	0.094	0.086	0.078	0.070	0.062
2500 RPM 16 bar	0.28	0.18	0.11	0.07	0.05	0.032	

A3. Model settings, full engine models

Reference Engine VW EA211 TSI evo

For this model, a C_u value of 3.65 is chosen, which is an experience value.

The friction model is calibrated according to following: At 2000 RPM, 12 bar BMEP, FMEP is 0.6 bar. At 3500 RPM, 12 bar BMEP, FMEP is 0.75 bar. These values are in accordance to the discussions during the steering committee of the research project “ICE2025+: Ultimate System Efficiency”.

Furthermore, it is assumed that the pressure after the turbine at the rated power is 1.15 bar. This value is in accordance to the discussions during the steering committee of the research project “ICE2025+: Ultimate System Efficiency”. The friction multipliers at the exhaust gas aftertreatment elements are matched accordingly.

The heat transfer multiplier at the cylinders is calibrated as following: Several operating points with lower loads are considered, of which the brake specific fuel consumption (BSFC) can be determined with the help of the published engine map of VW EA211 TSI evo. At lower loads no knock occurs, i.e. the mfb50% is set to the value of 8°CA. Then the heat transfer multiplier $C_{Woschni}$ is calibrated so that the model predicts the BSFCs accurately. The suitable value for $C_{Woschni}$ is 1.15. It is further assumed, that this value stays constant throughout the engine map.

The calibration of the knock model is as follows: Several operating points with higher loads are considered, of which the BSFC can be determined with the help of the published engine map of VW EA211 TSI evo. At these points, knock occurs and the mfb50% is greater than 8°CA and BSFC is higher than what could have been achieved with an optimal mfb50%. The value for x_{ub} is calibrated so that the model predicts the BSFC at higher loads accurately. The suitable value for x_{ub} is 0.25.

High Efficiency Engine, Full Load Water Injection Engine, A-Segment Engine, J-Segment Engine

For simulating the high turbulence concept C_u is doubled, i.e. the new value is 7.3. The discharge coefficients of the intake valve are multiplied by 0.85, which is an experience value for the high turbulence concept.

C_u is then further corrected for EGR according to the following formula:

$$C_u(EGR\ Rate) = C_{u,ref} - 0.15 \cdot \left(C_{u,ref} \cdot \frac{EGR\ Rate}{30\%}\right) \tag{5.1}$$

C_u is also corrected for water injection:

$$C_u(WI\%) = C_{u,ref} - 1.1 \cdot \frac{WI\%}{100\%} \tag{5.2}$$

where $WI\%$ is the mass of injected water divided by the mass of injected fuel in percent.

$C_{Woschni}$ needs also an EGR correction. Otherwise, the efficiency increase with the EGR is underestimated in comparison to the experimental data. Thus:

$$C_{Woschni} = C_{Woschni,ref} - 0.6 \cdot EGR\ Rate \tag{5.3}$$

The chosen x_{ub} is 0.25 as in the Reference Engine, but is modified in case of EGR or water injection:

$$x_{ub}(EGR\ Rate) = x_{ub,ref} \cdot 0.8^{\left(\frac{EGR\ Rate}{5\%}\right)} \tag{5.4}$$

$$x_{ub}(WI\%) = x_{ub,ref} - 0.05 \cdot \frac{WI\%}{100\%} \tag{5.5}$$

It should be noted that the x_{ub} has a strong exponential dependency on EGR. Also, this calibration is only suitable for lower and medium loads. For higher loads, an even stronger dependency on EGR would be necessary. But at higher loads the engine is operated without EGR so that the approach shown above yields accurate results.

Methanol Engine

Since the fitting Cu value for methanol is lower than the fitting value for gasoline at the experimental setup, the Cu for full engine methanol models must also be adjusted. Therefore, C_u is set 6.0 for the methanol engine. The EGR correction remains unchanged. Also, $C_{Woschni}$ is 1.15 and is constant.

The knock model is deactivated.

Blend Engine

Blend is considered similar to gasoline, but has longer burn durations and has a higher knock resistance. The suitable C_u is 5.5 and x_{ub} is 0.18. The suitable $C_{Woschni}$ remains unchanged and is 1.15.

These values are then corrected as in the High Efficiency Engine as described above.

Lean High Efficiency Engine, Lean Full Load Water Injection Engine

For the accurate simulation of the lean combustion, following corrections are necessary:

$$C_u(\lambda) = C_{u,ref} \cdot (1 - 0.25 \cdot (\lambda - 1)) \tag{5.6}$$

$$C_{Woschni} = C_{Woschni,ref} \cdot (1 - 0.25 \cdot (\lambda - 1)) \tag{5.7}$$

The knock model is deactivated.

Lean Methanol Engine

For the lean methanol engine C_u and $C_{Woschni}$ need also to be corrected. But in contrast to the gasoline engines, the correction trend is reversed:

$$C_u(\lambda) = C_{u,ref} \cdot (1 + 0.2 \cdot (\lambda - 1)) \tag{5.8}$$

$$C_{Woschni} = C_{Woschni,ref} \cdot (1 + 0.1 \cdot (\lambda - 1)) \tag{5.9}$$

A4. Estimation of the benefits with load point shifting

Here, the efficiency benefit of the load point shifting from 2000 RPM 100 Nm to 2000 RPM 80 Nm for the High Efficiency Engine is estimated. For this reason, the engine's operation is divided into two phases: In Phase 1, the engine is operated with an efficiency of the operating point 80 Nm or 100 Nm. In Phase 2, the engine is operated with an initially unknown efficiency. The overall efficiency during the both phases is 36.1% as in the P1 hybrid configuration.

$$\eta_2 = \frac{W_2}{Q_{f,2}} = \frac{W_{tot} - W_1}{Q_{f,tot} - Q_1} = \frac{W_{tot} - W_1}{Q_{f,tot} - \frac{W_1}{\eta_1}} \tag{5.10}$$

W: Mechanical energy output of the internal combustion engine

Q_f: Fuel energy

η: Efficiency of the internal combustion engine

Indices 1,2, tot: Phase 1, Phase 2, total respectively

Known or easily calculable quantities:

η_1 = 40.4% (2000 RPM 80 Nm)

W_{tot} = 2.95 kWh

$Q_{f,tot}$ = 8.17 kWh

W_1 = 1.88 kWh. Explanation: If 0.47 kWh electrical energy is used for a load point shifting of 20 Nm, the engine is operated at 80 Nm torque with the same engine speed would deliver (80 Nm/20 Nm) x 0.47 kWh = 1.88 kWh energy.

As a result, the efficiency during the Phase 2 is:

η_2 = 30.4%

In the second step, it is assumed that the same engine is operated without the hybridization and without the load point lifting.

Known or easily calculable quantities in this step:

W_{tot} = 3.22 kWh (as in the case of Reference Engine without hybridization)

W_2 = 2.95 kWh – 1.88 kWh = 1.07 kW

$W_1 = W_{tot} - W_2$ = 2.15 kWh

η_1 = 37.8% (2000 RPM, 100 Nm)

η_2 = 30.4% (calculated in the previous step)

$$Q_{tot} = Q_1 + Q_2 = \frac{W_1}{\eta_1} + \frac{W_2}{\eta_2} \tag{5.11}$$

According to the equation, the total fuel energy Q_{tot} in this case is 9.21 kWh. The efficiency of the internal combustion engine is as a result 35.0%.

A5. Complementary Engine Maps

Here, further engine maps generated with the simulation models are presented that were not shown during the main part of this work, but are still important and/or interesting. The considered quantities are, BSFC, FMEP, PMEP, EGR rate, compression ratio, indicated efficiency, mfb50%, burn duration 10-90%, maximum cylinder pressure, maximum gradient of pressure rise in bar/°CA, intake pressure (taken after throttle), and the shift of intake valve (with a value of 0°CA for latest possible and plausible intake valve opening timing and negative °CA values for earlier intake valve opening timings (i.e. Miller). The maps for quantities with constant values are not shown, i.e. for example no EGR rate diagram is shown, if the engine does not have EGR. Brief complementary comments are added, if necessary.

Reference Engine

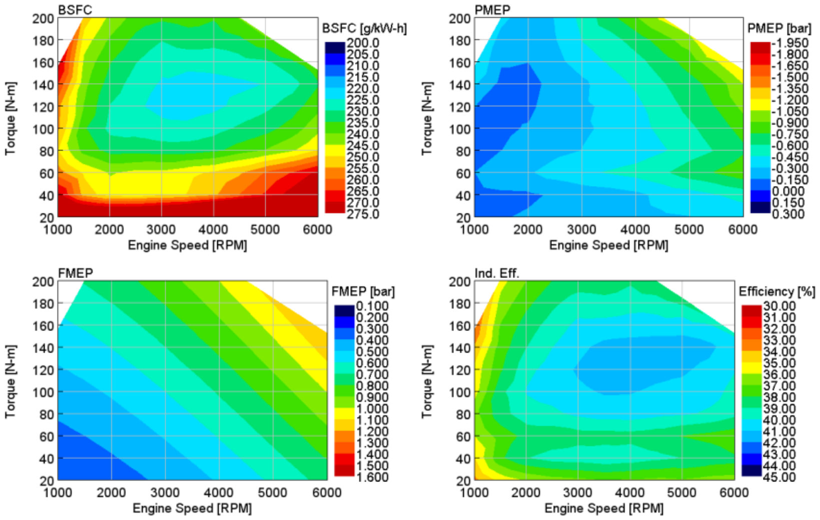

Figure A. 1. Complementary engine maps for the Reference Engine (I)

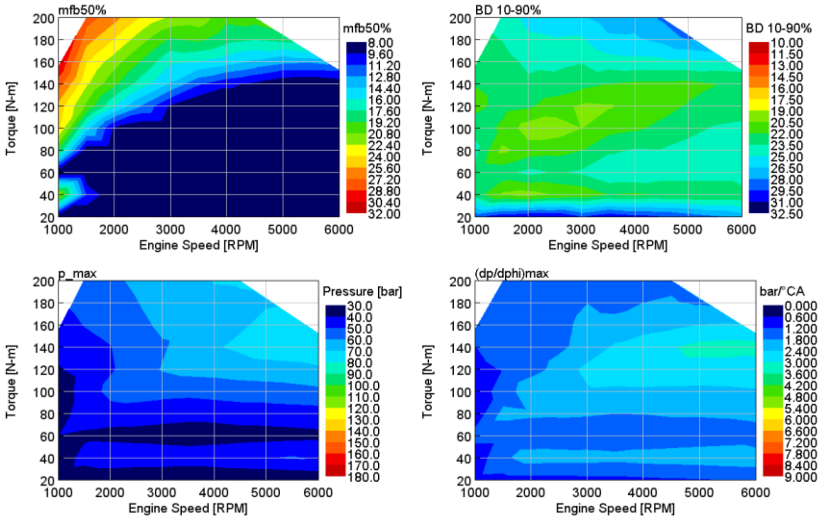

Figure A. 2. Complementary engine maps for the Reference Engine (II)

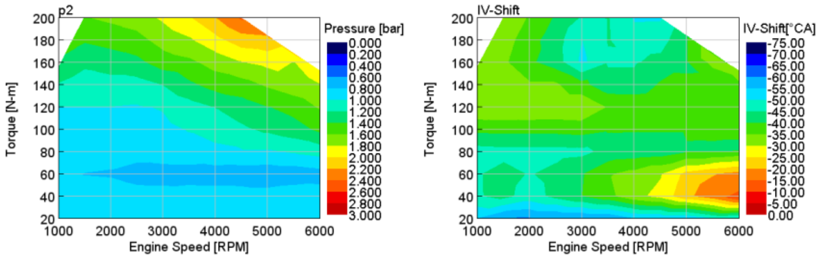

Figure A. 3. Complementary engine maps for the Reference Engine (III)

The most notable remark about the maps of the Reference Engine is the effect of cylinder deactivation along 40 Nm line. Many quantities like pumping losses or burn durations along 40 Nm are better than the values at 60 Nm where the engine is not operated with cylinder deactivation.

High Efficiency Engine

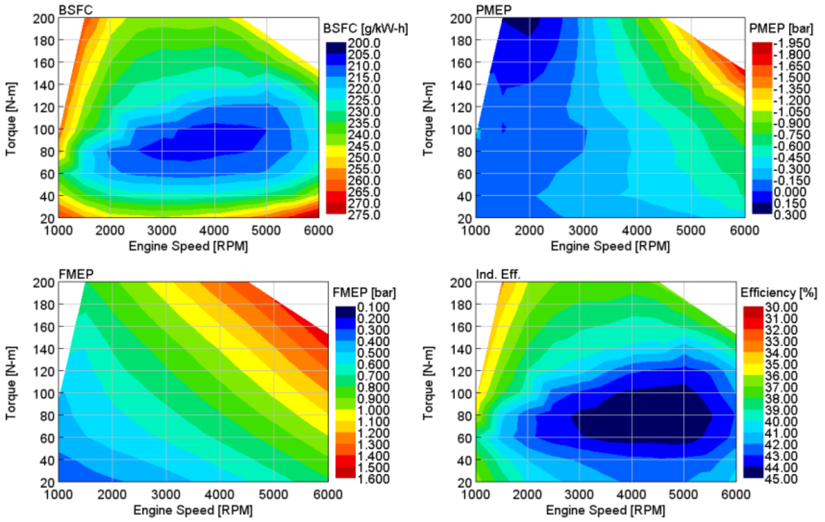

Figure A. 4. Complementary engine maps for the High Efficiency Engine (I)

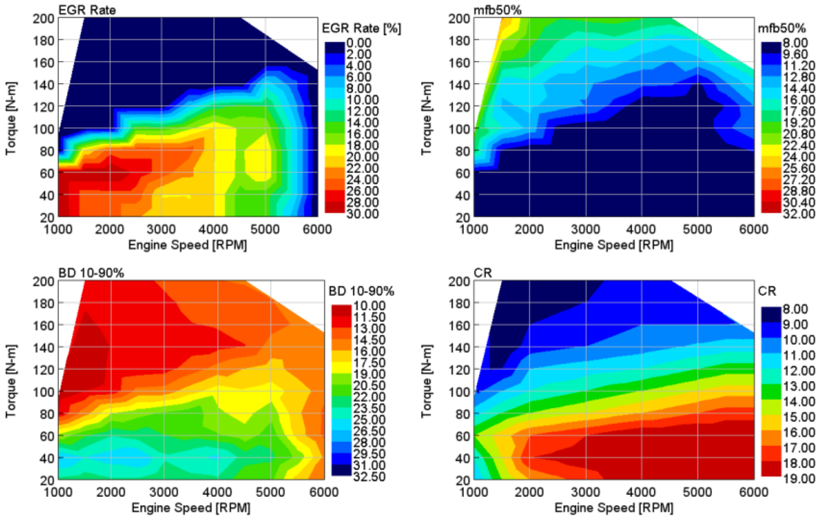

Figure A. 5. Complementary engine maps for the High Efficiency Engine (II)

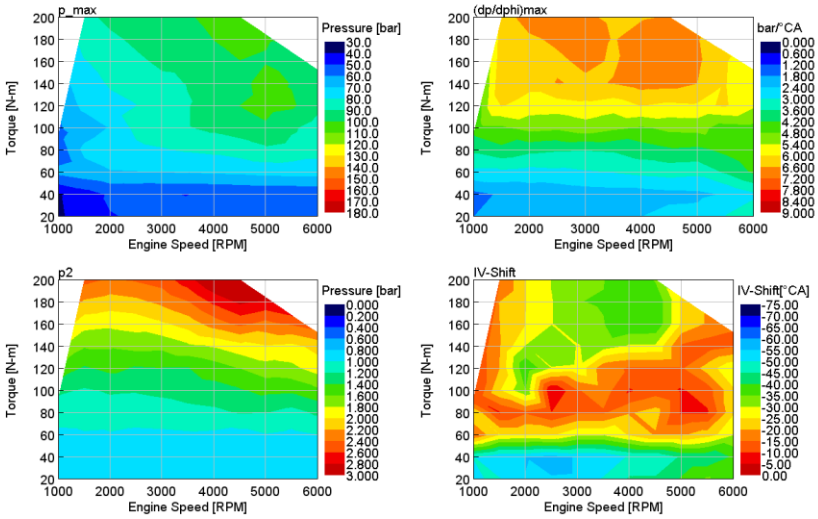

Figure A. 6. Complementary engine maps for the High Efficiency Engine (III)

On contrary to the Reference Engine, the High Efficiency Engine does not have cylinder deactivation at 40 Nm. Due to aggressive downsizing, the cylinder deactivation is only advantageous to up until about 20 Nm where the cylinder deactivation is utilized. Therefore, the characteristics of the maps of the High Efficiency Engine differ at lower loads from the Reference Engine. Similarly, since all of the following engines share the level of power density (and thus the same level of downsizing), they share similar characteristics at lower loads. The exceptions are the Methanol Engines.

A-Segment Engine

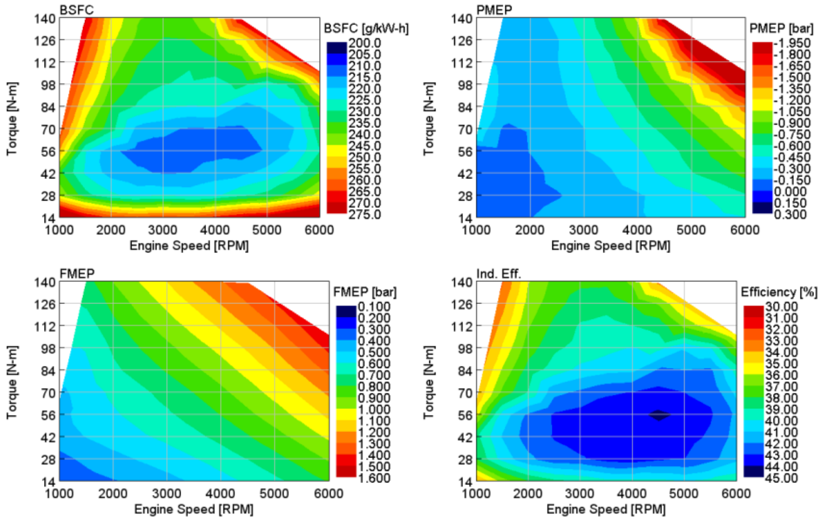

Figure A. 7. Complementary engine maps for the A-Segment Engine (I)

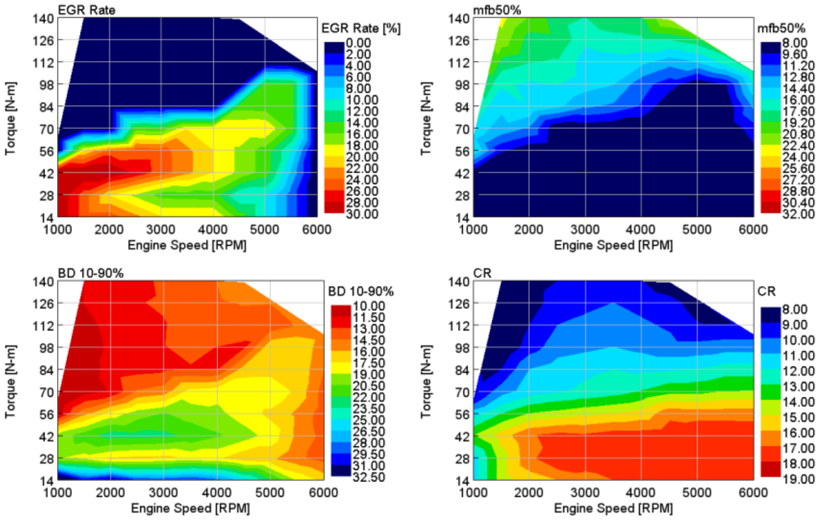

Figure A. 8. Complementary engine maps for the A-Segment Engine (II)

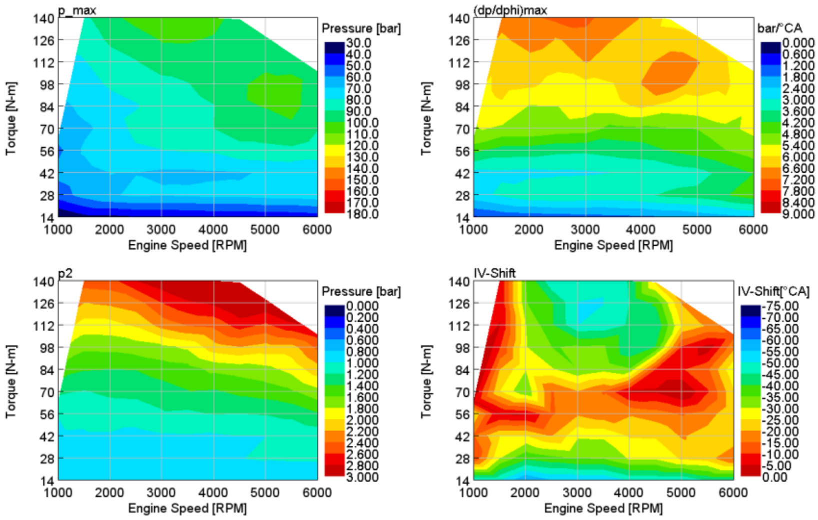

Figure A. 9. Complementary engine maps for the A-Segment Engine (III)

J-Segment Engine

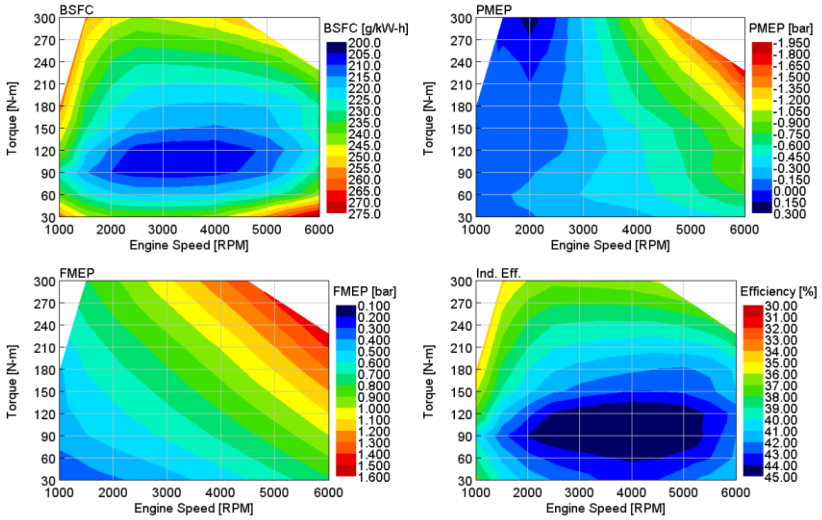

Figure A. 10. Complementary engine maps for the J-Segment Engine (I)

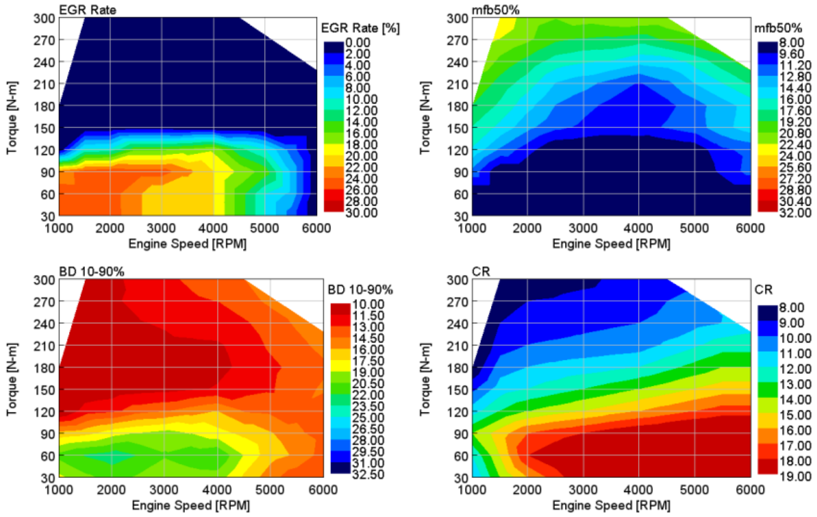

Figure A. 11. Complementary engine maps for the J-Segment Engine (II)

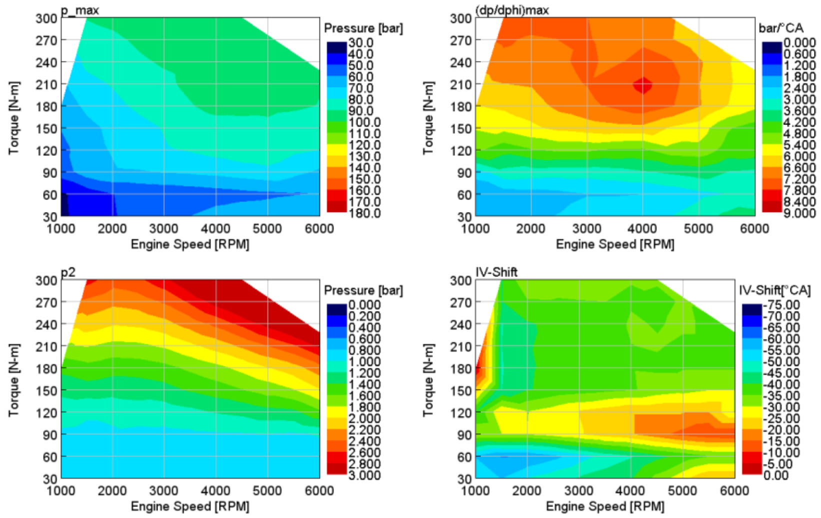

Figure A. 12. Complementary engine maps for the J-Segment Engine (III)

Methanol Engine

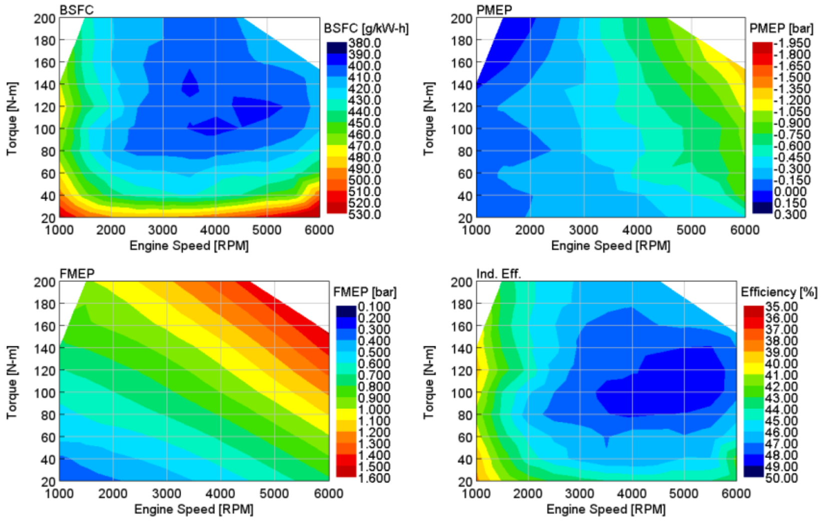

Figure A. 13. Complementary engine maps for the Methanol Engine (I)

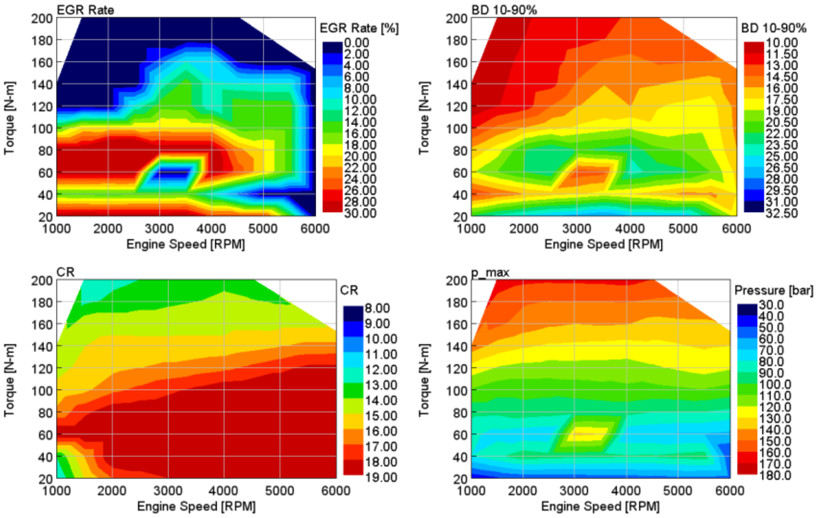

Figure A. 14. Complementary engine maps for the Methanol Engine (II)

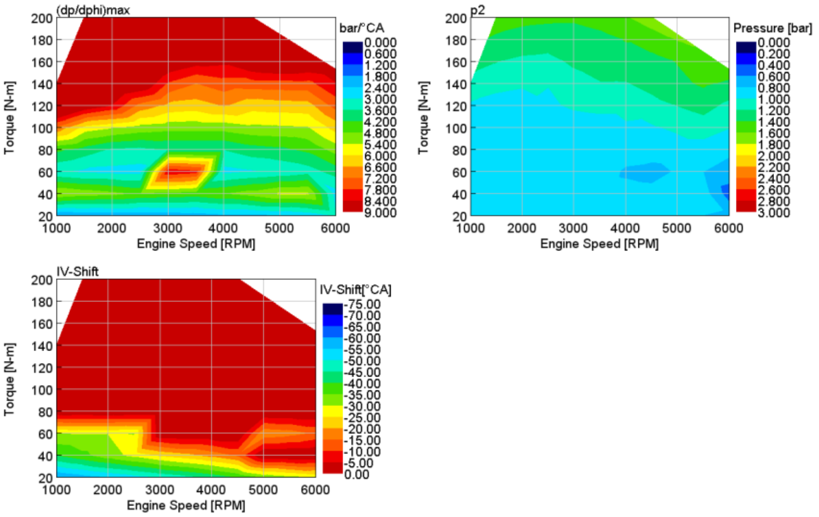

Figure A. 15. Complementary engine maps for the Methanol Engine (III)

The cylinder deactivation strategy of the Methanol Engine differs from the other High Efficiency Engines. Since methanol is very knock resistant, cylinder deactivation can be utilized at higher loads. Roughly speaking, cylinder deactivation can be regarded as advantageous as long as no boosting is necessary for the Methanol Engine. Thus, the cylinder deactivation is utilized at 40 Nm, and between 3000 RPM and 3500 RPM even for 60 Nm. This explains the sudden change at the maps for these two operating points: With the presence of cylinder deactivation, the operation of the engine at these points happens to be most efficient, when no EGR is utilized. Thus, the burn durations at these operating points differ greatly than the values in their vicinities.

Other than that, the combination of short burn durations, optimal mfb50% and a high compression ratio leads to a very high pressure gradient at full load. This is often associated a high noise, vibration and harshness (NVH).

Full Load Water Injection Engine

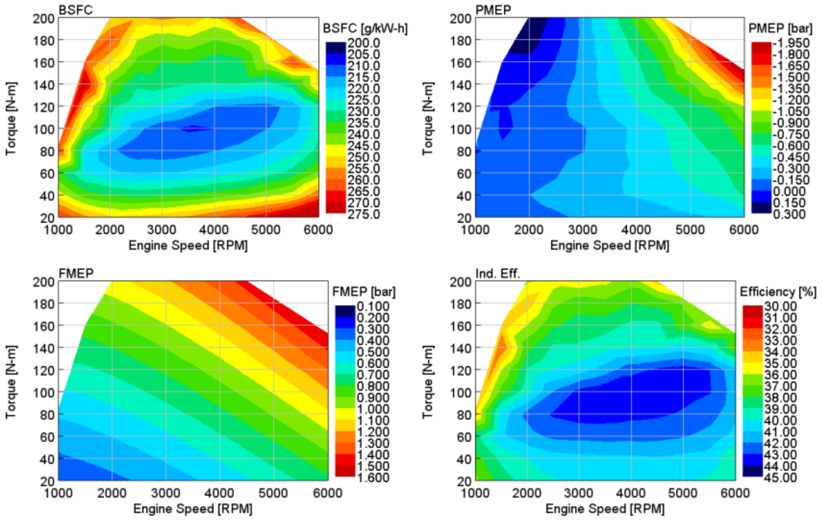

Figure A. 16. Complementary engine maps for the Full Load Water Injection Engine (I)

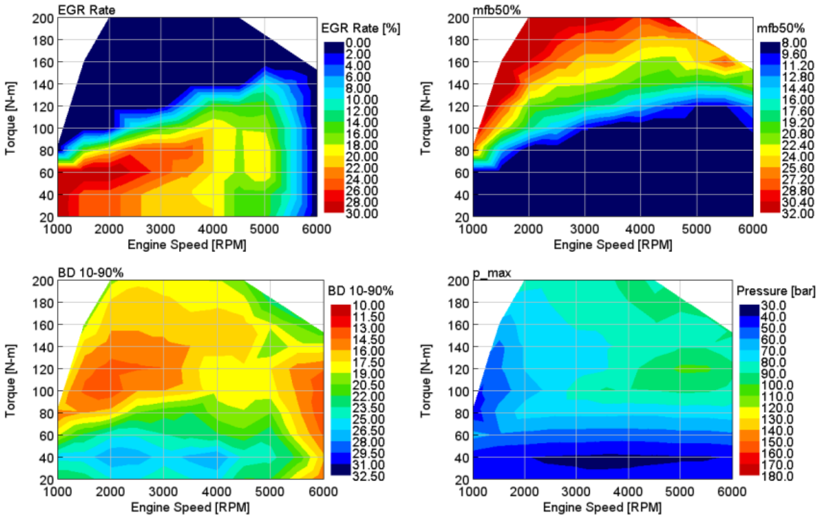

Figure A. 17. Complementary engine maps for the Full Load Water Injection Engine (II)

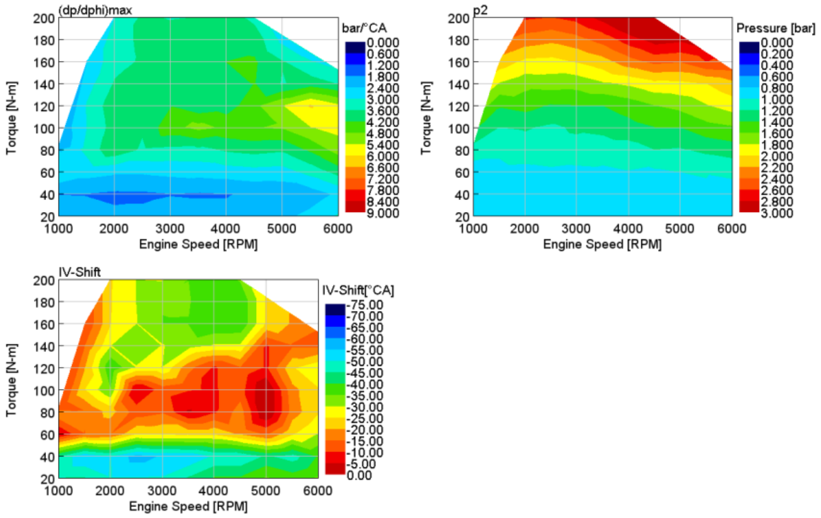

Figure A. 18. Complementary engine maps for the Full Load Water Injection Engine (III)

Lean High Efficiency Engine

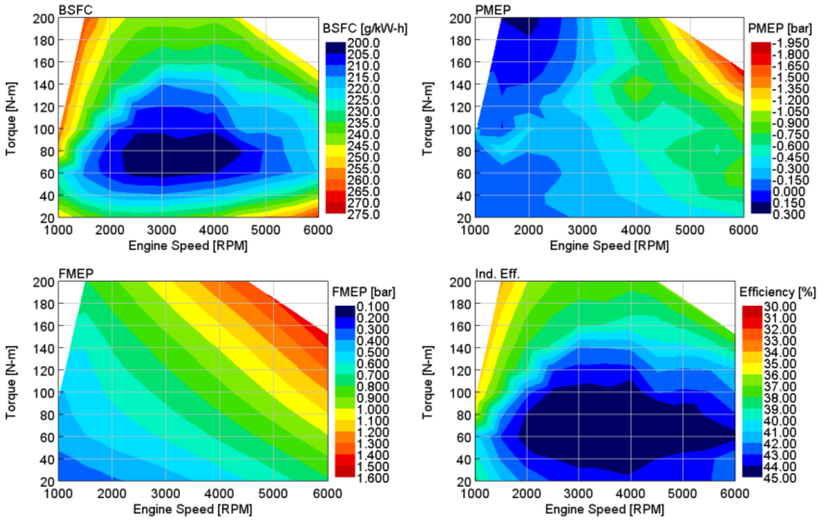

Figure A. 19. Complementary engine maps for the Lean High Efficiency Engine (I)

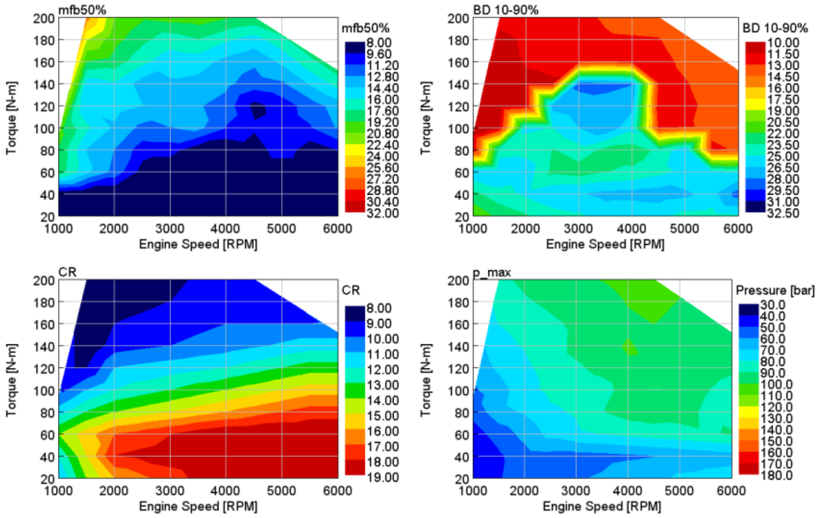

Figure A. 20. Complementary engine maps for the Lean High Efficiency Engine (II)

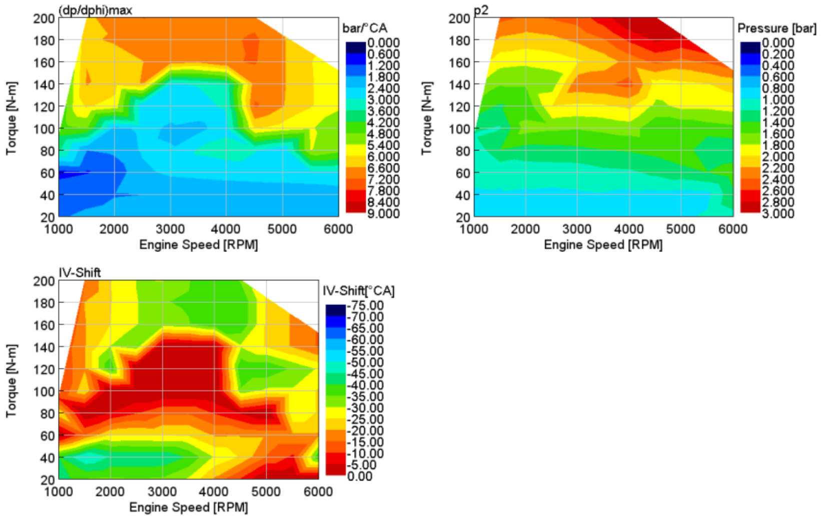

Figure A. 21. Complementary engine maps for the Lean High Efficiency Engine (III)

The map zone where the engine is operated lean is easily recognizable by the burn duration map. Moreover, the maps of the intake valve shift reveal how the presence of the lean concept limits the usage of an efficient Miller strategy.

Also interesting is the comparison of mfb50% of the stoichiometric and lean High Efficiency Engines. With the absence of EGR and a milder Miller strategy, the engine knock starts at significantly lower loads.

Lean Full Load Water Injection Engine

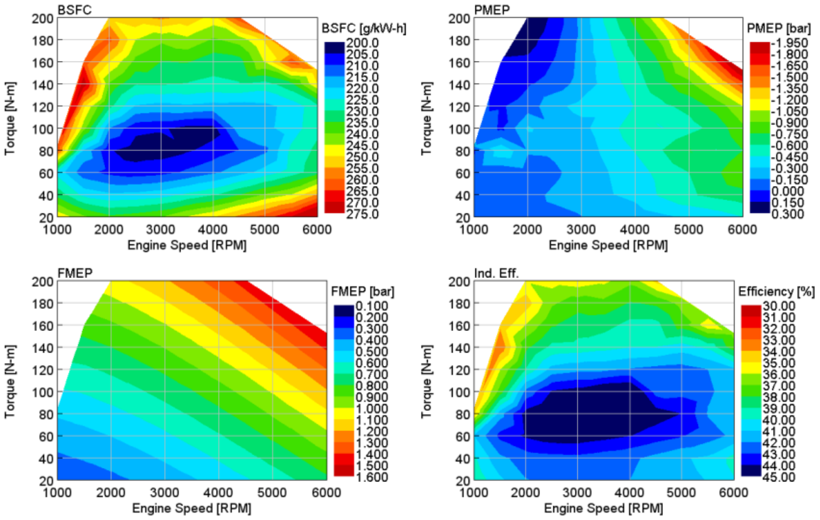

Figure A. 22. Complementary engine maps for the Lean Full Load Water Inj. Engine (I)

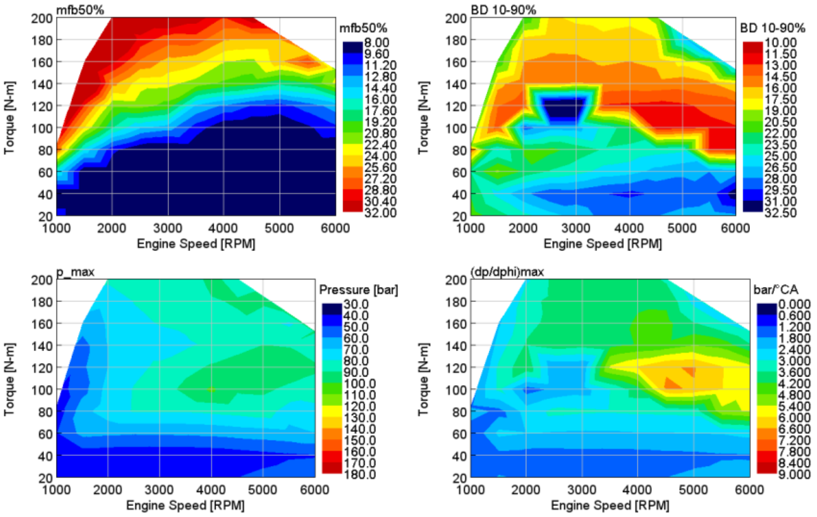

Figure A. 23. Complementary engine maps for the Lean Full Load Water Inj. Engine (II)

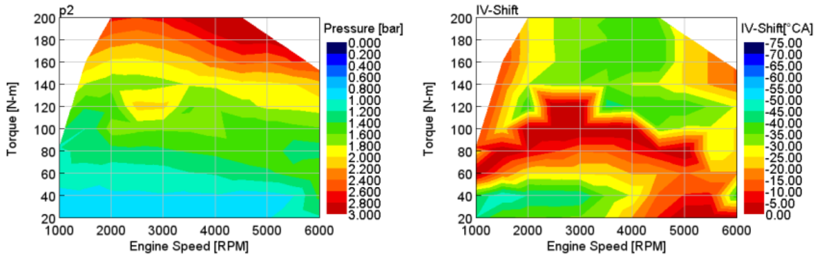

Figure A. 24. Complementary engine maps for the Lean Full Load Water Inj. Engine (III)

Lean Methanol Engine

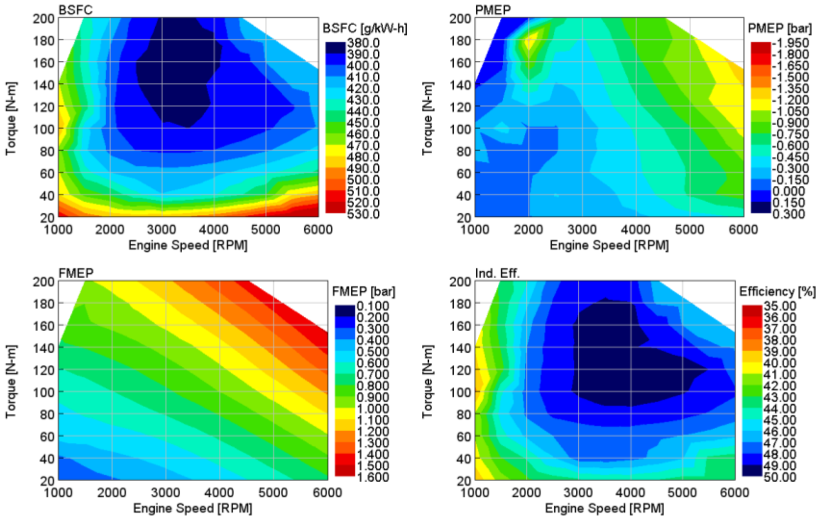

Figure A. 25. Complementary engine maps for the Lean Methanol Engine (I)

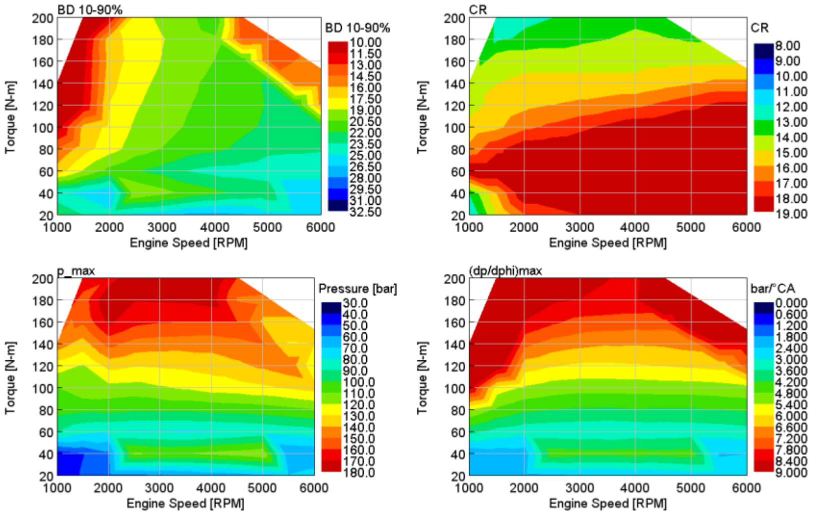

Figure A. 26. Complementary engine maps for the Lean Methanol Engine (II)

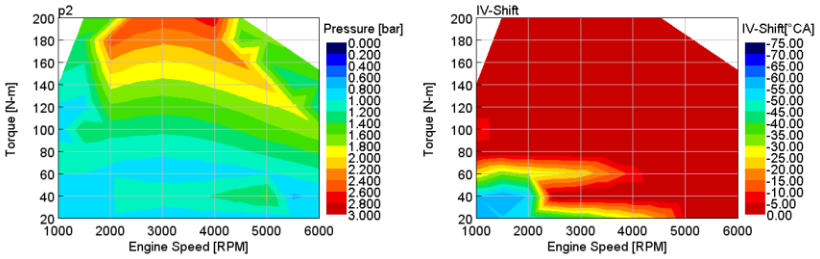

Figure A. 27. Complementary engine maps for the Lean Methanol Engine (III)

Curriculum Vitae

Name: Cihat Feyyaz Negüs

Date of Birth: April 6, 1988

Place of Birth: Sisli, Turkey

Citizenship: Turkish

Education:

04.2013 - 04.2016	RWTH Aachen University Field of Study: Energy Engineering Degree: Master of Science
10.2007 - 03.2013	RWTH Aachen University Field of Study: Mechanical Engineering Degree: Bachelor of Science
09.2002 - 06.2007	Deutsche Schule Istanbul

Professional Experience:

05.2018 - current	Research Associate Institute of Automotive Engineering (IFS) University of Stuttgart
04.2017 - 04.2018	Research Associate Research Institute of Automotive Engineering and Vehicle Engines Stuttgart (FKFS)
03.2013 - 02.2015	Student assistant Institute for Combustion Technology RWTH Aachen University
03.2012 - 10.2012	Internship Deutz AG, Cologne